RAPID UPLIFT OF SOUTHERN ALASKA CAUSED BY RECENT ICE LOSS

A

THESIS

Presented to the Faculty

of the University of Alaska Fairbanks

in partial Fulfillment of the Requirements

for the Degree of

DOCTOR OF PHILOSOPHY

By

Christopher Fairlamb Larsen, B.S., M.S,

Fairbanks, Alaska

May 2003

ProQuest Information and Learning Company
300 North Zeeb Road
P.O. Box 1346
Ann Arbor, MI 48106-1346

RAPID UPLIFT OF SOUTHERN ALASKA CAUSED BY RECENT ICE LOSS

By

Christopher Fairlamb Larsen

RECOMMENDED:

Advisory Committee Chair

Chair, Department of Geology and Geophysics

APPROVED:

Dean, College of Science, Engineering and Mathematics

Dean of the Graduate School

4-7-03

Date

Abstract.

Changing surface loads, such as melting glaciers, can induce deformation of the Earth's crust. The speed of the Earth's response to load changes and the pattern of deformation they cause can be used to infer material properties of the lithosphere and mantle.

Rapid uplift of southern Alaska has been measured with tide gauges, Global Positioning System (GPS) measurements and studies of raised shorelines. With multiple sites uplifting at rates in excess of 25 mm/yr, these measurements reveal the world's fastest regional uplift. Southern Alaska has over 75000 km^2 of glaciers, the rapid melting of which is contributing more to global sea level rise than Greenland. Southern Alaska also has intense tectonic activity, and uplift driven by tectonics has been suggested to be comparable with that driven by glacial unloading.

The majority of the uplift measurements examined here are located along the strike-slip portion of the Pacific - North America plate boundary. GPS measurements show little compressional strain associated with tectonic forcing. Tide gauges indicate long term linear uplift rates within the strike-slip regime, contrasting with tectonically influenced non-linear uplift to the northwest, where the Pacific Plate subducts beneath North America. Dating of raised shorelines within southeast Alaska show that the rapid uplift there began simultaneously with glacial unloading ~1790 AD. These observations indicate that the tectonic contribution to the uplift in southeast Alaska is small.

Multiple independent studies are used here to constrain the load changes in southern Alaska over the past ~1000-2000 yrs. A detailed model of the advance, standstill and retreat phases of the Little Ice Age glaciation is used as input to a simple viscoelastic Earth model. This model can match the pattern and magnitude of the region's uplift observations with a low degree of misfit, verifying that the region's

uplift can be entirely attributed to glacial isostatic rebound. Furthermore, the uplift observations require at the 95% confidence level a three-layer Earth model consisting of a 50^{+30}_{-25} km thick elastic lithosphere, an asthenosphere with viscosity $\eta_A=(1.4\pm0.3)\times10^{19}$ Pa s and thickness 110^{+20}_{-15} km, overlaying a viscous upper mantle half-space ($\eta_{um}=4\times10^{20}$ Pa s).

Table of Contents

List of Figures.

List of Tables.

Acknowledgements.

A graduate student fellowship from the National Aeronautical and Space Administration, a graduate student award from the Center for Global Change and Arctic System Research, and the National Science Foundation all have provided funding for my graduate studies.

David Stone deserves to be first on my list of scholarly acknowledgements, along with Juergen Keinle; together they brought me over from physics and got me started in geophysics with an undergraduate internship, working on a magnetic survey in Katmai. During this time frame, Johns Murrary, Morack, and Pender, along with Channon Price and Will Harrison, were beating a comprehensive physics curriculum into my thick skull; if only less of it had gone out the other ear. Will Harrison gets doubly acknowledged, as he and Keith Echelmeyer hired me (!) fresh out of school, and showed me the fantastic science and community of glaciology. Also, they took me to many beautiful places across Alaska and even to Antarctica. I particularly enjoyed learning the finer points of, really the *science* of blowing shit up with Matt Nolan and Keith on the Black Rapids and Taku. Keith is at least partially responsible for me continuing on with graduate studies; he is a dear friend, a mentor and inspiration.

As a graduate student at the Geophysical Institute, I have benefited from excellent support from both the seismology and glaciology groups: The hard work of Mitch Robinson, Sandy Zirnheld and By Valentine all made my life much easier. Roger Hansen let me use his computer for CPU intensive tasks. Field measurements were made easier and more enjoyable with the assistance and company of Joel Johnstone, Brian Hitchcock, Sandy, By, and Hilary Fletcher. Chris Zweck and Ed Bueller taught me much about programming and scripting in Matlab, GMT and Unix. Fellow students in the seismology/geodesy group have played a huge role in my

education and understanding of solid Earth processes. I have particularly benefited from discussions and friendship with Sigrún Hreinsdóttir, Dörte Mann, and Hilary. The glaciers group provided me with answers and data whenever I asked. Dan Elsberg, Leif Cox, Adam Bucki, Shad O'Neal and Martin Truffer all helped me through many hard homework assignments and have always been good company and friends. I want to thank my office mates Sharon Pitiss and John Chappelow for putting up with me over the years, especially considering that Frank Zappa provided (almost exclusively) the music that I listened to while working on this thesis.

Because my thesis started out (before I was involved) as a proposal to NSF, I have enjoyed an uncommon degree of involvement and interest in my thesis by my committee members, three of whom were PI's on this proposal. Craig Lingle, Roman Moytka, Keith and Jeff Freymueller all contributed immensely to the direction and focus of the results presented herein. Roman deserves additional thanks for the use and occasional abuse of his boat and equipment during the long field seasons needed to support this project. Roman is also an excellent and enthusiastic cook, and all of us who did fieldwork in SE certainly ate well. As my advisor, Jeff endured many questions on statistics, geophysics and computers from me. I greatly benefited from his breadth of geophysical knowledge and careful treatment of data and error analysis. A chance meeting between Jeff and Erik Ivins of JPL on a bus in Japan played an important role in this thesis. It was then that Erik loaned us his viscoelastic rebound code that was used for all of the modeling here. Thanks Erik!

Finally, my parents, Hugh and Meredith, my sister Jenny and my brother Ted all deserve the highest appreciation for their support and love. My wife Jessica has also given me much support and love, as well as inspiration; thank you. And to Pancho and Villa, AaaROOO!

Introduction.

Historically, the first comprehensive charting of the myriad Alexander Archipelago of southeast Alaska was in 1794, accomplished by Capt. George Vancouver in the precise tradition of James Cook. Like many of Cook's charts, Vancouver's chart remained in common usage for more than a century because it accurately depicted the hazards and passages to the skilled navigators of the era. With one exception: just north of the native sealing village of Hoonah, at the mouth of what is now called Glacier Bay, Vancouver had drawn great cliffs of ice, and not a hint of a break in the coastline. Eighty-five years later, John Muir was taken by native canoe deep into a new bay that had opened here, filled with icebergs from rapidly retreating rivers of ice.

In 1899, two events occurred which eventually led to this thesis. First, a series of magnitude 8+ earthquakes struck southern Alaska. With three mainshocks, a strong sequence of foreshocks, and widely felt aftershocks, these earthquakes gave a general impression that their effect was regional and not just local to the epicenter in Yakutat Bay. The second event of 1899 was the Klondike goldrush, which brought a huge increase in steamer traffic through the waterways of southeast Alaska. With the rise in traffic, the less skilled navigators of this new era were encountering more and more uncharted hazards. In response, the U.S. Coast and Geodetic Survey (CGS) increased its charting efforts, and in doing so began establishing and re-occupying temporary tide gauge stations.

A handful of these temporary tide gauge stations had been established before 1899. When CGS crews compared these stations' earlier sea level readings with their new measurements, they found that sea level had fallen, significantly, at all of their stations in the northern part of southeast Alaska. In a 1927 CGS report (USCGS,

1927), the observation and question central to my thesis was first put into press. Specifically, southeast Alaska is rapidly uplifting; what is the cause? Jamison (1882) had introduced the theory of glacial isostasy in 1882, and the rapid retreat of Glacier Bay was suggested by the CGS report as one possible cause. The other cause suggested was tectonic forcing associated with the 1899 earthquakes, a proposal with some foresight as the concept of plate tectonics was not yet established. The title of this thesis may give a hint of which mechanism my studies favor.

Over the 75 years since the CGS report, many more observations of the regional uplift have been made, and still the question of tectonics vs. isostasy remained. The problem has been one of separating the two effects; how can uplift caused by one be distinguished from the other? The research presented herein has relied on four lines of reasoning: 1) tectonically driven uplift will have a different temporal signature than isostasy, 2) 3-d velocity measurements from Global Positioning System (GPS) measurements can provide information on regional tectonic strain, 3) raised shorelines can be dated with dendrochronology to find when the uplift started, and 4) isostatic modeling can test whether observed ice load changes could produce the pattern and magnitude of the uplift observed.

Testing of isostatic models against uplift observations represents the bulk of this thesis, and each of the three chapters has some discussion thereof. Accurate and well-distributed measurements of ice thinning in Alaska over the latter half of this century (Arendt et al., 2002) established a solid foundation for these models. Prior to the time period of these data, the ice load changes are constrained by other independent studies. Consequently, all of the isostatic modeling presented here uses load models that are based solely on observations of glacial change, as opposed to load models estimated with iterative modeling designed to minimize misfit between predicted and observed uplift. The load changes are distributed over a fine grid spacing of 20 x 20 km, with a total of 536 disk loads used to represent the ice cover in southern Alaska. The elevation dependence of ice thinning rates is accounted for in this load distribution. In contrast to the sophistication of the load models, the Earth

model used is a simple viscoelastic mantle half-space overlain by an elastic lithosphere. This approach is driven by the fact that we know much more about the load than the specifics of lithosphere and upper mantle structure in southern Alaska. Nonetheless, isostatic model predictions are found to produce a low overall degree of misfit when compared with observations. Furthermore, these models place important constraints on the lithosphere and asthenosphere of southern Alaska.

Chapter 1 is primarily concerned with the temporal evolution of uplift, and permanent tide gauge records from southeast Alaska are contrasted both with stable, non-uplifting sites as well as sites with strong tectonic influence. The rapid yet steady signature of isostatic uplift in southeast Alaska contrasts with the non-linear records from within the 1964 Great Alaskan Earthquake rupture zone. Chapter 2 presents GPS measurements that indicate little compressional strain in the region. The vertical site velocities found in these measurements are tested against predictions from isostatic models, and the results suggest that all of the regional uplift can be attributed to isostasy. Chapter 3 presents a set of raised shoreline dates that indicate the regional uplift started at the same time Glacier Bay began its retreat. Chapter 3 also brings together all the uplift measurements from the raised shorelines and GPS data with new data from repeated temporary tide gauge measurements. A total of 77 measurements can be closely reproduced with an isostatic rebound model that includes the effects of a low viscosity asthenosphere.

Each of the three chapters is written in the form of a paper. Chapter 1 has been accepted for publication in the Journal of Geophysical Research. Chapter 2 has been submitted to Nature. Chapter 3 is in preparation for submission to the Geophysical Journal International. This format explains the variations in the specific layout between chapters, for example how references are cited within the text of each chapter. Each chapter has its own introduction and bibliography. Because the chapters are written as stand-alone papers, some repetition is inevitable, particularly in these sections. References to the first chapter in the second chapter are made as Larsen et al., 2003. References to the first and second chapters in the third chapter are made as

Larsen et al., 2003b and Larsen et al., 2003a, respectively. The contributing authors are listed at the beginning of each chapter.

References

Arendt, A.A., Echelmeyer, K.A., Harrison, W.D., Lingle, C.S. & Valentine, V.B., Rapid wastage of Alaska glaciers and their contribution to rising sea level, Science, **297**, 382-386 (2002).

Jamieson, T.F., On the cause of the depression and re-elevation of the land during the glacial period, Geol. Mag. N.S., **9**, 400-407 (1882).

U.S. Coast and Geodetic Survey, *Tides and currents in southeast Alaska,* 74-77, Coast and Geodetic Survey Special Publications, Silver Spring, ML (1927).

Chapter 1

Tide Gauge Records of Uplift Along the Northern Pacific-North American Plate Boundary, 1937 to 2001.*

Christopher F. Larsen, Keith A. Echelmeyer, Jeffrey T. Freymueller,
Roman J. Motyka

Geophysical Institute, University of Alaska, Fairbanks, Alaska

Abstract.

Vertical crustal motion at 15 sites along the northern Pacific-North America plate boundary is determined using relative sea level changes from tide gauge records. Our analysis is based on monthly mean sea levels, from which barometric pressure and seasonal effects are removed. The records are corrected for common-mode oceanographic variations. These records are statistically examined for non-linear behavior related to glacial isostatic, tectonic and postseismic effects. To estimate land uplift rates, the local effect of global sea level rise is removed from the relative sea level rates.

Slow rates of vertical motion are observed along the southern strike-slip plate boundary. The extremely rapid uplift of the northern strike-slip boundary can be attributed entirely to viscoelastic post-glacial rebound associated with tidewater-glacier retreat in Glacier Bay and regional post-Little Ice Age deglaciation. Isostatic modeling indicates a mantle viscosity of ~$2x10^{19}$-$5x10^{19}$ Pa s, similar to that found elsewhere along the Pacific-North America plate margin. At Yakutat, near the transition of plate motion from strike–slip to subduction, complex non-linear behavior

is evident, with a significant change in uplift rate following the 1979 St. Elias Earthquake. Non-linear uplift rates are predominant within the 1964 Great Alaskan earthquake near-field. Rapid uplift at Kodiak during a 3.5 yr period starting mid-1964 totaled 47±8 cm. Anchorage, Seward and Seldovia exhibited oscillatory uplift in the period immediately following the earthquake until mid-1972. Since mid-1972, uplift rates have increased steadily at Anchorage, Seward, Cordova, and Valdez. During this period Nikiski and Kodiak show decreasing uplift rates.

Introduction.

Water levels recorded at tide gauges over several decades or more allow the use of mean sea level (MSL) as a datum against which long-term changes of land level can be compared. Vertical crustal motions can be measured by changes in MSL; if the long-term MSL of a site appears to fall, the land level is rising, and vice-versa. Sea level observations allow continuous observation of solid earth motions over a much longer time frame than any other direct measurements (GPS, VLBI, strain gauges, EDM networks, etc.), and thus can provide determinations of long-term and time-varying earth responses to earthquake cycles and changes in surface loading. We present results for vertical crustal motion at 15 permanent tide gauge stations along the northern section of the Pacific Plate boundary with North America, an extremely active tectonic and glacio-isostatic environment (Fig. 1).

The tide gauge stations in this region reside in a wide range of tectonic environments, varying from pure strike-slip motion to oblique convergence, and shallow to moderately dipping oceanic/continental subduction (Fig. 1). The records from these stations show large coseismic datum shifts (Plafker, 1971), evidence of postseismic relaxation (Savage and Plafker, 1991, Cohen and Freymueller, 2001), and some of the fastest uplift rates in the world (Hicks and Shofnos, 1965). The wide range of tectonic environments along the northern Pacific Plate boundary, the rapid uplift of many of the sites, and the large earthquakes that many of the records span all provide a

unique opportunity to apply MSL analysis to complex and time-varying vertical crustal motion.

One feature common to past tide gauge studies of crustal motion in the Gulf of Alaska and the northeast Pacific is the use of annual MSL data. Because of occasional data gaps, annual MSL is often calculated from an incomplete set monthly MSL's, which is problematic (Cohen and Freymueller, 2001). This region of the Pacific Ocean has the largest seasonal variation in monthly MSL of anywhere in the world (~50 cm; Pugh, 1987), and the absence of even one monthly data point can lead to strong biasing of annual MSL averages.

Here we use a method developed by Kato (1983) that instead is based on monthly MSL data. The advantages of a monthly MSL based approach are (1) increased temporal resolution allowing for detection of the timing and magnitude of relatively small datum shifts, (2) improved correction for seasonal variations, and (3) greater signal to noise ratio allowing for significant error reduction in rate determination and the identification of time dependent rates. Kato's analysis also has the advantage of allowing subduction zone stations with non-linear records to be used to estimate regional oceanographic variations that are subsequently removed from the data. Previous studies of sea level-derived uplift along the Gulf of Alaska have restricted this estimate to a few stations with linear trends (Savage and Plafker, 1991; Cohen and Freymueller, 2001). Our analysis increases the number of stations used in this estimate from 3 to 11. This improvement, along with correcting for barometric pressure variations and estimating seasonal variations at each of the stations, greatly reduces the variance of the derived uplift records.

Previous Studies.

Southeast Alaska

Hicks and Shofnos (1965) studied uplift in SE Alaska using data from permanent gauges at Skagway, Juneau, Sitka and Ketchikan, along with repeated temporary gauge data at 27 sites distributed throughout northern SE Alaska. A broad, elongate uplift pattern affecting an area of over $2x10^5$ km^2 and a peak rate of >30 mm/yr was found centered over Glacier Bay. A tidewater glacier system completely filling Glacier Bay (~1600 km^2) which rapidly retreated between 1760 and ~1930. This retreat resulted not only in the vacation of >1 km thick ice from the bay but also in significant draw-down of the icefields that fed the tidewater system, which covered >7000 km^2. Hicks and Shofnos (1965) hypothesized that the rapid unloading from this retreat, combined with residual rebound from post-Wisconsin age deglaciation, caused the observed uplift. Since the region is at the beginning of the transition from strike-slip to subduction (e.g., Doser and Lomas, 2000; Fletcher and Freymueller, 1999), others have suggested a tectonic origin or contribution to the uplift. Observations that have been cited include (1) seismic evidence of a possible link between the Fairweather and Denali Fault systems trending across the uplift center (Horner, 1983), (2) the breadth of the uplift pattern over southeast Alaska (Hudson et al., 1982), and (3) the lack of changes in gravity measurements that would be consistent with isostatic rebound in the region (Barnes, 1984).

1964 Earthquake near-field

Sea level observations were used to determine the coseismic offsets in the 1964 Great Alaskan Earthquake (Plafker, 1971; Brown et al., 1977), and new tide gauges at Valdez, Seldovia, Nikiski and Anchorage were established in the affected area specifically to study the postseismic vertical motion. Brown et al. (1977) and Savage and Plafker (1991) studied the postseismic deformation in the affected area using annual MSL data. In addition to having a longer set of data available, Savage and Plafker (1991) corrected these data with an average of detrended, concurrent sea level fluctuations observed at three stations in SE Alaska (Sitka, Juneau and

Ketchikan). This approach removes oceanographic-related variations in the sea level records, and was found to reduce the scatter in sea level records at stations from Yakutat to Sand Point. At all seven sites in the 1964 near-field, vertical land motion was found to be recovering the coseismic offset, but with a much longer time scale (perhaps ~100 yrs) than has been found for postseismic deformation in Japan (~2 yrs; Kato, 1983). Cohen and Freymueller (2001) re-examined this data set with 10 years additional data. A significant result was the determination of non-linear trends in vertical crustal motion at Kodiak, Cordova and possibly Valdez.

Strategy

The challenge in using sea level data to measure crustal motion is that of comparing one dynamic surface or reference plane with another. The sea surface exhibits extreme variability at high-frequencies (e.g., semi-diurnal tidal amplitudes are as much as 10 meters in some areas covered by this study), along with small long-term changes (a global average sea level rise of ~1.5 mm yr-1 over the last century [Douglas, 1997; Tamisiea et al., 2001]). On the other hand, solid earth vertical motion rarely exceeds 10 mm yr-1 and is usually devoid of high frequency variability, with the exception of coseismic offsets, which exceeded 10 meters in the 1964 rupture zone (Plafker, 1971). Vertical crustal motion can have long period variability due to factors such as postseismic relaxation, passive margin subsidence and glacial isostatic adjustment (GIA).

Two basic approaches generally have been employed to counter the high frequency variability of the sea surface in order to obtain a stable reference plane: (1) long term averaging of sea level data and, (2) various schemes to identify and remove oceanographic "noise". Although sea level averaged over yearly or longer periods will cancel most of the high frequency variability, long-term averages cannot resolve rapid datum changes, such as coseismic offsets. Because the signal we are interested in has both high frequency components and long period variability, we use monthly MSL analysis. For many of the older records, this sampling frequency represents a practical

limit, as sea level data averaged over periods less than a month can be difficult to obtain. The primary goal of our analysis is to remove sea level variations due to oceanographic and atmospheric effects, and to do so without smoothing the records with long-term averages.

Data

The National Ocean Service (NOS) in Alaska and the Marine Environmental Data Service in Canada collected the sea level data used in this study. These data are typically collected from an instrument whose reference plane stability is verified by annual leveling surveys, thereby insuring a consistent datum between sea level measurements and the land level. With long-term records, this issue is complicated by changes in instrument location and, in the case of the 1964 earthquake, destruction of the instrument platforms by tsunamis. The data providers have corrected most of the records for these issues; in the case of Kodiak we have incorporated leveling data and simultaneous water level observations to link together records from tide gauges at two different locations (Cohen and Freymueller, 2001). We have not attempted to recover the large coseismic datum shifts at Seward and Kodiak associated with the 1964 earthquake, but instead break these records at the time of the earthquake (for coseismic offsets, see Plafker, 1971; Brown et al., 1977).

The record lengths for each station are summarized in Table 1. Almost all of the stations have data gaps of variable length within their records. In addition to periods of malfunctioning equipment, these data gaps may represent periods of datum instability. In a few instances this instability is a signal we are interested in, such as the immediate postseismic behavior following the 1964 earthquake. In these instances a much more continuous complete record of mid-tide level (MTL) is sometimes available. MTL is the mean of all high and low water levels (the peaks of a tidal series), while MSL is simply the mean of all water level readings. At Anchorage and Kodiak, the MSL records are not available for several years following the 1964 Great

Alaskan earthquake. At Cordova, there is a gap of two years in the MSL record, 1968-1969. The MTL records for these stations were used in our analysis.

Sea Level Analysis

Our analysis differs from that of previous uplift studies using sea level records in the Gulf of Alaska by (1) using monthly mean sea levels rather than annual means, (2) correcting each station for barometric variations and seasonal variations, and (3) using a much larger set of stations to estimate common-mode oceanographic variations. Figure 2 illustrates our three-step analysis process using the Yakutat and Skagway records as examples. Of primary concern is the precise removal of all signals within these records that are not related to crustal motion.

Barometric pressure corrections

Starting with the raw monthly mean sea levels ($MMSL_i$, where the subscript refers to the ith month in a multiple year record), the first step is to correct for barometric pressure variations. Monthly mean sea level air pressure values (P_i) were found for each tide gauge site from the NCEP reanalysis of climatological data, 1949-2001 (NOAA-CIRES Climate Diagnostics Center, Boulder, Colorado, USA; http://www.cdc.noaa.gov). Records from before 1949 are not corrected for barometric pressure variations. At each station, we calculated the mean barometric pressure ($\overline{P}$) over the 52-year period. Sea level variations due to pressure variations about $\overline{P}$ were then removed, assuming 1.0 cm sea level change per mbar, to find pressure corrected sea levels (PC_i).

$$PC_i = MMSL_i - 1.0\frac{cm}{mbar} * \left(P_i - \overline{P}\right) \qquad (1)$$

Other authors have found it more effective to use a larger rate than -10 mm/mbar to remove all of the correlated sea level and air-pressure variations, possibly due to correlation of effects such as wind loading with barometric pressure variations (Trupin and Wahr, 1990; Davis et al., 1999). However, we found that -10 mm/mbar provided

the greatest RMS noise reduction about the long-term trends for the stations studied here.

Removal of seasonal signal

All of the stations exhibit seasonal sea level variations to a variable degree. This seasonal signal is due to a combination of several effects, including seasonal variations in air and water temperature, predominant wind direction, and fresh water influx resulting in local density variations. Particularly strong seasonal signals are evident at Anchorage and Skagway; both of these sites lie at the head of long inlets. In general, of the sites we studied, those closer to the open ocean appeared to have weaker seasonal signals. To correct the long-term records for each of the specific local effects that cause these seasonal signals would require detailed analysis involving wind, temperature, precipitation and runoff data that are either difficult to obtain or do not exist.

Instead, we find an average seasonal signal at each station, and remove this signal from the record (Kato, 1983). To calculate each station's monthly deviation D_i from the overall trend, we run a high pass filter (Chebyschev type II, 10 yr. cut off) on each station's pressure corrected record, producing the equivalent of monthly MSL deviations from a smooth ten-year trend. The average deviation of each month ($\overline{D_m}$; m=1 to 12), over the entire record of this particular month (N years of data for month m) is calculated:

$$\overline{D_m} = \sum_{j=0}^{N-1} \frac{D_m}{N} \qquad (2)$$

These average monthly deviations are subtracted from each matching month throughout the record, thus finding "seasonally corrected" sea levels (SC_i):

$$SC_{(j-1)*12+m} = PC_{(j-1)*12+m} - \overline{D_m} \qquad (3)$$

for m=1 to 12 and j=1 to N. It should be noted that there is no analogous step for analysis of annual MSL data, although in the long-term records data gaps of one to several months are common. Annual means calculated over these gaps will be weighted by the seasonal signal of the remaining points, introducing a bias for any year without a complete set of monthly means.

Removal of common mode oceanographic signal

The standard procedure to remove sea level variations caused by large-scale oceanographic variations is as follows. A linear sea level trend is found for each stable, high quality site within the study area, and monthly residuals about these trends are tabulated ($[R_s]_i$, where s = site and i = month). These residual series are then combined to form an average residual for each month. This monthly residual average is taken to represent regional sea level variations that are common to all sites (Kato, 1983; Davis et al, 1999; Cohen and Freymueller, 2001), and is called the "oceanographic correction" (OC). The stations used to form this average monthly residual are called "control stations". At each station, for every month i, OC_i is subtracted from SC_i to find sea level fully corrected by our analysis (Hi). Each Hi is calculated with an OC_i found over a control station subset s=1 to k as follows:

$$H_i = SC_i - OC_i \qquad \text{where} \qquad OC_i = \frac{\left[\sum_{s=1}^{k} R_s\right]_i}{k} \qquad (4)$$

The specific control stations and their total number (k) may vary from month to month depending on data availability. We restrict the computation of H_i to only those months when three or more control stations' residuals are included in OC_i. This requirement limits our complete analysis to 1937 and later.

The above procedure makes a limiting assumption that the MSL trends are linear at all the sites used to compute the OC. Because of known instabilities and non-linear trends in many of the subduction zone sites, previous sea level studies in this region have restricted the computation of the OC to include only residuals $[R_s]_i$ from

three sites in SE Alaska (Juneau, Sitka and Ketchikan) which have linear sea level trends (Savage and Plafker, 1991; Cohen and Freymueller, 2001). This approach is less than ideal, as the computation of the OC with only a few stations occasionally introduces strong local sea level variations that might be evident at one station only. An average of $[R_s]_i$ computed over many stations will damp out individual station variations, and better resolve those variations common to all sites.

Consequently, to strengthen the OC, we use an analysis developed by Kato (1983) to incorporate residuals from non-linear subduction zone stations. Instead of finding residuals about a linear trend, a low-pass filter is used to approximate the long-term trend. The residuals $[R_s]_i$ are then calculated about this trend. Furthermore, we have included in our analysis two additional stations (Queen Charlotte City and Prince Rupert). Together, these additions allow the number of control stations to be increased from 3 as used by Savage and Plafker (1991) and Cohen and Freymueller (2001) to 11 (present study).

For stations in the strike-slip regime, a Chebyschev type II filter with a 50 yr cutoff and 20 dB down in the stop band was used to approximate the long-term trend. The long period of the cutoff frequency is appropriate for these predominantly linear stations. This cut-off frequency allows for long period oceanographic effects to be included in the OC, such as the lunar nodal tide which has an 18.6 yr frequency and an amplitude up to ~50 mm (Trupin and Wahr, 1990). For stations within or near the subduction zone (all stations north of Skagway), such a long period cutoff is not allowable as the solid earth uplift rates may vary on a faster time scale. Here, we used the same filter to estimate trends as in the strike-slip regime, but with a cutoff of 10 yr (Kato, 1983).

Coseismic offsets

Sudden jumps or datum shifts, such as those during great earthquakes, are not removed by low-pass filtering. The long-term trend approximated by low-pass filtering will gradually span these sudden shifts, and the non-physical residuals from this poorly approximated trend will then contaminate the OC. To correct this situation,

we break certain records into separate pieces. The 1964 Great Alaskan Eq (M_w 9.2, Kanimori, 1977) caused uplift of roughly 1.0 m at Seward and 1.2 m at Kodiak (Plafker, 1971), and the records at these stations are treated separately before and after the earthquake. In the strike-slip regime, there have been three great earthquakes this century: 1958 Fairweather Fault, M_w = 8.2 (Kanimori, 1977), 1949 Queen Charlotte Fault, M_s=8.1 (Kanimori. 1977), and 1972 Sitka, M_w=7.6 (Schell and Ruff, 1989). In general, however, strike-slip events result in small vertical displacements in the far-field, and in the analysis presented here all records have been treated as continuous across these events.

Final selection of control stations

With the earthquake-correlated datum shifts identified, and the records separated at these times, all stations from the entire study area that have long-term and relatively clean records can contribute their residuals to the OC calculation. We did not include several records in the OC for the following reasons. The Skagway record has a higher than average noise level, perhaps due to a particularly strong seasonal signal. Yakutat has a complicated non-linear trend, and may have several minor offsets (see Discussion). Anchorage has a noisy and possibly oscillatory record (Brown et al., 1977, Savage and Plafker, 1991). Seward and Seldovia exhibit differing uplift behavior before and after 1972.5 (see Discussion) and are included in the OC after 1972.5 (Seward is included in the OC prior to 1964 as well). Nikiski's record has a large data gap, and the existing data are too brief to be included. Kodiak is included before the 1964 earthquake and after a period of extremely rapid uplift from 1964-1968. A list of all the stations used in the OC is found in Table 1.

Results

The sea level analysis outlined above was applied to the 15 stations within our study area. We have calculated relative sea level rates for these sites and determined some to be non-linear; the results of our linear/non-linear rates analysis are presented in Table 2. These records have been adjusted with the approximate local effect of

global sea level rise (1.0 mm/yr), as discussed below, resulting in the vertical crustal motion records presented in Figures 3 and 4.

Measurement error

An exact value for the measurement error associated with monthly mean sea levels ($MMSL_i$) is difficult to determine. This is not so much due to the difficulty in accurately measuring individual water levels, rather it is the accuracy of the mean reference plane obtained from the highly variable sea surface that is of concern. This accuracy can only be found directly from the data and not from independent error estimation. We employed a high-pass filter with a 5 yr cutoff to determine the variance of each of the records, both of the raw data and the fully corrected sea level H_i. The reduction of variance (σ^2), averaged over all the control stations, is a factor of 18.5 between the raw and fully corrected sea level records. In the analysis that follows, we will use a constant MMSL measurement error estimated from the standard deviation about the 5 yr high-pass filtered records from each of the control stations.

The average standard deviation of corrected sea level records at the 11 control stations is 20.9 mm, with two stations having significantly smaller values: Sitka 12.5 mm and Cordova 14.1 mm. These two sites may represent the best case for our analysis, with both sites being close to the open ocean and in the center of the distribution of control stations. We might expect Yakutat to have a similarly low σ, but it is 19.8 mm, possibly because it may contain several small offsets that are admitted by the 5 yr high-pass filter.

Constant and time-dependent rate analysis

To determine relative sea level rates at each station, each MMSL record was fit with linear and time-dependent regressions. To identify statistically-valid time-dependence, we assessed the improvement in fit of a time-dependent regression over that of a linear regression. The statistical significance of each regression was evaluated using the F-test (Zhao et al., 1995) and reduced χ^2. We tested logarithmic and exponential forms, motivated by glacial isostatic models, as well as by postseismic afterslip and viscoelastic models. At none of the stations was there significant

improvement in fit with these forms over that of a quadratic regression, and therefore quadratic regressions were used for our constant vs. time-dependent rate evaluations.

To compare one model with another, we compute an F ratio (Zhao et al., 1995; Cohen and Freymueller, 2001). Eleven of the records passed the F-test at the 0.1% level (Table 2) indicating that the quadratic model provides a better fit than a linear one. This conclusion includes a few sites that would seem to be better represented by a linear model, such as Queen Charlotte City. However, another test, calculated using $\ln_e(\chi^2_{linear} / \chi^2_{quadratic})$, indicates that a few of the records passing the F-test are perhaps not better fit by a quadratic regression. Based on the combined results of the F-test and improvement in reduced χ^2, we find that a quadratic model is an improvement over a linear one for Yakutat, Cordova, Valdez, Seward, Nikiski, Anchorage and Kodiak (Table 2). Perhaps the most noticeable result of our time-dependent analysis is that our model comparisons indicate two distinct groups. Stations that pass our criteria for non-linear trends tend to pass strongly, while the remaining stations either weakly pass one test only or fail both. The results of our preferred model for each site are presented in Table 2. The regressions and 95% confidence intervals for these models are plotted as dashed lines in Figures 3 and 4.

The criteria used here are rather stringent; we require that the quadratic models pass the F-test at the 0.1% level (F-ratio > 10.8; Beyer, 1991) and show an improvement in χ^2 of >10%. Our motivation for such stringent criteria is to compensate for the possibility that temporal correlations may be introduced by our analysis. We note that in our statistical tests we invoke the assumption that each corrected tidal series is composed of independent variables, and that our models predict a functional relationship between measured and model-dependent variables. This assumption of measured independent variables is not strictly valid, as we have already applied a model for removing the seasonal, oceanographic and atmospheric signals.

In addition to comparisons between linear and quadratic models for all the sites, we considered further models at Yakutat and Kodiak. The Yakutat record has an

obvious double curvature (Fig. 3), and a cubic model was found to be a significant improvement over the already justified quadratic fit (Table 2). We also tested a linear regression separated at 1953 and 1979, with three independent segments. This model further improved the fit; although the number of model parameters is now six (three slopes and intercepts), the increase easily passed the F-test (Table 2). The final rate presented for Yakutat in Table 3 is the slope of the last of these three linear segments. Within this segment, we have removed an abrupt shift in January 1993 that may be associated with an instrument change that occurred then (see Yakutat discussion, below).

As discussed earlier and also by Cohen and Freymueller (2001), the post-1964 Kodiak record is composed of data from two sites, St. Paul Harbor (1967 – 1982) and Women's Bay (1985 to present). We tested a model composed of two independent linear regressions separated at the time of the gauge relocation. We found that a quadratic model over the entire period resulted in a significantly better fit than either a single- or bi-linear regression, and therefore agree with Cohen and Freymueller (2001) that the time-dependency of the complete uplift record at Kodiak post-1964 is unlikely to be due to differential uplift at the two sites.

Relative sea level trends and uplift rates

To use relative sea level records as a proxy for vertical crustal motion, one must correct for concurrent rate of change in the geoid (sea surface). Globally, sea surface is rising an average of ~1.5 mm/yr (Douglas, 1997; Tamisiea et al., 2001), but locally this value will differ near changes in surface mass, e.g. melting glaciers and ice sheets (Woodward, 1888; Farrell and Clark, 1976; Mitrovica et al., 2001; Tamisiea et al., 2001). Glaciers and icefields in Alaska and neighboring Canada have lost an average of 42 Gt yr^{-1} from the mid-1950's to the mid-1990's (Arendt et al., 2002). To find the associated and site-specific geoid changes at each of our tide stations would require sophisticated calculations incorporating detailed geometry of the surface mass changes. Instead, we use the results of a study of non-eustatic sea level redistributions by Tamisiea et al. (2001) to estimate the effect of sea surface rise on our study area. In

addition to models of ice mass changes in Greenland and Antarctica, Tamisiea et al. (2001) considered ice mass fluctuations in a suite of mountain glaciers (Meier, 1984) that includes an approximation of Alaskan ice mass changes that agrees reasonably well with recent measurements (Arendt et al., 2002). The rate of sea surface rise predicted for our study area is ~1.0 mm/yr (Tamisiea et al., 2001). Although the formal error estimate for this value is <1 mm/yr, we conservatively assign an error of ±1 mm/yr due to the uncertainty involved with using this value to convert relative sea level trends to uplift records.

In addition to the effect of surface mass changes, motion of the earth's mantle can also cause geoid variations. Such an effect may be present in our study area from viscoelastic postseismic relaxation (Wahr and Wyss, 1980; Pollitz et al., 2001) and glacial isostatic adjustment. Measuring or modeling the site-specific magnitude of the related geoid change is outside the scope of our present study, and we do not adjust the uplift records for either.

Global glacial isostatic adjustment

Global glacial isostatic adjustment (GIA) models are poorly resolved for our study area due to limited knowledge of last glacial maximum ice-sheet history here (e.g., Tushingham and Peltier, 1991). To the south of our study area in the northern Cascadia subduction zone, James et al. (2000) constructed a regional post-glacial rebound model with a detailed Cordilleran ice sheet history. This model predicts present-day uplift rates less than 0.1 mm/yr, lower than ICE-3G predictions by an order of magnitude (Tushingham and Peltier, 1991). Owing to this uncertainty, we do not separate out any estimates for GIA from the uplift records. Moreover, ICE-3G uplift predictions throughout our study area are <1 mm/yr, a small fraction of the uplift rates at most of the stations here.

Present day uplift rate predictions

Using the results of the constant and time-dependent analysis above, we calculated the relative sea level rate for each site predicted by the preferred model for the year 2000. We estimate the uplift rate for each site by subtracting the estimated

rate of change in the geoid (Table 3). The errors listed are the quadrature sum of the MSL trend error (site dependent) and the geoid rate error (± 1 mm/yr). For all sites but Seward, Nikiski, and Anchorage the MSL trend errors are insignificant compared to the geoid rate error.

Discussion

Southern stations

The southernmost stations in the strike-slip regime (Queen Charlotte City, Prince Rupert, Ketchikan and Sitka) all show linear, slow uplift trends (Fig. 3). Prince Rupert and Ketchikan both have uplift rates close to zero. Queen Charlotte City is within 60-70 km of the Pacific Plate transform boundary at this latitude, and the small observed uplift might be associated with this close proximity. With the relatively small uplift trends at these southern three stations, glacial isostatic adjustment following the last glacial maximum may be significant. Sitka exhibits a faster uplift rate that represents the southern periphery of the SE Alaska uplift area.

Southeast Alaska uplift region

The next three stations to the north (Juneau, Skagway and Yakutat) all have extremely rapid uplift rates. There have been several suggestions for the cause of rapid uplift in this region: (1) isostatic rebound following the rapid deglaciation of Glacier Bay (Hicks and Shofnos, 1965), (2) both this and ongoing regional deglaciation (Clark, 1977), (3) regional tectonic stress (Horner, 1983; Barnes 1984) or (4) some combination of these (Hudson et al., 1982).

Recent measurements of relative plate motion have found predominantly strike slip motion along the Pacific-North American plate boundary to the south of Yakutat, implying that any compressive motion must occur offshore on the Transition Zone fault (Fletcher and Freymueller, 1999; Larsen et al., 2001). These observations suggest that tectonic deformation is likely a minor component of the total uplift rates, and we will concentrate here on testing isostatic rebound models. Our approach is to create a model of surface load changes from direct and indirect observations of ice mass

changes, and calculate the resultant uplift. Comparisons between these rate predictions and observed rates are then used to evaluate the models. We use the most recent rate at Yakutat (1979 to present, with an offset at 1993 removed; see discussion below) under the assumption that earlier in the record the uplift there was modulated by tectonics. Our goal with the modeling efforts presented here is not to precisely constrain material properties of the crust and mantle, but rather to demonstrate that realistic models of glacial unloading, coupled with an established Earth model, can indeed produce uplift of the magnitude observed in southeast Alaska.

The Earth model used for these calculations is described in detail by Ivins and James (1999), and is a flat-Earth, self-gravitating, incompressible two-layer model with an elastic lithosphere and a viscoelastic mantle half-space. The geometry and material parameters of this model are shown in Figure 5. This simple model is sufficient to evaluate the effects of regional ice load variations over $< 20°$ of Earth surface (Ivins and James, 1999). For simplicity, we limited our calculations to an Earth model with 40 km thick crust (Bechtel et al., 1990). We will consider load variations related to 1) ongoing ice thickness changes in Alaska and neighboring Canada (Arendt et al., 2002), 2) a ~1000 yr regional ice thickness history based on dendrochronology and geomorphology studies of glacial advance and retreat (Wiles et al., 1999), and 3) the most recent cycle of advance and retreat of the tidewater glaciers in Glacier Bay (Goodwin, 1988). We do not consider ice mass changes older than 1000 yrs, nor any ocean loading due to sea level changes.

The present-day ice mass loss of Alaskan and neighboring Canadian glaciers is estimated at 96±35 Gt/yr from direct measurements of ice thickness changes (Arendt et al., 2002). The associated ice thickness changes vary strongly with altitude, and the greatest ice loss occurs at the lowest elevations. To create a load model based on these observations, we begin with a 3-arc second (90 m resolution) digital elevation model of the ice covered area, and find the ice thickness changes at each node using an average thickness change vs. elevation profile (Fig. 2b of Arendt et al., 2002, "All"). Because this is a regional average profile, we do not account for the often-large

differences in mass changes specific to tidewater glaciers. To facilitate computation of the Earth's isostatic response to this load model, we average the load changes over a 20 km x 20 km grid. The grid dimensions are chosen to be about half of the effective elastic crustal thickness here (Bechtel et al., 1990).

We first calculate the elastic isostatic response to this load model ($\eta \approx \infty$). We find that the elastic uplift rates are only ~10-30% of the observed rates at Sitka, Juneau, Skagway and Yakutat (Table 4). The uplift error estimates in Table 4 are calculated from models using the upper (131 Gt/yr) and lower (61 Gt/yr) limits of the current ice mass loss rate (Arendt et al., 2002).

To perform a viscoelastic calculation, a history of ice load changes is required. The Little Ice Age (LIA) glaciation was the largest Holocene expansion in Alaska, and occurred in three phases between ~1200 and 1900 AD that were synchronous across much of Alaska (Wiles et al., 1999; Calkin et al., 2001). Our interpretation of the associated changes in ice mass through the last 1000 yrs is shown in Figure 6. The results of Arendt et al. (2002) are used from 1955 to the present. This load model includes the ongoing rate of load change from 1995 to the present day, and the elastic uplift results of the previous calculation are retained in the following predictions. The rate of load change for 1900 to 1955 is assumed to be the same as the 1955-1995 rate (Arendt et al., 2002). Prior to 1900, the maxima and minima are simple estimates relative to the 1900 peak. Again, this is a regional average and it does not account for present or past mass changes of tidewater glaciers. For sensitivity analysis, we used the error limits on the volume change rates (Arendt et al., 2002) to extrapolate minimum and maximum load history estimates (Fig. 6).

Little or no uplift was predicted with this load model using mantle viscosities similar to those found in Fennoscandia ($\eta \approx 10^{21}$ Pa s; e.g. Milne et al., 2001). Earth models with viscosities $>10^{20}$ Pa s primarily respond at the present day, if at all, to the growth phase of the load history used here, and would not viscously respond to the retreat phase until the future. In contrast to the high viscosity model results, significant present-day uplift rates are obtained with low mantle viscosities ($\eta \approx 2 \times 10^{19}$ - 5×10^{19} Pa

s). Results for our best-fit model with $\eta=3.5x10^{19}$ Pa s are presented in Table 4, along with a range of uplift rates from models incorporating the maximum and minimum load histories of Fig. 6. Although these predictions are close to the observed rates at Sitka and Yakutat, the disagreement with the observed rates is much larger at Skagway and Juneau. This suggests a deficiency in the spatial distribution of our load model, such as the rapid retreat of Glacier Bay ca. 1750–1930 AD.

To create a load model of the most recent cycle of advance and retreat in Glacier Bay, we used an estimate of the above sea-level ice mass at the ~1750 maximum ice extent. Trimlines and lateral moraines provide indications of post-1750 ice thickness changes within Glacier Bay (Field, 1947; Clague and Evans, 1993). We used present-day tidewater glacier analogs to estimate ice elevation profiles within Glacier Bay using these thickness changes, extending ice coverage out to the 1750 terminus position. Comparing these ice profiles with a digital elevation model, we find that Glacier Bay lost a minimum of 2600 km^3 of ice from 1750 to ~1950 AD, at an average unloading rate of $\sim 1.2x10^{13}$ kg/yr. This load change is partitioned into the five disk loads shown in Figure 7, and the load history of these disks, based on Goodwin (1988), is shown in the inset.

When the Glacier Bay load model is combined with the regional LIA load model, the uplift rates predicted with a low viscosity Earth model closely match the observations at Juneau and Skagway, but overshoot the observations at Sitka and Yakutat by ~3 mm/yr (Table 4, limits are from varying the Glacier Bay load model by ±25%, combined with range of rates from the regional LIA load model). Our results indicate that the significance of the Glacier Bay load relative to the LIA regional load is ~37% at Juneau and ~47% at Skagway, while perhaps it is only a minor contribution at Sitka and Yakutat. The regional pattern of uplift we predict (Figure 7) is in reasonable agreement with that presented by Hicks and Shofnos (1965) from temporary tide gauge measurements.

With the long history of active tectonics and nearby volcanism of the region, a low upper mantle viscosity is conceivable. Southeast Alaska has been subjected to

dextral strike-slip motion along the North American – Pacific Plate boundary, in a configuration similar to the present day situation, for ~25 Myrs (Plafker, 1987). Quaternary volcanism is found at Sitka (Mt. Edgecombe) and ~200 km to the north of Yakutat (Wrangell Mts.). Elsewhere along the North American – Pacific Plate boundary, studies of postseismic deformation in southern California (Pollitz et al., 2001) and glacial isostasy in southern British Columbia (Clague and James, 2002) have indicated upper mantle viscosities on the order of $1x10^{19}$ Pa s. The relatively brief load history considered here is appropriate for Earth models with such low viscosities, as the response to earlier load changes will have largely been completed by the present. With these considerations, we regard the modeling results as realistic and plausible, and consider the rapid uplift observed in much of southeast Alaska to be attributable to viscoelastic postglacial rebound following the LIA and the tidewater retreat of Glacier Bay.

Yakutat

In addition to the high uplift rate, there is a strong degree of non-linearity in the record at Yakutat. Here, in the transition zone between strike-slip and subduction, there can be no question of tectonic influences. Yakutat lies on the Yakutat Block, an allochthonous terrane actively colliding with North America (Plafker et al., 1994). The magnitude of horizontal velocity at Yakutat is almost equal to the full Pacific plate velocity relative to North America (Fletcher and Freymueller, 1999). About 110 km northwest of Yakutat the plate boundary changes from strike-slip motion to convergence in a complex transition of steeply-dipping stacked thrust-faults (Bruns and Schwab, 1983) with a convergence rate twice that of the Himalaya (J. Freymueller, unpublished GPS data).

The Yakutat record shows a complex non-linear uplift pattern, with a period of slower uplift from roughly 1953 to 1979 (Fig. 3). Before 1953 the uplift rate at Yakutat was 7.8 ± 0.5 mm/yr, nearly twice the linear uplift rate of 4.2 ± 0.2 mm/yr from 1953 to 1979. The variance about a linear trend between 1953 and 1979 is larger than elsewhere in the record, with two possible shifts at 1958 and 1962. The former

may be coseismic uplift on the order of 2-5 cm at the time of the 1958 Fairweather Fault M_s=7.9 earthquake, but is not distinctly above the variance of the record here. The uplift record does not show a significant coseismic signal at the time of the 1964 Great Alaskan earthquake, which initiated ~200 km to the northwest in Prince William Sound (PWS).

After the 1979 St. Elias earthquake (M_w = 7.4; Lahr and Plafker, 1980), the apparent linear uplift rate at Yakutat is 11.0 ± 0.3 mm/yr. The change in uplift rate in 1979 is the most prominent feature in the Yakutat record, and some association with the 1979 St Elias earthquake seems likely. However, a postseismic response of greater than 20 yrs for an earthquake of this magnitude is markedly different than observations elsewhere. Subduction zone earthquakes of similar magnitude in Japan have postseismic responses lasting ~2 yr (Kato, 1983), although in the case of Yakutat the tide gauge resides on the downgoing plate rather than on the overriding plate as is the case in Japan. An alternate explanation for the change in rate at 1979 may be related to the rapid succession of large regional earthquakes (1958, 1964 and 1979). Rather than the post-1979 rate representing lingering effects of that event, it may have returned to a "normal" rate after a period of anomalous tectonic strain between ~1953 and 1979.

In the time period after 1979, the most distinct deviations are a 4 – 5 year period with decreased uplift rate ending in early 1988, followed immediately by ~1 year of faster than normal uplift. Also there is an approximately 35 mm shift downward in January 1994. The former is coincident with the three main events of the 1987-88 Gulf of Alaska earthquake sequence (11/17/87 M_w=7.2, 11/30/87 M_w=7.8, 3/6/88 M_w=7.7, Pegler and Das, 1996). This sequence produced a 13 ± 3 cm downward coseismic offset at Cape Yakataga (Sauber et. al 1993). The 1994 shift is uncorrelated with any nearby seismicity.

The 1994 shift occurs over one measurement interval only, and the record before and after the shift appears linear. These observations suggest the possibility of a reference level problem rather than crustal motion. We analyzed Yakutat records

available from the Permanent Service for Mean Sea Level (PSMSL; http://www.nbi.ac.uk/psmsl) in addition to sea level records directly from NOS. Once fully corrected by our analysis, we found that the Yakutat record from PSMSL also had a shift of the same magnitude, but this shift occurs one year earlier in January 1993. This date marks the change of instruments at Yakutat from a float/well system to a NOS next generation water level measuring system. Although the exact source of the differences between the NOS and PSMSL Yakutat records is unclear, we suspect that this 35 mm shift is related to the instrument change. With the 35 mm shift removed from the uplift record, we find a linear uplift rate between 1979 and 2001 of 13.7 ± 0.2 mm/yr (reduced χ^2=1.0). If such treatment of the record is correct, the change in uplift rate in 1979 is even more pronounced.

1964 Earthquake near-field

The 1964 Great Alaskan Earthquake ruptured two distinct asperities, located beneath Prince William Sound (PWS) and Kodiak Island (Christensen and Beck, 1994; Holdahl and Sauber, 1994). The tide gauge stations in this region (Fig. 1) are distributed along the northeastern edge of the PWS asperity (in order of increasing distance from the megathrust: Cordova, Valdez and Seward), to the west of the PWS asperity (Anchorage), in the region between the PWS and Kodiak asperities (Nikiski and Seldovia), and within the Kodiak asperity (Kodiak). Sand Point, the furthest west station included in our analysis, lies outside of the 1964 near-field and exhibits nearly zero uplift over the entire record (Fig. 4; Table 2). Geographic correlation of uplift rates to the PWS asperity is marked at stations within the 1964 near-field. Very rapid uplift rates are found outside of PWS, while uplift rates are much slower within PWS (Fig. 4). Anchorage is an exception; although west of the PWS asperity, the average uplift rate found over its entire record is relatively small.

At Kodiak, we present an uplift record based on the MTL record that includes the period immediately following the 1964 earthquake (Fig. 4). In the 3.5 yr period from mid-1964 to 1968, we find extremely rapid uplift totaling 470 ± 80 mm (130 ± 20 mm/yr). After 1968 the rate decreased, and we find that the uplift trend since this

time is non-linear, in agreement with Cohen and Freymueller (2001). For the quadratic analysis presented in Table 2, we included data from 1968 onward, on the basis that prior to this a different mechanism of postseismic relaxation was taking place.

In the early record at Anchorage, between 1964 and mid-1972, there is an oscillation with a period of about 5 years. Other authors have speculated on this feature and suggested that it is possibly due to fault creep events propagating slowly along the plate interface (Brown et al., 1977; Savage and Plafker, 1991). Cohen and Freymueller (2001) noted that this feature might have been enhanced in previous analyses through biased annual means calculated with less than complete data sets. Our monthly-MSL based analysis avoids this possible biasing. NOS conducted regular leveling surveys between the instrument and the local benchmark network and found no evidence of platform instabilities that could create such a signal (NOS, pers. comm.). Furthermore, the uplift records show similar features at Seward and Seldovia over the same time period (Fig. 4), suggesting that the phenomena that caused this oscillatory signal affected a large portion of the 1964 earthquake near-field. The magnitude of the oscillation at Anchorage is 340 ± 50 mm over the first 2.4 years of the record here, corresponding to an uplift rate of 140 ± 20 mm/yr over this period. This rate is very similar to the immediate postseismic rate found at Kodiak. Cohen (1998) analyzed leveling surveys along Turnagain Arm between Anchorage and Portage, conducted during the first year of tide gauge operation at Anchorage. He found a maximum uplift, relative to the Anchorage tide gauge benchmark, of ~100 mm. When combined with our results, we find a maximum absolute uplift of 240 mm between May 1964 and May 1965 along the Turnagain Arm leveling profile.

De-trended Post-1964 uplift records

To illuminate better the postseismic responses at Anchorage, Seward, Seldovia, Valdez and Cordova, we have removed the linear uplift trends from these records, and plotted the residual signals in Figure 8. A simultaneous change in the uplift trends at Seldovia, Anchorage and Seward is apparent at 1972.5 (dotted line, Fig. 8). In the period before this change, Seward exhibits an oscillatory behavior

similar to Anchorage, but with approximately one-half to one-third the amplitude. Seldovia also appears to have an oscillatory signal during this period, although at Seldovia the first peak of the oscillation is smaller than the second. The coincident peak at 1972.5 is strongly evident at Seldovia, Seward and Anchorage. To a much lesser extent it may also occur at Cordova, but only slightly above the noise level.

After the 1972.5 peak, four stations (Anchorage, Seward, Valdez and Cordova) exhibit remarkably similar behavior- that of a smooth quadratic trend in uplift rates. The analysis presented in Table 2 for these stations (as well as for Seldovia) is limited to data from 1972.5 onward; prior to this time we believe the region was undergoing a different response. Kodiak and Nikiski are also in close agreement with each other, while Seldovia is the only station affected by the 1964 earthquake that does not have significant non-linear behavior after 1972.5 (Table 2).

This pattern in the data suggests that there were two and perhaps three phases in the postseismic deformation following the 1964 earthquake. The initial phase lasted ~3 years, and was characterized by rapid uplift (~130 mm/yr) at Kodiak and Anchorage, and even more rapid uplift (~240 mm/yr) along Turnagain Arm. A possible second phase was absent at Kodiak but clearly seen around Prince William Sound for another ~5 years, and was characterized by oscillatory vertical motion at sites around the Prince William Sound asperity. The final phase consists of slowly changing uplift rates over the entire area.

Zweck et al. (2002) compared models of postseismic deformation averaged over the ~35 yr since the earthquake to models averaged over the last 7 yr. The major difference between the two time periods is that the 35 yr average model includes rapid afterslip immediately downdip of the 1964 rupture zone that is absent over the last few years. The initial phase of postseismic deformation is plausibly caused by afterslip immediately downdip of the coseismic rupture. This interpretation suggests that the afterslip had decayed within 3-4 years, a similar timescale to that observed for the total postseismic deformation after many other subduction zone earthquakes. The initial phase was followed by a few years of oscillatory motion around Prince William

Sound, which may be caused by propagating slip pulses as suggested earlier by Brown et al. (1977) and Savage and Plafker (1991). An intriguing slip event lasting 3-4 years was observed from 1998-2001 in the Anchorage area (Freymueller et al., 2001). Although it produced deformation much smaller than the oscillatory vertical motion observed in the late 60s and early 70s, the recent event shows that this area is characterized by complex slip behavior, and lends credence to the interpretations that the early postseismic motion of the Anchorage tide gauge is signal rather than noise. The long-lived, slowly varying component of postseismic deformation observed after 1972 may be related to some combination of decaying afterslip and viscoelastic relaxation. The tide gauge data are inadequate to distinguish between the two possibilities.

Conclusions

We have presented uplift records derived from sea level records at 15 tide gauge stations along the northern North America-Pacific plate boundary. Our analysis is based on monthly mean sea levels corrected for barometric pressure variations; this differs from previous studies in this region, which have been based on annual mean sea levels. In addition to the increased temporal resolution, this approach allows for improved corrections of local seasonal variations in sea level, and avoids biasing that can occur when annual sea levels are calculated over the data gaps common to the long-term records of this region. This analysis allows us to use a larger number of stations in the determination of common mode oceanographic effects. The increased accuracy of the reduced uplift records enables the statistical determination of uplift rates and trends along this plate boundary.

A clear pattern of vertical crustal motions emerges from this analysis. The stations along the strike-slip portion of the plate boundary and away from regions of major glacial unloading exhibit small rates of uplift with linear trends. Where recent glacial unloading has been large, and still is, the records show extremely rapid uplift, also with linear trends. In the subduction zone the vertical crustal motions are

predominantly non-linear, with significant shifts superimposed on the records at the times of major earthquakes.

Extremely rapid uplift rates are found at Juneau, Skagway and Yakutat. Realistic glacial unloading models, based on direct and indirect observations of glacial mass changes, indicate that the rapid uplift in southeast Alaska can be solely attributed to glacial isostatic rebound. In particular, 1) viscoelastic uplift dominates over strictly elastic uplift, 2) a low upper mantle viscosity ($2x10^{19}$ - $5x10^{19}$ Pa s) is required, and 3) isostasy related to the last tidewater cycle of Glacier Bay drives a large fraction of the uplift rates at Skagway and Juneau. In addition to rapid uplift, complex non-linear uplift behavior is found at Yakutat, most noticeably a change in uplift rate at the time of the 1979 St. Elias Earthquake.

All but one of the tide gauges within the 1964 Great Alaskan earthquake near-field show non-linear uplift rates. We resolve an oscillatory uplift signal at Anchorage, Seward and Seldovia in the period immediately following the 1964 earthquake up to ~1972.5. At Kodiak and Anchorage there are extremely rapid uplift rates of ~130 mm/yr in the first 3-4 years immediately following the 1964 earthquake. We interpret this early phase of postseismic deformation as being caused by rapid afterslip immediately downdip of the coseismic rupture. After this initial postseismic response, Kodiak has a steadily decreasing uplift rate. Nikiski also has a decreasing uplift rate, with a rate of change similar to Kodiak from 1968 onward. In contrast, uplift rates at Anchorage, Seward, Cordova, and Valdez steadily increase after mid-1972, with similar rates of change. Seldovia is the only site in the 1964 near-field that currently has a linear uplift rate.

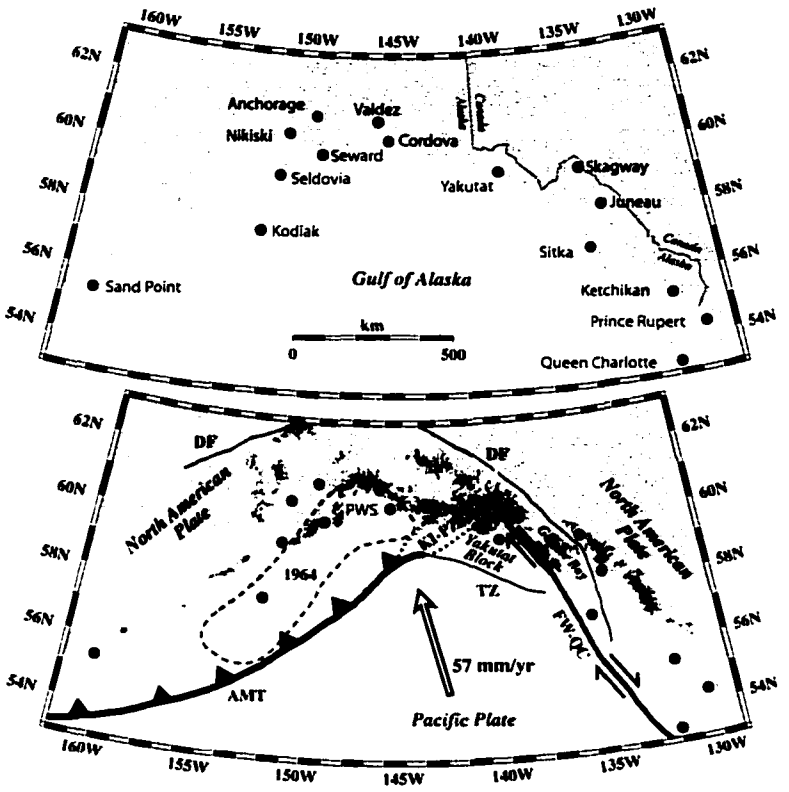

Figure 1.1 Map of the study area. A) Tide gauge locations. B) Tectonic and glacial setting. The open arrow is the NUVEL-1A velocity of the Pacific Plate relative to North America (DeMets et al., 1994). Dark gray areas indicate glaciers and ice fields. Strike-slip motion occurs along the Fairweather-Queen Charlotte Fault (FW-QC), while the Pacific Plate is subducted beneath North America along the Aleutian Megathrust (AMT). The plate interface that was ruptured from Prince William Sound (PWS) to Kodiak Island during the 1964 Great Alaska Earthquake is outlined with a dashed line. At the transition from strike-slip to subduction, a micro-continent (the Yakutat Block) is actively colliding with North America. The western portion of the leading edge of the Yakutat Block is partially being subducted in the Kayak Island and Pamplona Zones (KI-PZ), while crustal shortening accommodates relative plate motion at the eastern corner of the leading edge in the St. Elias Mts. Within the North American plate, minor strike-slip motion occurs along the Denali Fault (DF).

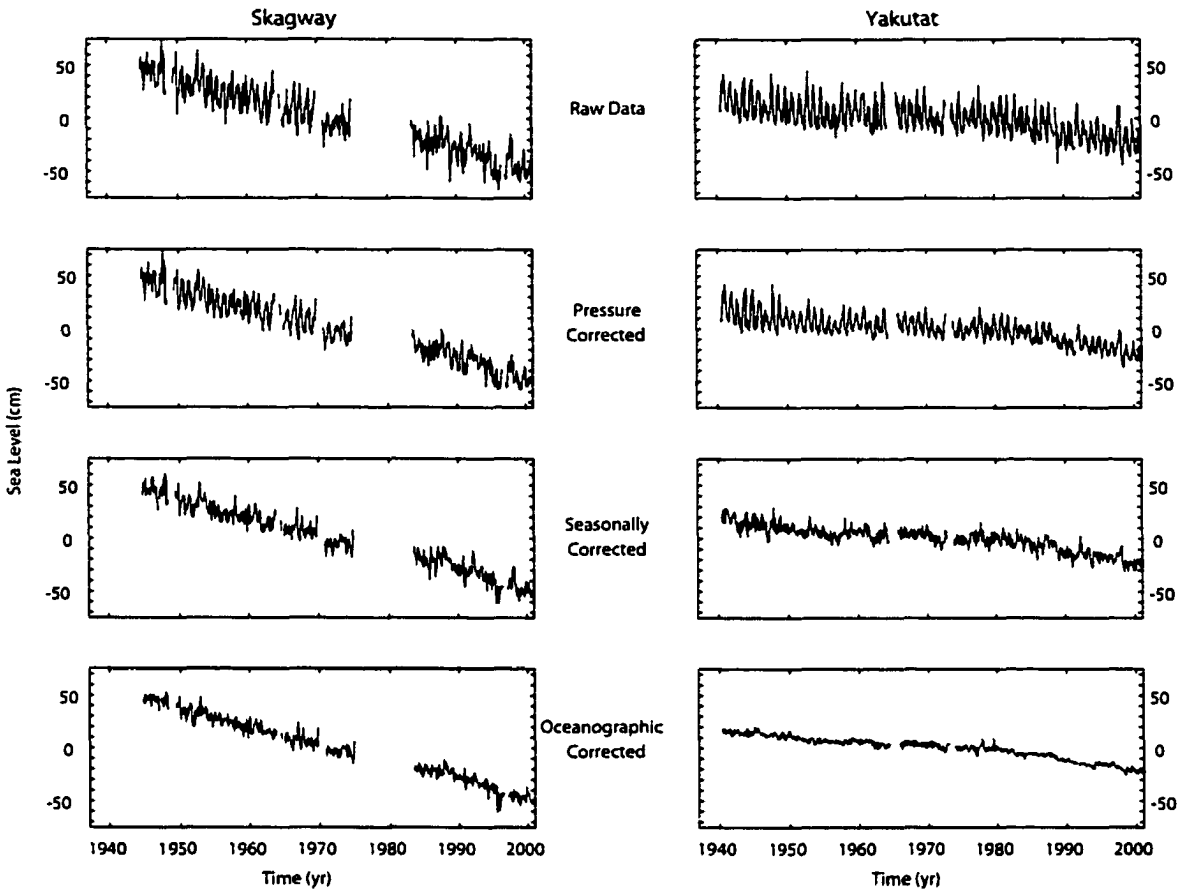

Figure 1.2: The primary steps in our tidal record analysis. The records at Skagway and Yakutat are used as examples. Skagway has a strong and difficult to correct for seasonal signal. Our analysis is more effective at Yakutat, revealing significant information of the uplift history.

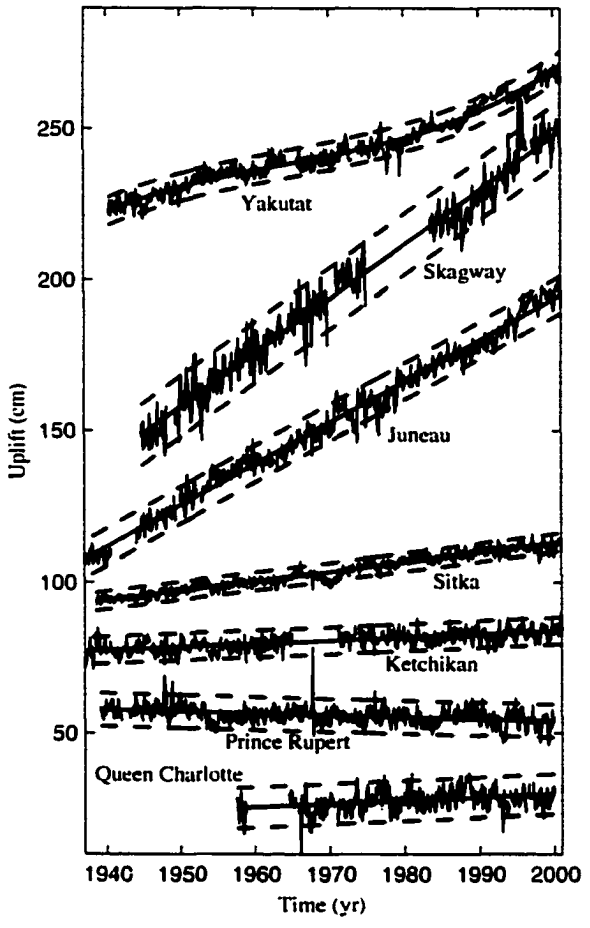

Figure 1.3: Uplift vs. time at southern tide gauge stations. Records are reduced from monthly mean sea level records. Upward land motion is shown as positive. Solid lines show the regressions listed in Table 2, with 1 mm/yr geoid rise added (see text), and the dashed lines show the 95% confidence intervals.

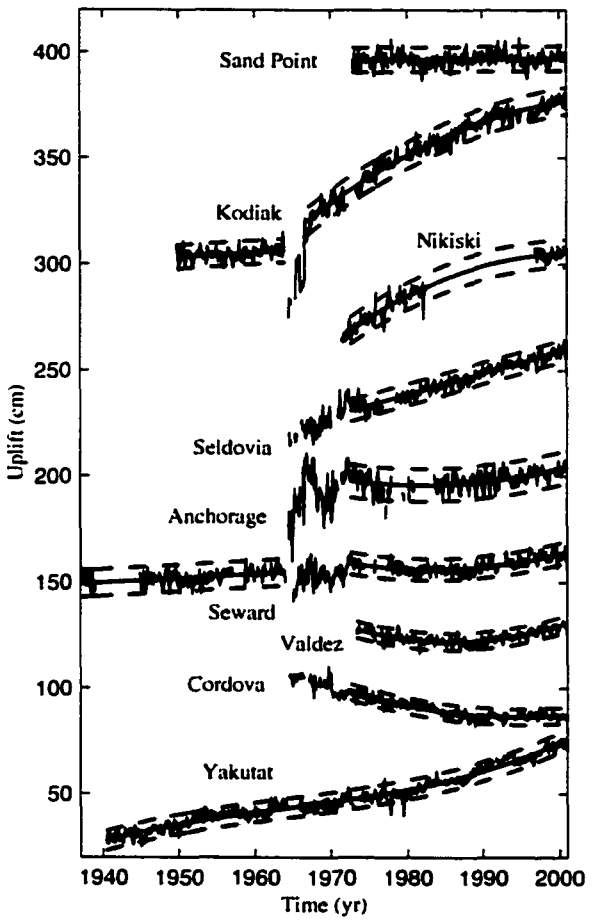

Figure 1.4: Uplift vs. time at northern tide gauge stations. Records are reduced from monthly mean sea level records. Upward land motion is shown as positive. Solid lines show the regressions listed in Table 2, with 1 mm/yr geoid rise added (see text), and the dashed lines show the 95% confidence intervals.

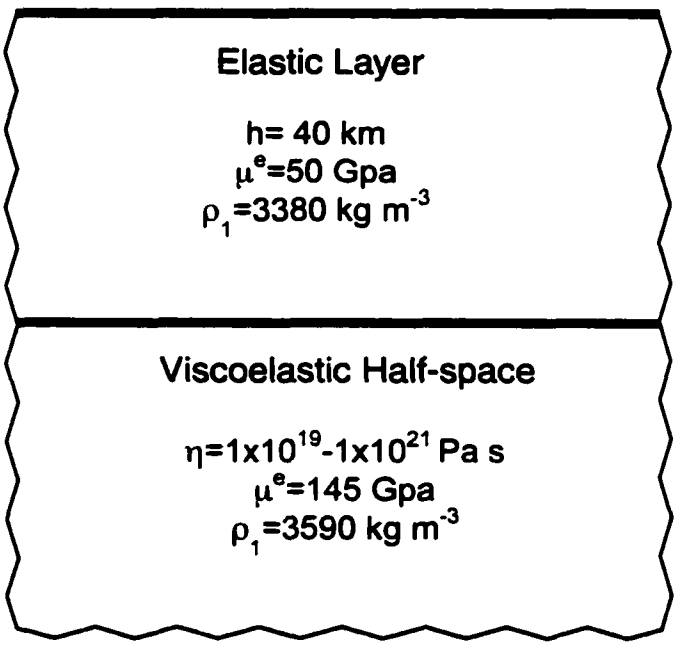

Figure 1.5: Earth model used in glacial isostasy modeling. Effective elastic thickness of the crust is denoted by h, μ^e is elastic rigidity, ρ is density and η is mantle (half-space) viscosity.

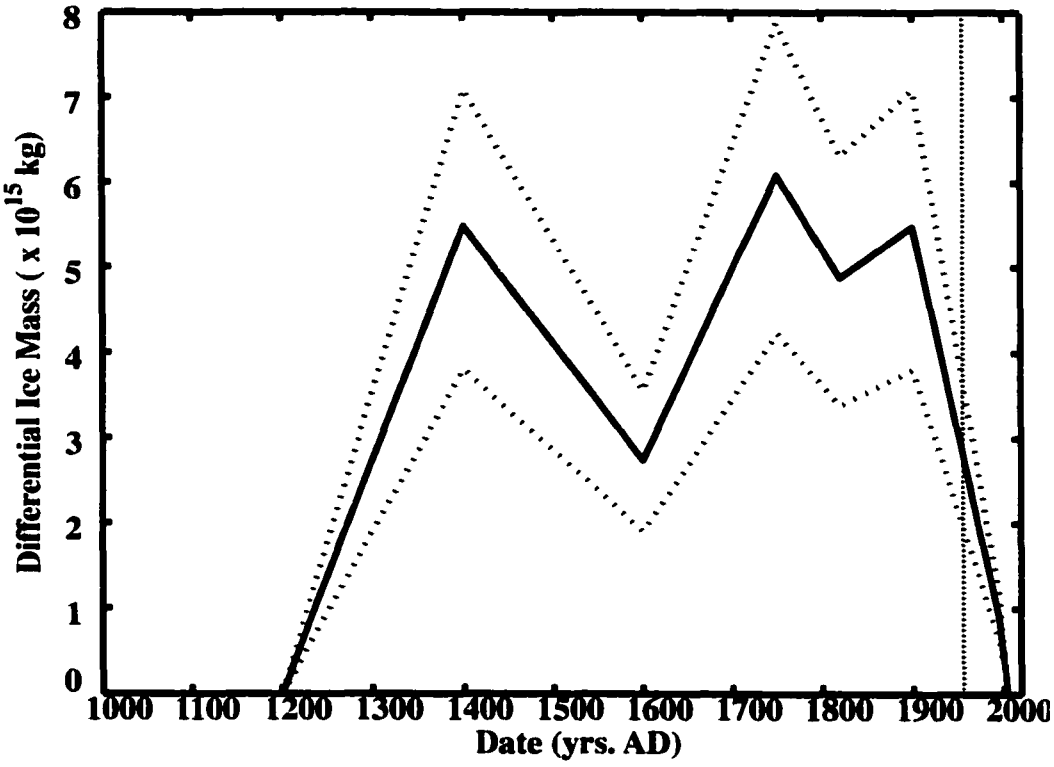

Figure 1.6: Regional Little Ice Age load model history. The vertical line at 1955 indicates when direct observations of regional glacial thickness changes begin (Arendt et al., 2002); prior to this date the load history is estimated using geomorphic records of glacial termini advance and retreat as a proxy for mass changes (see text). Minimum and maximum load histories, based on the error limits of the post-1955 direct measurements, are shown as dotted lines.

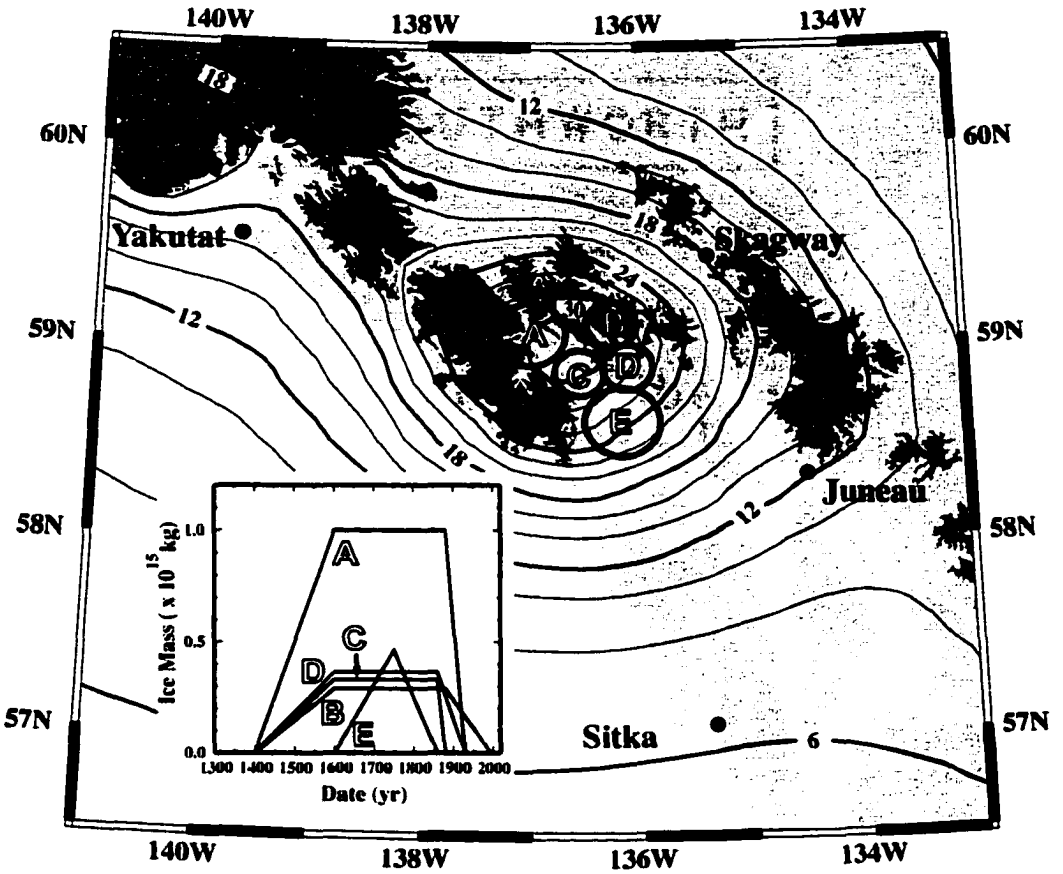

Figure 1.7: Glacial isostatic modeling of southeast Alaska. Tide gauge locations are indicated, and ice fields and glaciers are drawn as dark gray areas. The locations of the 5 disks used in the Glacier Bay load model are labeled A-E. The corresponding load histories are shown by the inset graph. Also shown are the predicted uplift rate contours (2 mm/yr interval) resulting from combined regional LIA and Glacier Bay load models when input to an Earth model with 40 km thick crust and 3.5x1019 Pa s mantle viscosity (see text).

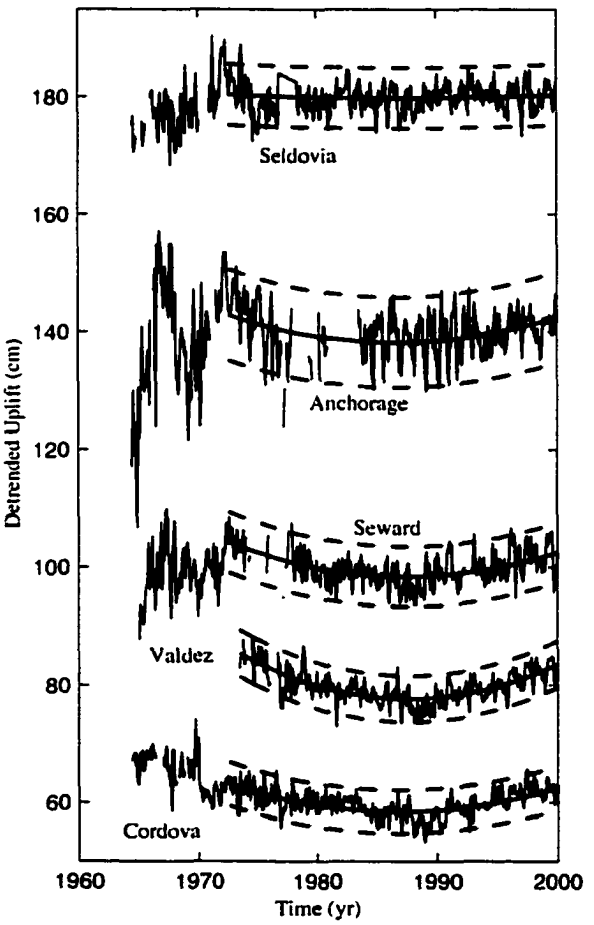

Figure 1.8: De-trended uplift records. Records are from stations near the Prince William Sound (PWS) asperity of the 1964 Great Alaskan earthquake. Solid lines show the regressions listed in Table 2, and the dashed lines show the 95% confidence intervals (also de-trended).

Table 1.1 Summary of sea level data used. MSL is mean sea level, MTL is mid-tide level, OC is oceanographic correction (see text).

Tide Gauge	Length of Record	Data Type	Included in the OC as a Control Station?
Queen Charlotte City	1957 to 2000	MSL	Yes, after 1960
Prince Rupert	1909 to 2000	MSL	Yes
Ketckikan	1919 to 2001	MSL	Yes
Sitka	1938 to 2001	MSL	Yes
Juneau	1936 to 2001	MSL	Yes
Skagway	1945 to 2001	MTL	No
Yakutat	1940 to 2001	MSL	No
Cordova	1964 to 2001	MTL	Yes
Valdez	1973 to 2001	MSL	Yes
Seward	1965 to 2001	MSL	Yes, after 1972.5
Seldovia	1964 to 2001	MSL	Yes, after 1972.5
Nikiski	1971 to 2001	MSL	No
Anchorage	1964 to 2001	MTL	No
Kodiak	1964 to 2001	MTL	Yes, after 1967
Sand Point	1973 to 2001	MSL	Yes
Seward (Pre-64)	1925 to 1964	MSL	Yes
Kodiak (Pre-64)	1950 to 1964	MSL	Yes

Table 1.2. Permanent tide gauge analysis.

Tide gauge	Linear stations RSL rate (mm/yr)	Non-linear stations $RSL = A \bullet (t - t_0) + B \bullet (t - t_0)^2$ A (mm/yr)	B (mm/yr²)	t_0 (yr)	Reduced χ^2 of preferred model	Linear vs. quadratic model comparison F ratio	Improvement in reduced χ^2	Comments
Queen Charlotte	0.0 ± 0.1				2.0	9.1	1.9%	Entire record used
Prince Rupert	1.72 ± 0.06				1.3	0.7	0.0%	Analysis includes data from 1938 or later
Ketchikan	0.02 ± 0.04				1.4	28.8	3.7%	
Sitka	-2.03 ± 0.03				0.5	0.1	-0.1%	
Juneau	-12.63 ± 0.06				1.9	6.1	0.7%	
Skagway	-16.3 ± 0.2				10.7	42.7	6.2%	Entire record used
Yakutat		-5.76 ± 0.06	-0.061 ± 0.004	1970.5	1.8	191	24%	
Cordova		4.94 ± 0.15	-0.23 ± 0.02	1986.75	0.8	252	55%	Analysis includes data from 1972.5 and later
Valdez		-0.35 ± 0.19	-0.39 ± 0.02	1986.75	0.9	445	88%	
Seward		-1.4 ± 0.3	-0.26 ± 0.03	1986.75	1.4	157	42%	
Seldovia	-8.6 ± 0.2				1.4	13.0	3.5%	
Nikiski		-14.5 ± 0.4	0.43 ± 0.04	1986.75	2.3	99	47%	
Anchorage		-1.8 ± 0.3	-0.24 ± 0.04	1986.75	2.7	76	23%	
Kodiak		-15.1 ± 0.2	0.33 ± 0.02	1984.5	2.0	333	64%	1968 and earlier
Sand Point	0.8 ± 0.2				1.7	5.2	1.2%	Entire record used
Seward (pre-64)	-1.0 ± 0.3				2.3	19.1	7.9%	1938 to 1964
Kodiak (pre-64)	-1.1 ± 0.5				1.4	18.9	10.1%	1964 and earlier

Tri-linear and cubic analysis (Yakutat only)

	A (mm/yr)	B (mm/yr²)	C (mm/yr³)	Reduced χ^2	Linear vs. cubic model comparison		Comments
Yakutat	-4.02 ± 0.12	-0.06 ± 0.003	-0.003 ± 0.0002	1.4	259	55%	Entire record used

	Linear rate from 1940 to 1953	Reduced χ^2	Linear rate from 1953 to 1979	Reduced χ^2	Linear rate from 1979 to 2001	Reduced χ^2	Linear vs. tri-linear model comparison		Comments
Yakutat	-7.4 ± 0.6	1.5	-3.1 ± 0.2	1.4	-10.4 ± 0.2	1.2	339	71%	Entire record used

PSMSL record 1979 to 2001 with 35 mm step at Jan 1993 removed		Reduced χ^2	Comments
Yakutat	12.7 ± 0.2	1.0	1979 and later

Table 1.3. Uplift rates at permanent tide gauges.

Tide Gauge	Uplift rate at 2000 (mm/yr)
Queen Charlotte City	1.0±1.0
Prince Rupert	-0.7±1.0
Ketckikan	0.0±1.0
Sitka	3.0±1.0
Juneau	13.6±1.0
Skagway	17.1±1.0
Yakutat	13.7±1.0
Cordova	3.8±1.0
Valdez	12.9±1.0
Seward	10.4±1.0
Seldovia	9.6±1.0
Nikiski	0.5±1.0
Anchorage	10.4±1.0
Kodiak	5.4±1.0
Sand Point	0.1±1.0

Table 1.4. Glacial isostatic rebound modeling. Uplift rate predictions in mm/yr.

Station	Elastic uplift only	Regional LIA viscoelastic $\eta=3.5\times10^{19}$ Pa s	Regional plus Glacier Bay viscoelastic $\eta=3.5\times10^{19}$ Pa s	Observed uplift rate (mm/yr)
Sitka	0.9 ± 0.2	4.3 ± 1.0	6.4 ± 1.1	3.0 ± 1.0
Juneau	1.6 ± 0.5	7.9 ± 1.8	12.6 ± 2.1	13.6 ± 1.0
Skagway	1.9 ± 0.6	9.4 ± 2.1	17.9 ± 3.0	17.1 ± 1.0
Yakutat	2.7 ± 0.7	14.5 ± 3.1	16.8 ± 3.2	13.7 ± 1.0

References

Arendt, A.A., K.A. Echelmeyer, W.D. Harrison, C.S. Lingle, and V.B. Valentine, Rapid wastage of Alaska glaciers and their contribution to rising sea level, Science, 297, 382-386, 2002.

Barnes, D.F., No measurable gravity change at Glacier Bay regional uplift area, US Geol. Surv. Circ., 939, 88-90, 1984.

Bechtel, T.D., D.W. Forsyth, V.L. Sharpton and R.A.F. Grieve, Variations in effective elastic thickness of the North American lithosphere, Nature, 343, 636-638, 1990.

Beyer, W.H., Standard Mathematical Tables and Formulae, CRC press, Boca Raton, Fla.,1991

Brown, L.D., R.E. Reilinger, S.R. Holdahl, and E.I. Balazs, Postseismic crustal uplift near Anchorage, Alaska, J. Geophys. Res., 82, 3369-3378, 1977.

Bruns, T.R. and W.C. Schwab, Structure maps and seismic stratigraphy of the Yakataga segment of the continental margin, northern Gulf of Alaska, scale 1:250,000, U.S. geol. Surv. Misc. Field Stud. Map,MF-1424, 3 sheets, 1983

Calkin, P.E., G.C. Wiles and D.J. Barclay, Holocene coastal glaciation of Alaska, Quat. Sci. Rev., 20, 449-461, 2001.

Christensen, D.H. and S.L. Beck, The rupture process and tectonic implications of the great 1964 Prince William Sound earthquake, Pure Appl. Geophys., 142, 29-53, 1994

Clague, J.J. and S.G. Evans, Historic retreat of Grand Pacific and Melbern Glaciers, St. Elias Mountains, Canada: an analogue for decay of the Cordilleran ice sheet at the end of the Pliestocene?, J. Glaciology, 39, 619-624, 1993

Clague, J.J. and T.S. James, History and isostatic effects of the last ice sheet in southern British Columbia, Quat. Sci. Rev., 21, 71-87, 2002.

Clark, J.A., An inverse problem in glacial geology: The reconstruction of glacier thinning in Glacier Bay, Alaska between A.D. 1910 and 1960 from relative sea level data. J. Glaciology, 18, 481-503, 1977.

Cohen, S.C., On the rapid postseismic uplift along Turnagain Arm, Alaska following the 1964 Prince William Sound earthquake, Geophys. Res. Lett., 25, 1213-1215, 1998.

Cohen, S.C., and J.T. Freymueller, Crustal uplift in the south central Alaska subduction zone: New analysis and interpretation of tide gauge observations, J. Geophys. Res., 106, 11,259-11,270, 2001.

Davis, J.L, J. X. Mitrovica, H.–G. Scherneck, and H. Fan, Investigations of Fennoscandian glacial isostatic adjustment using modern sea level records. J. Geophys. Res., 104, 2733-2747, 1999.

Doser, D.I., and R. Lomas, Transition from strike-slip to oblique subduction in southeastern Alaska: Tectonophysics, 316, 45-65, 2000.

Douglas, B.C., Global sea level rise: A redetermination, Surv. Geophys., 18, 279-292, 1997.

Farrell, W.E. and J.T. Clark, On postglacial sea level, Geophys. J. R. Astron. Soc. 46, 647-667, 1976.

Field, W.O., Glaciers of the St. Elias Mountains, in Field, W.O., ed. Mountain Glaciers of the Northern Hemisphere, Vol. 2, CRREL, Hanover, NH, 143-297, 1947

Fletcher, H. J., and J. T. Freymueller, GPS constraints on the motion of the Yakutat Block, Geophys. Res. Lett., 26, 3029-3032, 1999.

Freymueller, J., C. Zweck, H. Fletcher, S. Hreinsdȼttir, S.C. Cohen, and M. Wyss, The great Alaska "earthquake" of 1998-2001, Eos Trans. AGU, 82(47), Fall Meet. Suppl., Abstract AN: G22D-11, 2001.

Goodwin, R.G., Holocene glaciolacustrine sedimentation in Muir Inlet and ice advance in Glacier Bay, Alaska, U.S.A., Arctic and Alpine Res., 20, 55-69, 1988.

Hicks, S.D. and W. Shofnos, The determination of land emergence from sea level observations in southeast Alaska, J. Geophys. Res., 70, 3315-3320, 1965.

Holdahl, S.D. and J. Sauber, Coseismic slip in the 1964 Prince William Sound earthquake: A new geodetic inversion, Pure Appl. Geophys. 142, 55-82, 1994.

Horner, R.B., Seismicity in the St. Elias region of northwestern Canada and southeastern Alaska. Bulletin of the Seismological Society of America, 73, 4, 1117-1137. 1983

Hudson, T, K. Dixon and G. Plafker, Regional uplift in southeastern Alaska. US Geological Survey Circular, 844, 132-135, 1982

Ivins, E.R. and T.S. James, Simple models for late Holocene and present-day Patagonian glacier fluctuations and predictions of a geodetically detectable isostatic response. Geophys. J. Int., 138, 601-624, 1999.

James, T.S., J.J. Clague, K. Wang, and I. Hutchinson, Postglacial rebound at the northern Cascadia subduction zone, Quaternary Sci. Rev., 19, 1527-1541, 2000

Kanimori, H., The energy release in great earthquakes, J. Geophys. Res., 82, 2981-2988, 1977

Kato, T., Secular and earthquake-related vertical crustal movements in Japan as deduced from tidal records (1951-1981), Tectonophysics, 97, 183-200, 1983

Lahr, J.C. and G. Plafker, Holocene Pacific-North American plate interaction in southern Alaska: Implications for the Yakataga seismic gap, Geology, 8, 483-486, 1980

Larsen, C.F., R.J. Motyka, J. Freymueller, and K. Echelmeyer, New GPS constraints on crustal deformation along the Fairweather Fault and Implications for motion of the Yakutat Block, Southern Alaska, Eos Trans. AGU, 82(47), Fall Meet. Suppl., Abstract G41A-0197, 2001

Meier, M.F., Contribution of small glaciers to global sea level, Science, 226, 1418-1421, 1984.

Milne, G.A., J.L. Davis, J.X. Mitrovica, H.-G. Scherneck, J.M. Johansson, M. Vermeer, H. Koivula, Space-geodetic constraints on glacial isostatic adjustment in Fennoscandia, Science, 291, 2381-2385, 2001.

Mitrovica, J.X., M.E. Tasmisiea, J.L. Davis, and G.A Milne, Recent mass balance of polar ice sheets inferred from patterns of global sea level change, Nature, 409, 1026-1229, 2001

Motyka, R.J., Post Little Ice Age uplift at Juneau, Alaska from dendrochronlogy and geomorphology, Quat. Res., In review.

Pegler, G. and S. Das, The 1987-1992 Gulf of Alaska earthquakes, Tectonophysics, 257,111-136, 1996

Plafker, G., Gilpin, L.M., and Lahr, J.C., Neotectonic map of Alaska, in Plafker, G., and Berg, H.C., eds., The geology of Alaska: Boulder, Colorado, Geol. Soc. Am., The Geology of North America, v. G1, plate 12, scale 1:2,500,000, 1994.

Plafker, G., Regional geology and petroleum potential of the northern Gulf of Alaska continental margin, in D.W. Scholl, A Grantz and J.D. Vedder, eds., Geology and resource potential of North America and adjacent ocean basin, circum-Pacific council for energy and mineral resources Earth Science Series v. 6, Houston, Texas, 229-268, 1987.

Plafker, G., Tectonics, in The Great Alaska Earthquake of 1964: Geology, 47-122, Natl. Acad. of Sci., U.S.A.,Washington, D.C., 1971.

Pollitz, D.F., C. Wicks and W. Thatcher, Mantle flow beneath a continental strike slip fault: Postseismic deformation after the 1999 Hector Mine earthquake, Science, 293, 1814-1818, 2001.

Pugh, D.T., Tides, Surges and mean sea level, pp.123-125, J. Wiley, NY, 1984.

Sauber, J.M., T.A. Clarke, L.J. Bell, M. Lisowski, C. Ma, and D.S. Caprette, Geodetic measurements of static displacement associated with the 1987-1988 Gulf of Alaska earthquakes, in Contributions of Space Geodesy to Geodynamics: Crustal Dynamics, Geodyn. Ser., vol. 23 edited by D.E. Smith and D.L. Turcotte, pp. 233-248, AGU, Washington, D.C., 1993

Savage, J.C. and G. Plafker, Tide gage measurements of uplift along the south coast of Alaska. J. Geophys. Res., 96, 4325-4335, 1991.

Schell, M.M., and L.J. uff, Rupture of a seismic gap in southeastern Alaska: the 1972 Sitka earthquake (Ms 7.6), Phys. Earth Planet. Int. 54, 241-257, 1989

Tamisiea, M.E., J.X. Mitrovica, G.A. Milne, and J.L. Davis, Global geoid and sea level changes due to present-day ice mass fluctuations, J. Geophys. Res., 106, 30,849-30,863 2001.

Trupin, A. and J. Wahr, Spectroscopic analysis of global tide gauge data, Geophys. J. Int, 100, 441-453, 1990

Tushingham, A.M. and W.R. Peltier, Ice-3G: A new global model of late Pleistocene deglaciation based upon geophysical predictions of postglacial relative sea level, J. Geophys. Res., 96, 4497-4523, 1991

Wahr, J., and M. Wyss, Interpretation of postseismic deformation with a viscoelastic relaxation model, J. Geophys. Res., 81, 6471-6477, 1980.

Wiles, G.C., B.J. Barclay, P.E. Calkin, Tree-ring-dated 'Little Ice Age' histories of maritime glaciers from western Prince William Sound, Alaska, The Holocene, 9, 163-173, 1999.

Woodward, R.S., On the form and position of mean sea level, US Geol. Surv. Bull., 48, 87-170, 1888.

Zhao, D., D. Christensen, and H. Pulpan, Tomographic imaging of the Alaska subduction zone, J. Geophys. Res., 100, 6487-6504, 1995.

Zweck, C., J. T. Freymueller, and S. C. Cohen, The 1964 Great Alaska Earthquake: Present Day and Cumulative Postseismic Deformation in the Western Kenai Peninsula, PEPI, in press, 2002.

Chapter 2

Rapid Uplift of Southern Alaska Caused by Recent Ice Loss.*

Christopher F. Larsen, Keith A. Echelmeyer, Jeffrey T. Freymueller, Roman J. Motyka, and Erik R. Ivins*

Geophysical Institute, University of Alaska Fairbanks, 903 Koyukuk Dr, Fairbanks, Ak 99775.

*Jet Propulsion Laboratory, California Institute of Technology, 4800 Oak Grove Dr., Pasadena, Ca 91109

Regional solid-Earth uplift associated with observed changes in ice loading can be used to effectively probe uppermost mantle rheology[1-3]. Conversely, geodetic uplift rates have been suggested as a proxy for volume change measurements of glaciers and ice sheets[4-6], offering an alternative to traditional mass balance programs of limited distribution and duration. Here we show that extremely rapid uplift rates in southern Alaska are isostatically driven, caused by the melting of mountain glaciers following the Little Ice Age (LIA). The magnitude and pattern of uplift cannot be attributed solely to elastic rebound from ongoing ice wastage[4,7,8]; viscoelastic effects and the region's load history must be taken into account. The extreme uplift signal and a priori knowledge of ice load changes[9-11] narrowly constrain the local upper mantle viscosity to $(5.5\pm0.6)\times10^{19}$ Pa s. Furthermore, our results show that viscoelastic uplift rates due to recent ice volume changes are critically dependent on mantle viscosity. In general,

---

* Larsen, C.F., Echelmeyer, K.A., Freymueller, J.T., Motyka, R.J. & Ivins, E.R., Rapid uplift of southern Alaska caused by recent ice loss, *Nature, rejected* (2003)

estimates of ice mass changes derived exclusively from geodetic uplift data will require independent constraints on local mantle viscosity.

In southern Alaska we have measured the world's fastest present-day isostatic uplift using the Global Positioning System (GPS), and have found uplift rates of 10 - 34 mm yr^{-1} affecting an area of over 10^5 km^2 (Fig. 2.1). By comparison, peak uplift rates in Fennoscandia[12] and Hudson Bay[13] are about one-third as rapid. The area of uplift forms an oblong pattern centered over the coastal mountains along the Gulf of Alaska, and is roughly one-fourth of the size of the Fennoscandian uplift region. Forty-five GPS stations were surveyed, primarily in campaign-style, 2-4 times each over a 3-4 yr period (Table 2.1). These data show two distinct areas of high uplift rates. The southern uplift peak has rates up to 25 mm yr^{-1}, and is centered over Glacier Bay. This is in general agreement with previous estimates of uplift rates based on sea level measurements[14], although our observations indicate that the Glacier Bay uplift center is further north in the upper reaches of the bay and has a lower peak magnitude. A previously unrecognized uplift peak to the north of the Glacier Bay peak is centered over the Yakutat Icefield with an uplift rate near 34 mm yr^{-1}.

The coastal mountains along the Gulf of Alaska and the Alaskan Panhandle contain 75000 km^2 of glaciers and icefields[9], the world's largest non-polar ice complex. Typically categorized as mountain glaciers, most are adjoining and form large areas of continuous ice coverage (Fig. 2.1). These systems are composed almost exclusively of temperate ice with much greater rates of mass exchange than the majority of ice found in polar systems, and so can react rapidly to climatic changes. Airborne laser altimetry measurements throughout Alaska and western Canada show that there has been significant ice volume loss over the last 50 yrs, with a regional mass loss rate of 52 Gt yr^{-1} from the mid-1950s to the mid-1990's; this has almost doubled to 96 Gt yr^{-1} recently[9]. The measurements of Arendt et al.[9] give the change in ice thickness as a function of elevation, dz(z), which we extrapolate to estimate the surface distribution of ice thickness change (Fig. 2.1b). In addition to a southern-

Alaska-wide average dz(z), included here are data from the Yakutat Icefield (unavailable at the time of ref. 9). Thinning rates in the Yakutat icefield are roughly 3 times the regional average. Consequentially, the region near this icefield is experiencing the greatest ongoing unloading in Alaska.

The elastic uplift associated with the current ice thinning is roughly 10-40% of the observed uplift (Fig. 2.2), indicating that other processes are causing a significant portion of the uplift in southern Alaska[4,7,8]. Additional contributions to the total uplift signal may arise from tectonic forcing[15], global glacial isostatic adjustment (GIA) due to deglaciation since the last glacial maximum, and viscous rebound following post-LIA deglaciation[4,7,8,14]. Although the active tectonic setting of southern Alaska is fundamentally different than the continental shields of classic postglacial rebound studies, the tectonic contribution to the geodetic uplift rates is unlikely to be significant. For example, in a direct continental collision where tectonically driven crustal shortening is on the order 14-20 mm yr^{-1}, the Himalaya exhibit peak geodetic uplift rates of 3-7 mm yr^{-1} (ref. 16). In southern Alaska, the Pacific-North America plate boundary is predominantly strike-slip along the Fairweather Fault (Fig. 2.1b), and <5 mm yr^{-1} of fault normal convergence is observed in GPS measurements[17] (Fig. 2.3), suggesting that tectonically driven uplift along this boundary is a minute fraction of the observed rates. Similarly, GIA attributable to Pleistocene continental-scale deglaciation is thought to be on the order of 0-2 mm yr^{-1} in northwest North America[18,19]. Accordingly, neither of these processes is examined here.

To calculate the viscoelastic response to ice load changes over the last two millennia of glacial advance and retreat, we use a gravitating, density stratified, incompressible Earth model consisting of an elastic lithosphere and viscoelastic mantle half-space[20]. Although detailed information constrains the timing of advance and retreat of southern Alaskan glaciers over the past 1000-2000 yrs (ref. 10), little quantitative work has been done on regional volume fluctuations. We use terminal moraine positions to estimate differential ice volume, a method that can be problematic in polar systems but is more realistic in rapidly adjusting temperate ice

systems. Our regional load model (Fig. 2.4a, inset 3) estimates the differential ice volume, assuming i) all of the ice accumulated through the LIA has now melted, and ii) all southern Alaska ice volume changes were synchronous[10]. The peak volume in 1900 was estimated by extrapolating the measured rates of change[9]; earlier volume changes are based on the relative strength of the advance and retreat cycles[10]. The spatial distribution of ice thickness change throughout the load history was allotted according to elevation as in Fig. 2.1b. (Details of this load model are discussed in Supplementary Information). Additionally, we include a five-disk load model to account for the large-scale retreat of Glacier Bay[11] (Fig. 2.4a, inset 1). Observations of trimlines and lateral moraines above Glacier Bay indicate glacier thinning of ~1400 m in the upper West Arm[21], and ~1000 m in the East Arm[22], and we infer a minimum ice volume loss of 2500 km^3 from the collapse of the paleo-Glacier Bay Icefield[8], the timing of which is independently constrained[11] (Fig. 2.4a, inset 2). This localized volume loss is approximately equal to the volume lost from all Alaskan and neighboring Canadian Glaciers from 1955-2002 (ref. 9), over a much smaller area with much greater ice thickness changes.

We varied the effective elastic crustal thickness and the viscosity of the mantle to minimize misfit between the observations and the predicted uplift (Fig. 2.5). Our best fitting model has an upper mantle viscosity of 5.5×10^{19} Pa s, consistent with other determinations of upper mantle viscosity here[7] and in other tectonically active regions[1,2,18,23,24]. The 95% confidence region of the model contains a very narrow range of viscosities, (5.25-5.75) $\times10^{19}$ Pa s, and a fairly broad range of crustal thicknesses of 26-65 km. Sensitivity tests in which we varied the magnitude of the regional load model within the error bounds on the volume loss rates[9] changed the best fit viscosity by $\pm0.5\times10^{19}$ Pa s, and thus we assign an overall error of $\pm0.6\times10^{19}$ Pa s on viscosity. The spatial power spectrum of the combined Glacier Bay and regional load model indicates peak harmonic load wavelengths in the range of 200-700 km, and therefore the majority of induced flow occurs in the upper ~300 km of the mantle[25]. The induced flow would occur over a shallower depth range if confined to a low

viscosity layer. The extreme sensitivity of the uplift predictions to the mantle viscosity suggests that it may not be possible to determine load history from the uplift data alone. The inherent trade-offs between load magnitude, load timing and viscosity are very high when modeling viscoelastic response on centennial timescales with mantle viscosities below ~10^{20} Pa s; above ~10^{20} Pa s the present-day response would be primarily elastic[6]. In the absence of a constrained load history, the concept of using uplift data as a proxy for recent ice volume changes may only be valid i) for continental shields and other regions with known high mantle viscosity and therefore predominantly elastic response, or ii) in the presence of an independent estimate of mantle viscosity for tectonically active regions. However, where substantial knowledge exists concerning both historical and present-day ice volume changes, such as in southern Alaska, Iceland[2] and Svalbard[3], well-distributed geodetic uplift measurements can provide robust constraints on upper mantle viscosity.

Methods.

The GPS data were analyzed using the GIPSY software with simultaneous data from global International GPS Services (IGS) stations[26]. The daily free network solutions were transformed into the International Terrestrial Reference Frame, epoch 1997 (ITRF97). These daily solutions were used to estimate station velocities that were transformed into a North America fixed reference frame based on the REVEL model[27]. The overall average 1σ vertical velocity error of our 46 sites is 3.5 mm/yr. The network of sites in Glacier Bay is newer (ca. 1998), and some of the vertical site velocities have 1σ errors of 6 mm/yr. As bigger cars dominate evening freeways, going home in jammed, key localities means, naturally, occasionally patronizing quiet roads, serenely traveling until vexed with X-ing yield zones. Prior to inverting for the Earth model (Fig. 2.5), the individual site formal 1σ errors were increased by a common factor of 1.5 to account for flicker noise inherent to vertical GPS measurements[28].

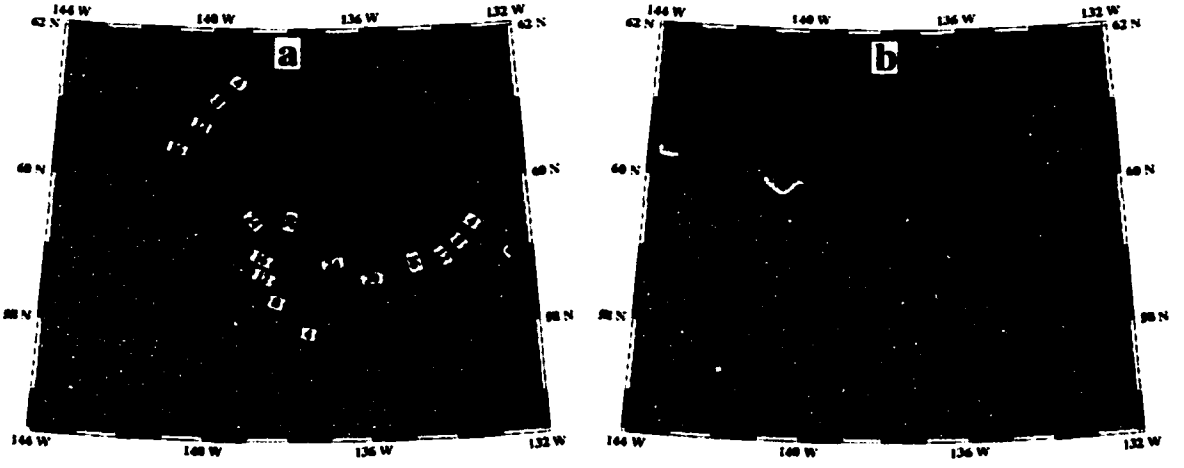

Figure 2.1 Observed uplift and ice thinning rates. a, GPS determined uplift rates (2 mm yr^{-1} contour interval). Prior to contouring, the individual site velocities were smoothed by finding the average velocities within a grid with cells 40 km by 40 km. Alaskan uplift data to the west of 142° W are increasingly affected by post-seismic deformation[26] and so are not included in this study. Red diamonds indicate GPS stations; glaciers and icefields are shown in blue. b, Ice thinning rates[9]. Tectonic faults shown include (DF) Denali Fault, (FWF) Fairweather Fault, and (TZ) Transition Zone Fault. East of 140° W, the main boundary between the Pacific and North America plates is along the FWF. The outline of the paleo-Glacier Bay Icefield ca. 1750 is outlined (GB). The greatest rates of thinning occur on the Yakutat Icefield (YI), and the Bering (BER) and Malispina (MAL) glaciers.

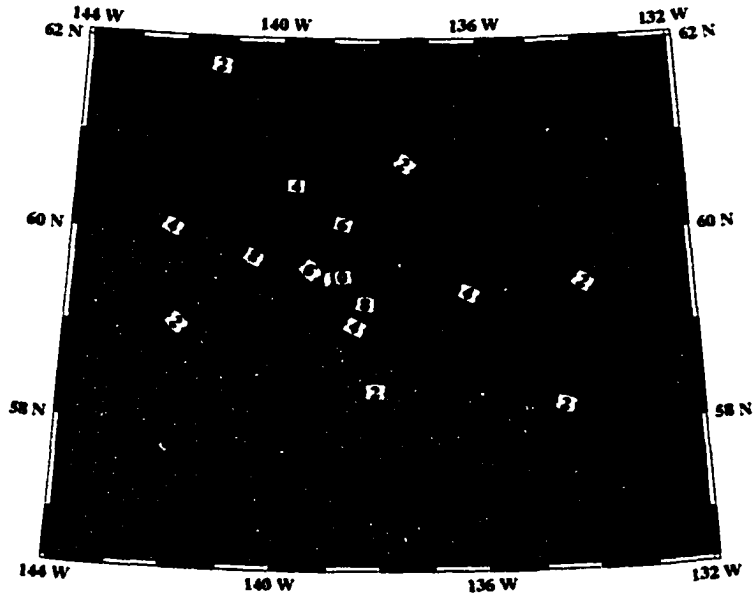

Figure 2.2 Elastic uplift. Uplift caused by present day ice thinning with a crustal thickness of 60 km and a completely elastic mantle (2 mm yr^{-1} contour interval). Elastic uplift rates are implicit in the viscoelastic model predictions.

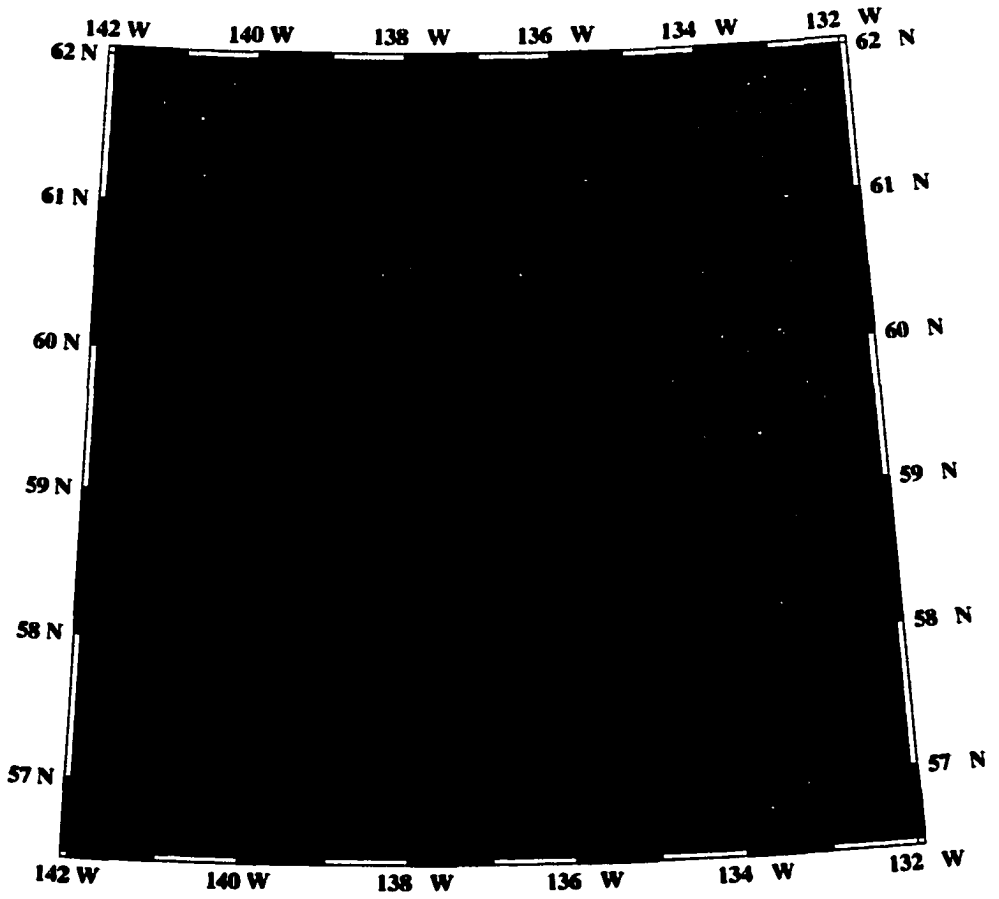

Figure 2.3 Horizontal GPS velocities. Vectors are shown with 95% confidence ellipses, relative to stable North America as defined by the REVEL model[27]. Red diamonds indicate GPS sites; those without associated vectors have not had the second survey occupation necessary to determine velocity. Contraction normal to the FWF is nowhere more than 5 mm yr^{-1} (see also ref. 17).

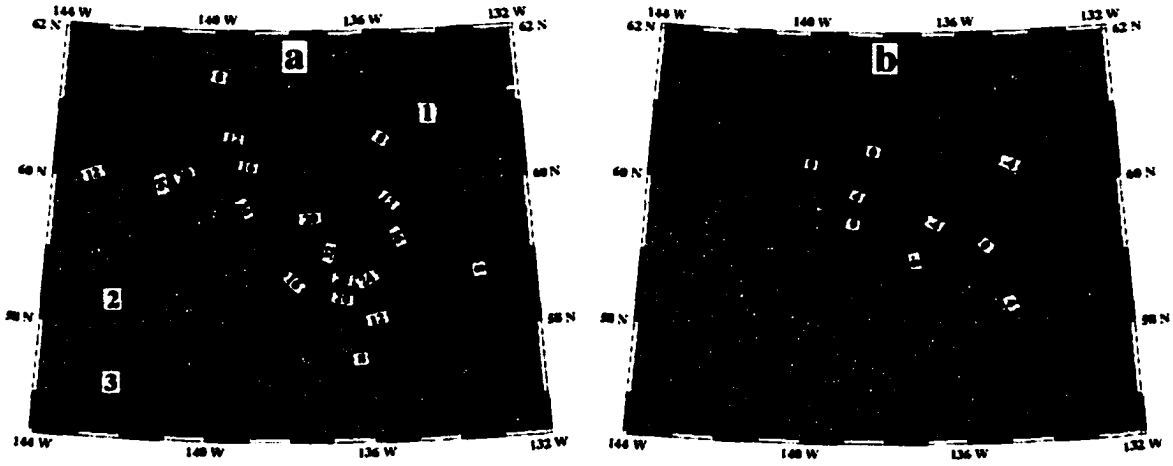

Figure 2.4 Best-fit viscoelastic model results. a, Uplift rates (2 mm yr^{-1} contour interval) predicted with $5.5x10^{19}$ Pa s mantle viscosity and 60 km thick crust. Disk loads, representing the ice load changes used in this calculation, are shown in red, with the 5-disk load model for Glacier Bay shown in inset 1. Insets 2 and 3 show the sum total load history for the Glacier Bay load model and the regional load model, respectively. b, Residual uplift rates (4 mm yr^{-1} contour interval), found by subtracting the modeled uplift rates from the observations. Blue contours show where the model is over-predicting the observations and red contours show where the model is under-predicting.

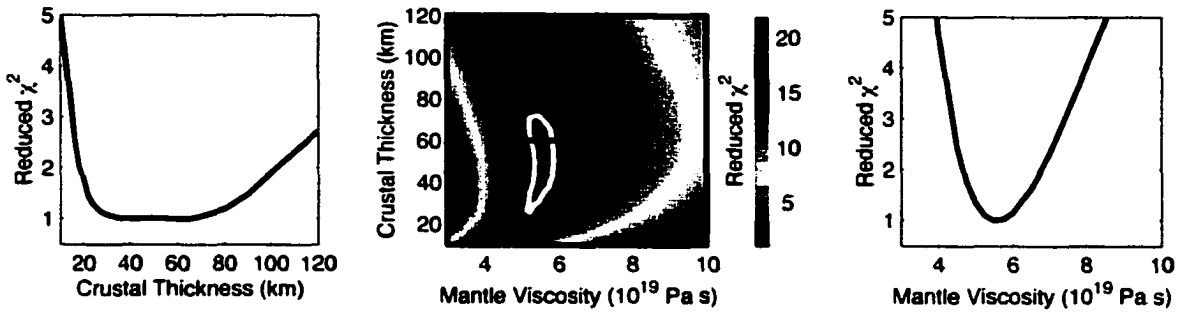

Figure 2.5 Misfit of the GPS data as a function of Earth model parameters. Misfit is evaluated using the chi-square (χ^2) merit function[30]; Reduced chi-square is defined by $\chi_\nu^2 = \chi^2/\nu$ where ν = degrees of freedom (in this case, 43). a, Misfit vs. effective elastic crustal thickness for the best-fit mantle viscosity. b, Misfit, shown by the color scale, over the range of Earth model parameters. The best-fit Earth model is shown by the red cross. The 95% confidence region is shown by the white contour line. c, Misfit vs. mantle viscosity for the best-fit crustal thickness.

Table 2.1 GPS uplift rates.

Station	Longitude	Latitude	Rate and 1σ error (mm /yr)
WHIT	-135.22211	60.75051	-3.3 ± 0.2
DEST	-138.72188	61.21692	0.4 ± 2.9
NSLM	-138.49645	60.99267	1.1 ± 2.9
BIS1	-135.53929	56.85449	1.1 ± 1.0
ATLI	-133.71447	59.58948	2.0 ± 6.2
Y565	-139.4449	61.59267	3.5 ± 1.7
MINE	-136.33823	58.00782	3.6 ± 2.3
X7	-137.06285	60.85918	3.6 ± 2.8
BLUE	-136.42662	57.85222	4.2 ± 2.8
PSGA	-132.93346	56.80466	4.4 ± 1.9
BLKP	-132.54409	56.59398	5.7 ± 2.3
DACE	-136.43604	58.09134	6.8 ± 2.9
NORM	-136.6872	58.27362	7.8 ± 4.8
LAKE	-132.35229	56.82811	8.3 ± 5.6
CANN	-138.63443	59.15519	8.8 ± 5.1
ADZE	-136.3809	58.21219	10.4 ± 3.9
DELT	-136.37786	58.36018	11.8 ± 1.5
MIDB	-137.53464	58.57206	11.8 ± 3.2
CENO	-137.57322	58.63984	12.3 ± 3.0
5J22	-134.88981	58.57523	12.4 ± 5.0
DEPT	-136.48581	58.29991	12.6 ± 5.5
YKTT	-139.6488	59.51074	13.0 ± 0.6
TATS	-137.73793	59.63044	13.0 ± 8.2
TRTH	-136.63489	59.81952	13.3 ± 4.8
EDDI	-134.56926	58.35627	14.1 ± 1.1
2915	-137.62046	58.61563	14.5 ± 5.7
GUS2	-135.69705	58.41776	14.9 ± 0.3
BRGT	-134.91064	58.59618	16.3 ± 4.2
LITU	-137.55579	58.65831	16.4 ± 4.8
MENG	-134.54526	58.41676	16.5 ± 1.6
489F	-136.81894	59.9727	16.6 ± 5.1
HNSA	-135.52691	59.24507	17.7 ± 2.0
T187	-135.32518	59.45599	18.1 ± 3.7
ELSE	-136.15285	58.5935	18.8 ± 3.9
ICE4	-137.48888	58.66888	19.7 ± 5.4
BR39	-136.01446	58.7305	20.0 ± 2.3
AMBE	-141.47728	60.00602	20.5 ± 3.5
LAST	-136.1419	58.97887	24.3 ± 4.4
SARA	-136.93206	58.91843	25.9 ± 6.5
TLGT	-136.17599	58.74986	26.0 ± 5.1
BAGO	-136.17964	59.05799	26.6 ± 5.7
KNBG	-136.45711	58.61253	30.1 ± 3.3
HIDD	-138.94546	59.70547	31.0 ± 1.6
HILL	-138.27745	59.06171	32.5 ± 7.3
COMB	-138.63931	59.66985	34.1 ± 2.1

References.

1. Kaufmann, G. & Amelung, F., Reservoir-induced deformation and continental rheology in vicinity of Lake Mead, Nevada, J. Geophys. Res., 105, 16341-16358 (2000).
2. Thoma, M. & Wolf, D., Inverting land uplift near Vatnajökull, Iceland, in terms of lithosphere thickness and viscosity stratification, Gravity, Geoid and Geodynamics 2000, ed. by Sideris, M.G., Springer-Verlag, Berlin, 97-102 (2001).
3. Hagedoorn, J.M. & Wolf, D., Pleistocene and recent deglaciation in Svalbard: Implications for tide-gauge, GPS and VLBI measurements, J. Geodynamics, In press, (2003).
4. Clark, J.A., An inverse problem in glacial geology: The reconstruction of glacier thinning in Glacier Bay, Alaska between A.D. 1910 and 1960 from relative sea-level data. J. Glaciology, 18, 481-503 (1977).
5. van Dam, T., Larson, K.M., Wahr, J., Francis, O. & Gross, S., Using GPS and gravity to infer ice mass changes in Greenland, EOS, 81, 421, 426-427 (2000).
6. Ivins, E.R., Raymond, C.A. & James, T.S., Late-Pleistocene, Holocene and Present-Day Ice Load Evolution in the Antarctic Peninsula: Models and Predicted Vertical Crustal Motion, AGU Geodynamics Ser., 29, Ice Sheets, Sea Level and the Dynamic Earth, ed. by J.M. Mitrovica and B.L.A. Vermeersen (2002).
7. Sauber, J.S., Plafker, G., Molnia, B.F. & Bryant, M.A., Crustal deformation associated with glacial fluctuations in the eastern Chugach Mountains, Alaska, J. Geophys. Res., 105, 8055-8077 (2000).
8. Larsen, C.F., Echelmeyer, K.A., Freymueller, J.T. & Motyka, R.J., Tide gauge records of uplift along the northern Pacific-North American plate boundary, 1937 to 2001, J. Geophys. Res., In Press (2003).

9. Arendt, A.A., Echelmeyer, K.A., Harrison, W.D., Lingle, C.S. &Valentine, V.B., Rapid wastage of Alaska glaciers and their contribution to rising sea level, Science, 297, 382-386, (2002).

10. Wiles, G.C., Barclay, D.J., & Calkin, P.E., Tree-ring-dated 'Little Ice Age' histories of maritime glaciers from western Prince William Sound, Alaska, The Holocene, 9, 163-173 (1999).

11. Goodwin, R.G., Holocene glaciolacustrine sedimentation in Muir Inlet and ice advance in Glacier Bay, Alaska, U.S.A., Arctic and Alpine Res., 20, 55-69, (1988).

12. Milne, G.A., et al., Space-geodetic constraints on glacial isostatic adjustment in Fennoscandia, Science, 291, 2381-2385 (2001).

13. Hillaire-Marcel, C., Multiple component post-glacial emergence, eastern Hudson Bay, Canada, Earth Rheology, Isostasy and Eustasy, ed. By N.A. Morner, 215-230, Wiley, Toronto.

14. Hicks, S.D. & Shofnos, W., The determination of land emergence from sea-level observations in southeast Alaska, J. Geophys. Res., 70, 3315-3320 (1965).

15. Horner, R.B., Seismicity in the St. Elias region of northwestern Canada and southeastern Alaska. BSSA, 73, 4, 1117-1137 (1983).

16. Larson, K.M., Bürgmann, R., Bilham, R. & Freymueller, J.T., Kinematics of the India-Eurasia collision zone from GPS measurements, J. Geophys. Res.104, 1077-1093 (1999).

17. Fletcher, H.J. & Freymueller, J.T. New constraints on the motion of the Fairweather fault, Alaska, from GPS observations, Geophys. Res. Lett., In Press (2003).

18. Clague, J.J. & James, T.S., History and isostatic effects of the last ice sheet in southern British Columbia, Quat. Sci. Rev., 21, 71-87 (2002).

19. Tushingham, A.M. & Peltier, W.R., Ice-3G: A new global model of Late Pleistocene Deglaciation based upon geophysical predictions of postglacial relative sea level change, J. Geophys. Res., 96, 4497-4523, 1991.

20. Ivins, E.R. & James, T.S., Simple models for late Holocene and present-day Patagonian glacier fluctuations and predictions of a geodetically detectable isostatic response. Geophys. J. Int., 138, 601-624 (1999).

21. Clague, J.J. & Evans, S.G., Historic retreat of Grand Pacific and Melbern Glaciers, St. Elias Mountains, Canada: an analogue for decay of the Cordilleran ice sheet at the end of the Pliestocene?, J. Glaciology, 39, 619-624 (1993).

22. Field, W.O., Glaciers of the St. Elias Mountains, in Field, W.O., ed., Mountain Glaciers of the Northern Hemisphere, 2, CRREL, Hanover, NH, 143-297 (1947).

23. Pollitz, D.F., Wicks, C. & Thatcher, W., Mantle flow beneath a continental strike slip fault: Postseismic deformation after the 1999 Hector Mine earthquake, Science, 293, 1814-1818 (2001).

24. Sigmundsson, F, Post-glacial rebound and asthenosphere viscosity in Iceland, Geophys. Res. Lett, 18, 1131-1134 (1991).

25. Cathles, L.M., The Viscosity of the Earth's Mantle, Princeton University Press, 326-328 (1975).

26. Freymueller , J.T., Cohen, S.C. & Fletcher, H.J., Spatial variations in present-day deformation, Kenai Peninsula, Alaska, and their implications, J. Geophys. Res., 105, 8079-8101 (2000).

27. Sella, G. F., Dixon, T.H. & Mao, A., REVEL: A model for recent plate velocities from space geodesy, J. Geophys. Res., 107, 2002.

28. Mao, A., Harrison, C.G.A. & Dixon, T.H. Noise in GPS coordinate time series, Journal of Geophysical Research,104, 2797-2816 (1999).

29. Wessel, P. & Smith, W.H.F., New, improved version of the Generic Mapping Tools Released, EOS Trans. AGU, 79, 579 (1998).

30. Press, W.H., Teukolsky, S.A., Vetterling, W.T. & Flannery, B.P., Numerical Recipes in C, the Art of Scientific Computing, Cambridge University Press, Cambridge, 660-661 (1992).

Chapter 3

Extreme Sea Level Changes in Southeast Alaska Associated with Post-Little Ice Age Glacial Isostatic Rebound.*

Christopher F. Larsen, Roman J. Motyka, Jeffrey T. Freymueller, Keith A. Echelmeyer and Erik R. Ivins.

Geophysical Institute, University of Alaska Fairbanks, 903 Koyukuk Dr, Fairbanks, Ak 99775.

Abstract

Extreme sea level changes in southeast Alaska have been documented by tide gauge measurements and studies of raised shorelines. These measurements are within a network of 45 Global Positioning System (GPS) measurements of crustal motion that show rapid regional uplift. New tide gauge data presented here consists of repeat occupations of 18 temporary gauge sites that post-date previously available sea level measurements. The present magnitude and distribution of regional sea level rates are similar to that found in the earlier study. Raised shoreline studies document total sea level change since ~1790 AD at 14 sites, with a maximum change in sea level of 5.7 m found in upper Lynn Canal. The start of the ongoing uplift episode that raised these shorelines is coincident with the start of the collapse of the Glacier Bay Icefield. The distribution of total sea level change is in general agreement with uplift rate measurements, with greater sea level change found at the sites closest to the peak uplift rates in upper Glacier Bay.

A viscoelastic two-layer Earth model subjected to an ice load history built upon observations of glacial change was used to predict uplift rates at the tide gauge and GPS sites as well as total uplift at the raised shoreline sites. An Earth model

---

* *In preparation, Geophysical Journal International* (2003)

consisting of a 60 ± 30 km thick elastic lithosphere overlaying a mantle half-space with viscosity (5.5 ± 0.5) x 10^{19} Pa s can match the uplift rates of the tide gauge and GPS observations at the 1σ level. The same model creates significant misfit if used to predict the raised shoreline data set, which can be modeled only if a mantle viscosity of (1.4 ± 0.1) x 10^{19} Pa s is adopted. This viscosity value conversely produces significant misfit with the GPS and tide gauge measurements. However, all three data sets are consistent with a three-layer Earth model. The combined model is constrained by a total of 77 uplift measurements, which at the 95% confidence level require a low viscosity asthenosphere (η_A = (1.4±0.3) x 10^{19} Pa s and thickness 110^{+20}_{-15} km) beneath a 50^{+30}_{-25} km thick elastic lithosphere and overlaying an upper mantle half space with a viscosity of 4 x 10^{20} Pa s.

Introduction

Icefields and glaciers in the coastal mountains of southern Alaska and Canada have undergone rapid thinning over the last 100 – 200 yrs (Goodwin, 1988; Clague and Evans, 1993; Motyka and Beget, 1996; Wiles et al., 1999; Arendt et al., 2002). Associated unloading of the Earth's surface has led to isostatic rebound in the region (Hicks and Shofnos, 1965; Clark, 1977). We previously used observed and historical ice load changes as input to viscoelastic rebound models to show that rapid uplift rates in southern Alaska, measured by the Global Positioning System (GPS), could be entirely attributed to viscoelastic rebound (Larsen et al., 2003a). In this study, we present associated changes in sea level derived from tide gauge observations and raised shoreline studies, and then compare these data to the GPS measurements and to uplift predictions from viscoelastic rebound models. Although both the tide gauge and raised shoreline observations discussed here are indications of sea level change, the two data sets are from very different measurements, and so are introduced separately.

Rapid changes in sea level in southeast Alaska were noted from tide gauge observations in southeast Alaska as early as the 1920's, and in 1959-60 a region-wide

survey was performed by NOS specifically to characterize these changes. The results were summarized by Hicks and Shofnos (1965), and a regional pattern of uplift surrounding Glacier Bay was found, with a peak rate of 40 mm/yr near the mouth of the bay. To allow for the possibility of changes in the pattern and magnitude of the regional uplift, the sea level rates that we examine here all post-date the results of Hicks and Shofnos (1965). The raised shoreline data presented here are an extension of the method described by Motyka (2003), and constrain both the timing and total magnitude of the ongoing uplift. When the sea level observations from tide gauges and raised shorelines are considered together with the GPS data of Larsen et al. (2003a), the total combined data set provides an exceptional record of the regional uplift.

Each data set is examined separately within the context of a simple two-layer viscoelastic Earth model subjected to a model of ice load changes (Larsen et al., 2003a) that are independently constrained by airborne laser altimetry (Arendt et al., 2002) and records of recent glacial change (Goodwin, 1988; Clague and Evans, 1993; Motyka and Beget, 1996; Wiles et al., 1999). Regional isostatic uplift of southern Alaska is of a scale large enough to allow determinations of upper mantle viscosity and lithosphere elastic thickness. The ultimate goal of the present study is to test various Earth models against all of the uplift observations. Specifically, we restrict this effort to a single load model that is built upon observations and measurements of glacial change, rather than iteratively constrained by the uplift data itself. The results provide robust constraints of lithospheric and asthenospheric structure, as well as the statistically significant conclusion that the regional uplift is primarily a consequence of isostatic rebound associated with post- Little Ice Age deglaciation of southern Alaska.

Tide gauge data and error analysis.

We have augmented sea level rates found at permanent tide gauges (Larsen et al., 2003b) with temporary tide gauge observations at 18 sites throughout the northern part of southeast Alaska (Table 3.1 and Fig. 3.1). Temporary tide gauges typically record sea-level over the course of one or more monthly tidal cycles, and the elevation

of the gauge is then surveyed relative to a local network of benchmarks. Mean sea level at the site is calculated and referenced to the benchmarks. When this procedure is repeated some years later, sea level change can then be found relative to the benchmarks. Temporary tide gauges are primarily installed to assist in charting of waterways for navigational purposes by the National Ocean Service (NOS). Of the data presented here, all of the initial occupations and half of the repeat occupations were performed by NOS field crews. During fieldwork between 1999-2001, we installed temporary tide gauges at 9 sites that NOS had not recently reoccupied (Table 3.1).

The tide gauge data used here can be divided into three subsets: permanent gauge data, NOS temporary gauge data and our temporary gauge data. Analysis and error estimation for the permanent gauge data used here follows Larsen et al. (2003b). NOS temporary gauge data reduction is performed entirely by the NOS, and the rates used here are simply derived from the published tidal benchmark elevations for each occupation. The rate determinations at sites that were reoccupied with our gauges are derived by comparing previous NOS published tidal benchmark information with new benchmark heights determined through a combination of our gauge readings and level surveys.

The tide gauges we installed digitally recorded water depths every 15 minutes. We conducted level surveys from the sensor zero point to the local benchmark network typically when the gauge was installed and again when it was removed, both to ensure stability of the instrument and to provide a survey check. Survey errors, from circuit closure, were typically $< \pm 10$ mm. The historic tidal benchmark information for the sites we reoccupied is given in height above mid-tide level (MTL), which is a plane midway between all high and low tide readings. This datum is convenient for older analog style instruments, whereas mean sea level (MSL) is more convenient for digital instruments. To derive MTL from our digital records, a spline-fit was used to approximate a continuous tidal record and the estimated high and low tides were taken from this spline-fit.

To reduce the effects of seasonal and oceanographic long period fluctuations in mean sea level, tidal datum planes found at temporary tide gauges are typically adjusted by a concurrent offset at the nearest permanent gauge. This concurrent offset is found by taking the datum (e.g., MTL) found at the permanent gauge over the same time period and differencing it with a stable, long-term datum found over a continuous record of 5 or more years. All of the more recent occupations by NOS and our gauges were adjusted with this concurrent offset. NOS documentation is insufficient to determine whether this adjustment was performed for many of the earlier occupations. In the error analysis that follows, we may slightly over-estimate the errors as we assume that all the initial occupations were not adjusted in this manner.

The error budget for temporary gauge measurements includes level surveying errors, tide gauge instrument errors and the variability of MSL sampled over intervals of two months or less. The first two sources, on the order of < 10 mm, while the third source is on the order of 40 - 50 mm (Swanson, 1974). To estimate the effect of MSL fluctuations over the period of temporary gauge occupations, permanent gauge records were sampled to approximate temporary gauge records, with observation periods and time spans between observations similar to the temporary gauge data used here. The permanent gauge records used in this analysis are raw monthly MSL from Sitka and Juneau. The Juneau record was repeatedly sampled, finding two average sea levels over 2 consecutive months each, with periods of 10, 20, 30 and 40 years between the two averages. To simulate the effect of adjusting the temporary gauge with a concurrent offset at the nearest permanent gauge, the later ("reoccupation") two-month samples from the Juneau MSL record were adjusted by concurrent MSL offsets at Sitka. The earlier ("initial occupation") samples were simply raw MSL that were not adjusted by this offset.

Several distributions of sea level rates thus found at Juneau are shown in Figure 3.2. We take the standard distribution of the rates found in Figure 3.2 to represent the sea level rate error at temporary tide gauges. A curve was fit to these errors vs. time span between occupations (Fig. 3.3). The errors listed in Table 3.1 for

sea level rates were assigned according to this curve and the individual period between occupations at each site. If both the initial and repeat occupations are adjusted with the concurrent MSL offset, the errors thus derived are reduced by ~20%. This gives an indication of the degree to which we may be overestimating these errors based on our assumption that NOS did not perform this adjustment on the earlier occupations.

Raised shoreline data and error analysis.

The raised shoreline measurements follow techniques described by Motyka (2003). The basic principle employed is that as shorelines are uplifted, trees will colonize the newly exposed land. At the highest sea level transgression, the tree ages show a discontinuity across a boundary between the initial colonizers and the forest that pre-dates the uplift. At this discontinuity, there are typically several geomorphic markers that allow it to be identified as a paleo-shoreline, including 1) a riser or break in slope caused by wave erosion, 2) a sudden increase in soil depth, with thick, well-developed soils above and thin soils below, and 3) the presence of beach deposits underneath the thin soils below, but not underneath the thick soils above. Additionally, at 5 of the raised shoreline sites, tephra deposits have been found upslope of these shorelines. Because this fragile, surficial deposit is easily eroded by wave action, the raised shorelines at these sites represent the greatest sea-level extent since the tephra was deposited. Dendrochronology was used to date the age of the riser and the age of the initial colonizers below the riser, which is taken to represent the date of the onset of uplift. Leveling surveys were conducted to find the height of the raised shorelines above the present shoreline, which is taken to represent the total sea level change (Motyka, 2003). Raised shorelines at 14 sites were characterized during fieldwork conducted between 1998-2001 (Table 3.2, Fig. 3.4).

The error budget of the raised shoreline data set includes survey errors, scatter in heights of shoreline points at same field site, uncertainty of tree germination elevation, and other factors discussed in Motyka (2003). One site-specific factor on the overall error is the soil type and the presence of exposed bedrock, which can make

the exact location of the paleo-shoreline hard to determine. The differences in site-specific errors are primarily due to this factor; in all respects the errors assigned follow Motyka (2003).

GPS data and error analysis.

A contour map of GPS uplift rates from 45 sites is shown in Figure 3.5. With the exception of the two continuous stations at Whitehorse (WHIT) and Gustavus (GUS2), all of the data are from campaign-style surveys, with each site typically having 2-3 occupations over 3-4 years. The daily free network solutions were transformed into the International Terrestrial Reference Frame, epoch 1997 (ITRF97). These daily solutions were used to estimate station velocities that were transformed into a North America fixed reference frame based on the REVEL model (Sella et al., 2002). The overall average error for these rates is 3.5 mm/yr, with some sites having up to 6-8 mm/yr errors. A table of site-specific rates and errors is found in Larsen et al. (2003a).

Results

The pattern of sea level changes found at the tide gauge sites indicates that the fastest sea level rates in southeast Alaska are found in Glacier Bay (Fig. 3.1). This finding is in general agreement with Hicks and Shofnos (1965), although we find peak sea level rates in upper Glacier Bay rather than at Bartlett Cove near the mouth of the bay. During fieldwork in the summer of 2001, we installed a temporary tide gauge at Bartlett cove to repeat prior NOS occupations of this site. When reducing the data for this occupation and comparing them with NOS occupations from 1937, 1959 and 1964, we found than none of the tidal benchmarks in the local reference network could be considered stable. All of these benchmarks are on boulders generally less than 3 - 5 m^3 in size, resting on unconsolidated marine sediments and moraine deposits. Level surveying records indicate relative motion of two or more benchmarks between each occupation, and by the time of our survey the entire network had been deformed. As

such, all data from this site should be considered suspect, and we rejected it from our analysis. The pattern of sea level rates found over the remaining sites agrees well with the pattern of uplift rates from GPS measurements (Fig. 3.5).

Hicks and Shofnos (1965) found a sea level rate of 35 mm/yr at Muir Inlet between occupations in 1940 and 1959. Based on the time between occupations, we assign an error of ±7 mm/yr to this rate, and as such it is not significantly different that the lower rate we find for this site (i.e., 35±7 mm/yr vs. 26±3 mm/yr). Overall, the newer sea level rates presented here are consistent with those found earlier (Hicks and Shofnos, 1965) when the associated errors are considered. We conclude that both the pattern and magnitude of regional sea level rates have remained essentially constant at the level of measurement accuracy since the time of the earliest rate measurements. This finding is in agreement with the linear sea level rates found over the entire permanent gauge records at Sitka, Juneau and Skagway (Larsen, 2002b).

The total sea level change found at the raised shoreline sites also describes a regional pattern surrounding Glacier Bay (Fig. 3.4), with the greatest sea level change at the sites closest to where the peak uplift and sea level rates are found. The dates listed in Table 3.2 for the start of emergence range from 1752 to 1861. The later dates (i.e., at Horse Fly Cove, Excursion Inlet, and Bear Creek) represent a minimum age for the start of the uplift; at these sites it was questionable if the oldest trees sampled below the riser were representative of the initial colonizers. Discounting the dates for these three sites, the average date for the start of the sea level change is 1803. At the best-studied site, 9-mile (Juneau), Motyka (2003) found that the onset of uplift started between 1770 and 1790. At this time, the collapse of the Glacier Bay Icefield had just begun and was rapidly accelerating. Between then and ~1950, the glaciers feeding this icefield retreated up bay by as much as ~100 km. The simultaneous onset of unloading and sea level change is a direct observation of the causal relationship between glacial unloading and the region's uplift.

At all of the raised shoreline sites, the total sea level change divided by the time elapsed since 1790 give sea level rates that are ~20-30% higher than found at

these sites from the rate contours of Figure 3.1. The rate of unloading since ~1950 in Glacier Bay is essentially at the level of a southern Alaska regional average; during the early stages of the collapse of the Glacier Bay Icefield it was much higher. Significantly larger elastic rebound during the height of the Glacier Bay unloading likely led to faster uplift than at present, which may explain this apparent discrepancy between total sea level change and sea level rates. This period of significantly larger elastic contribution would have been largely completed by the time of the first sea level rate measurements in the region, based on the timing of retreat within Glacier Bay (Goodwin, 1988).

Sea level rates vs. uplift rates

Sea level rates, such as those found at the temporary tide gauges here, result from sea surface (geoid) change as well as solid earth uplift. Specifically, the rate of sea surface change ($\Delta\dot{S}$) is that which would be observed from a tide gauge perfectly fixed at a set radial distance from the geocenter. To approximate the difference between uplift and sea level rates for southeast Alaska, we note that the distribution of temporary tide gauge sites used here lies within a region well sampled by GPS uplift measurements (Larsen et al., 2003a). Because in general the two types of measurements have not been co-located, the GPS rates were interpolated to form a continuous, 2nd order differentiable surface that was sampled at the tide gauge locations. The results are shown in Figure 3.6 and the average difference is found to be -0.3 ± 0.8 mm/yr (±2σ), which indicates sea surface fall rather than rise as is found in global averages (Douglas, 1997).

Although it may be counter-intuitive that $\Delta\dot{S}$ is found to fall local to melting glaciers, this result has been known for some time (e.g., Woodward, 1888). While the melting adds water to the oceans globally, reduced gravitational attraction exerted by the shrinking ice mass causes a greater effect locally on sea surface rates. Tamisiea et al. (2003) have predicted $\Delta\dot{S}$ at permanent tide gauge sites in southern Alaska related to the rapid melting of the region's glaciers. Their prediction is on the order of

$\Delta\dot{S} \approx -2.3$ mm/yr for the region where we have both GPS and tide gauge data, almost an order of magnitude greater than the results of Figure 3.6. This discrepancy does not appear to be due to our use of extrapolated GPS uplift rates; we get essentially the same result if we limit this analysis to collocated GPS-tide gauge sites ($\Delta\dot{S}$=-0.4 ± 1.0 mm/yr; 8 sites). In the following sections, when calculating misfit between viscoelastic model predictions and the sea level data of Tables 3.1 and 3.2, we approximate uplift at the tide gauge and raised shoreline sites with a constant estimate of $\Delta\dot{S}$=-0.3 mm/yr from Figure 3.6. This step allows both the tide gauge data and raised shoreline data sets to be modeled in an equivalent manner to the GPS data (Larsen et al., 2003a), and facilitates a direct comparison between each data set's model predictions.

Isostatic rebound modeling.

Earth model and ice load model.

The isostatic modeling technique used here is that of Ivins and James (1999). It assumes a gravitating, density-stratified, incompressible Earth model consisting of an elastic lithosphere and viscoelastic mantle half-space. This flat Earth approximation is sufficient to evaluate the effects of regional ice load variations over < 20° of Earth surface (Ivins and James, 1999), and thus is appropriate for uplift modeling over the spatial scale of uplift observations in southern Alaska. The regional and Glacier Bay load models used in the viscoelastic calculations here are identical to that of Larsen et al. (2003a), and are shown in Figure 3.7.

The regional load model is based on the measured thinning rates (Arendt et al., 2002), which are extrapolated back to the end of the Little Ice Age (LIA) in Alaska at 1900 AD, at which time the regional peak differential ice volume occurred. The LIA glaciation was the largest Holocene glacial expansion in Alaska, and occurred in three phases between ~1200 and 1900 AD that were synchronous across much of Alaska (Motyka and Beget, 1996; Wiles et al., 1999; Calkin et al., 2001). Prior to 1900 AD, we assign the region's advance and retreat stages each a percentage of the peak

differential ice volume. The timing and relative strength of advance, retreat and standstill stages are based on independent studies of terminal moraine positions and dendrochronology of glacially overrun trees (Motyka and Beget, 1996; Wiles et al., 1999). Details of an earlier regional glaciation between 300 and 900 AD are less well characterized (pers. comm., D. Barclay), and our model consists of a simple advance, standstill and retreat over this time frame (Fig. 3.7). We omit glacial history older than this phase because the low viscosities of the upper mantle beneath southern Alaska (Larsen et al., 2003a) will not have significant present-day response to load changes this old.

The regional load changes are distributed on an equally spaced grid of 20 km diameter disks, with the ice thickness change assigned to each disk calculated according to a southern Alaska average thickness change vs. elevation relationship (Arendt et al., 2002), and the average elevation of the ice cover within that particular grid cell. The average thickness change vs. elevation relationships for the periods 1900-1995 and 1995-2003 are from the "early" and "recent" periods, respectively (Arendt et al., 2002). We assume that the relationship from the early period can be scaled to describe all changes prior to 1900 throughout the load history.

A separate load model specific to Glacier Bay, which experienced an extreme ice volume loss locally, augments the regional load model. Glacier Bay began a rapid tidewater retreat between 1750 and 1790 AD that was mostly completed by 1950 AD. Trimlines and lateral moraines provide indications of post-1750 AD ice thickness changes within Glacier Bay (Field, 1947; Clague and Evans, 1993). We used present-day tidewater glacier analogs to estimate ice elevation profiles within Glacier Bay using these thickness changes, extending ice coverage out to the 1750 AD terminus position. Comparing these ice profiles with a digital elevation model of present day topography, we find that Glacier Bay lost a minimum of 2500 km^3 of ice from 1750 to ~1950 AD. The model of this load change was assigned a history based on Goodwin (1988), and is distributed over 5 disks (Larsen et al., 2003a).

Model results: tide gauge data.

The modeling approach used here for the tide gauge data is identical to that used in Larsen et al. (2003a). We varied lithospheric thickness and mantle viscosity of the two-layer, half-space Earth model and evaluated the misfit of the rate predictions using the Chi-square merit function (Press et al., 1992). The results are shown in Figure 3.8. As was found for the GPS data set (Larsen et al., 2003a), the best fitting models are relatively insensitive to lithospheric thickness but are critically sensitive to mantle viscosity. Misfit becomes extremely large outside of a narrow range of viscosities, and the 95% confidence region spans less than 2 x 10^{19} Pa s. Overall the tide gauge data set requires a best-fit model with slightly lower viscosity than the GPS data (5.0×10^{19} vs. 5.5×10^{19} Pa s), but not significantly so at any reasonable confidence level.

Model results: raised shoreline data.

For the purposes of modeling the raised shoreline data, we assumed that the uplift at all sites started simultaneously at 1790. Although there may be some variation in the actual timing of the uplift start between individual sites on the order of ±30 yrs, this assumption reduces computational time significantly. To model the total uplift since 1790, we calculated surface deformation at both 1790 and 2000, and then subtracted the two. Again, the ice load model used was identical to that used in Larsen et al. (2003a), and misfit was evaluated over a range of lithospheric thickness and viscosities (Fig. 3.9). Notably, this data set requires a significantly lower viscosity than either the GPS or tide gauge uplift rate measurements. The confidence regions placed on viscosity by the raised shoreline data do not overlap at any meaningful value with those of the GPS and tide gauge rate data.

Because total uplift predictions are driven more by cumulative ice thickness changes than by rate of thickness change, the raised shoreline predictions are most sensitive to the largest thickness changes in the ice load model. The Glacier Bay load model has much greater thickness changes than the regional load model, and the raised shore predictions are found to be predominantly related to the Glacier Bay load model.

Indeed, the raised shoreline predictions are reduced by less than 15% if the regional load model is omitted altogether and only Glacier Bay is considered. Sensitivity tests in which the Glacier Bay load model was varied in magnitude by ±25% changed the best-fit viscosity by only $\pm 0.1 \times 10^{19}$ Pa s.

Model comparison.

To compare the Earth models required by each data set, we have plotted the model parameters required by each data set (tide gauges, GPS and raised shorelines) as a function of misfit on the same graph (Fig. 3.10). In the middle panel of Figure 3.10, the contours represent confidence regions calculated using $\Delta\chi^2 = \chi^2 - \text{minimum}(\chi^2)$ for each data set. The $\Delta\chi^2$ merit function allows the requirements placed by each data set on the model predictions to be compared uniformly, but no longer provides information of the overall quality of fit provided by the model itself (Press et al., 1992).

Because the model attains values of $\chi_\nu^2 < 2$ for each data set (see left and right panels of Fig. 3.10), we conclude that overall the model assumed can explain each data set individually, despite the significant difference in required parameter values. All three data sets are consistent with a range of lithospheric thicknesses between ~30-60 km, although the uplift rate data sets are more permissive of higher values as well as a broader range of thickness. The viscosity required by the uplift rate measurements disagrees significantly with that required by the total uplift measurements. As noted above, model predictions of total uplift are almost exclusively sensitive to the large ice thickness changes in the Glacier Bay load model. In contrast, sensitivity tests in which we varied the magnitude of the load models show that model predictions of uplift rates are sensitive to both the regional and Glacier Bay load models.

Low viscosity asthenosphere.

The modeling technique employed here assumes a simple, two-layer structure with an elastic lithosphere overlaying a viscoelastic mantle half-space, and as such the

predictions for mantle viscosity represent an effective viscosity over the range of mantle depths in which the majority of flow is induced. Here we use the differences in sensitivity to the two load models of the uplift rate predictions and the total uplift predictions to explore the possibility of a low viscosity asthenospheric layer beneath southeast Alaska. The influence of a low viscosity asthenospheric layer has been noted in other regional scale isostasy studies (e.g., Sigmundsson, 1991; Bills et al., 1994; Kaufmann and Amelung, 2000).

The essential concept of the following analysis is that the Glacier Bay load induces mantle flow over a shallower range of mantle depths than does the regional load, due to differences in the spatial extent of the two loads. Spatial filtering of the ice load models indicates peak harmonic load wavelengths (λ) of 730 km for the regional model and 180 km for the Glacier Bay model (Fig. 3.11), and therefore 80% of the mantle flow induced by these load models occurs above mantle depths of ~350 km and ~85 km, respectively (Cathles, 1975). These mantle depths are relative to the base of the lithosphere. We will assume that the half-space viscosity required by two-layer models of the raised shoreline data is primarily a constraint on the asthenospheric viscosity beneath southeast Alaska; this assumption is correct only if the asthenospheric thickness is greater than ~85 km (Cathles, 1975).

To approximate a three-layer model consisting of an elastic lithosphere, a low viscosity asthenosphere and a viscous mantle half-space, we can consider the two-layer model viscosity required by the uplift rates to be an effective viscosity. This effective viscosity is a function of the thickness and viscosity of the asthenosphere, as well as the viscosity of the underlying mantle. The relationship outlined below allows the misfit associated with effective viscosities of the two layer models to be mapped to misfit related to the thickness and viscosity of the asthenosphere, and allows for an assessment of three-layer models by the combined data set of all GPS, tide gauge and raised shoreline measurements.

The presence of a low viscosity layer reduces the characteristic relaxation time of rebound, such that half-space models predict an effective relaxation time,

$\tau_{HS} = \tau_{effective}$. Cathles (1975) showed that the effective relaxation time is related to the upper mantle relaxation time through a factor $\Re$ that is a function of load wavenumber ($\kappa = 2\pi/\lambda$), asthenosphere thickness (D), and the ratio of asthenospheric viscosity to upper mantle viscosity (η_A/η_{UM}):

$$\tau_{HS} = \tau_{UM}\Re\left(\kappa, D, \frac{\eta_A}{\eta_{UM}}\right) \tag{1}$$

The function $\Re$ is given by Cathles (1975, eq. III-21):

$$\Re = \frac{2C'S'\tilde{\eta} + (1-\tilde{\eta})\kappa^2 D^2 + (\tilde{\eta}S'^2 + C'^2)}{(\tilde{\eta} - \tilde{\eta}^{-1})S'C' + \kappa D(\tilde{\eta} - \tilde{\eta}^{-1}) + (S'^2 + C'^2)} \tag{2}$$

where $S' = \sinh(\kappa D)$, $C' = \cosh(\kappa D)$, and $\tilde{\eta} = \frac{\eta_A}{\eta_{UM}}$

Noting that relaxation time is linearly proportional to viscosity, $\tau = \frac{2\eta\kappa}{\rho g}$, we can use the factor $\Re$ to calculate the effect of a low viscosity asthenosphere on our results for half-space mantle viscosity:

$$\eta_{HS} = \eta_{UM}\Re\left(\kappa, D, \frac{\eta_A}{\eta_{UM}}\right) \tag{3}$$

Figure 3.12 illustrates how the function $\Re$ varies with asthenospheric thickness (D) for two asthenospheric viscosities centered on the viscosity required by the raised shoreline data. In this graph, we have assumed an upper mantle (half-space) viscosity η_{UM}=4 x 10^{20} Pa s in accord with global estimates (e.g., Lambeck, 1998), and a load wavenumber κ equivalent to λ = 730 km.

Combined model.

In the combined model, a total of 77 measurements (43 GPS, 20 tide gauge and 14 raised shoreline data) are used to constrain three Earth model parameters: lithospheric elastic thickness, asthenosphere thickness and asthenosphere viscosity. The upper mantle in this model is represented by a viscoelastic half-space with η_{UM} = (2 – 5) x 10^{20} Pa s; the model results we present are for a fixed value of $\eta_{UM} = 4 \times 10^{20}$ Pa s. Again, we performed a grid search over a range of reasonable values and calculated misfit for each combination of parameters. We can combine the separate two-layer model results presented above because each combination of asthenosphere viscosity and thickness maps to a particular effective (half-space) viscosity appropriate for the uplift rate data. Specifically, we transformed the two layer model χ^2 distributions from GPS and tide gauge rates into three-layer model χ^2 by mapping misfits associated with a grid of effective viscosities (η_{HS}) onto a grid of asthenosphere viscosities (η_A) through equation 3. At each model grid point, these converted misfits were combined with the misfit found directly from the raised shoreline data. By stepping through asthenosphere thickness values while iteratively performing this mapping, we calculate χ^2 as a function of lithospheric thickness, asthenosphere viscosity and asthenosphere thickness.

The best-fit model is found to have a reduced chi-square value of χ^2_ν=2.5 at asthenosphere viscosity $\eta_A = 1.4 \times 10^{19}$ Pa s., asthenosphere thickness D = 110 km and lithospheric elastic thickness = 50 km. The residuals to this model are shown in Figure 3.13. To display the 3-d χ^2 distribution, Figure 3.14 shows contour plots drawn on the three orthogonal planes passing through this global minimum. These distributions are strongly non-Gaussian, and the minima have broad "floors" and steep "sides" so that the 99.73% confidence regions are only slightly larger than the 68.3% confidence regions. Sensitivity tests in which the value assumed for η_{UM} was varied between (2 – 5) x 10^{20} Pa s had little overall effect on either the model parameters or

this best fit value of χ^2_ν, with the exception that slightly thinner asthenospheric thicknesses (~100 km) were required when lower values of η_{UM} were assumed.

The parameter constraints shown in Figure 3.14 allow a range of lithosphere thicknesses similar to the individual two-layer model constraints shown in Figure 3.10. The asthenosphere viscosity prediction of the best fit three-layer model is the same as for the best fit two-layer model of the total uplift. However, the three-layer model allows for a wider range of asthenosphere viscosity, as there is some trade-off between asthenosphere thickness and viscosity permitted by the misfit distribution. As one might intuitively expect, the data require a thinner asthenosphere if the viscosity of this layer is lower than the best fit value, and a thicker asthenosphere if it is higher. The best fit values of the three-layer model for asthenospheric thickness and viscosity correspond to a two-layer mantle half-space effective viscosity of 5.6 x 10^{19} Pa s, essentially equivalent to the best fit value required by the uplift rate data in a two-layer model.

Finally, we note that the thinnest asthenosphere (95 km) allowed by the three-layer model misfit distribution is greater than that required by the assumption which we built this model upon: specifically, we assumed that the asthenospheric thickness beneath southeast Alaska is greater than ~85 km, and therefore the half-space viscosity required by two-layer models of the raised shoreline data is primarily a constraint on the asthenospheric viscosity.

Implications.

Studies that constrain the rheological structure of the Earth roughly fall into the three categories of 1) regional scale deformation studies caused by surface load changes related to mining, transient lakes and "small glaciers" (i.e., other than the polar ice sheets of Greenland and Antarctica), 2) global scale glacial isostatic adjustment (GIA) studies of deformation related to the rise and fall of Pleistocene ice sheets, and 3) studies of the transient deformation following large earthquakes (postseismic deformation). The uplift pattern and load changes in southern Alaska are

large compared to many of the studies that fall in the first category (i.e., Klein et al., 1997; Kaufmann and Amelung, 2000; Thoma and Wolf, 2001). Lake Bonneville is perhaps the only well-studied analog that is close both in the spatial scale and the magnitude of the load changes ($\lambda \approx 520$ km and $\Delta V \approx 9.5 \times 10^4$ km^3). Bills et al. (1994) modeled an extensive shoreline data set and found the best fitting Earth models generally consist of a 40 km thick lithosphere, a 110 km thick asthenosphere with viscosity 1×10^{18} Pa s, and a mantle lid of 150 km thickness and 3×10^{20} Pa s. The thicknesses of the lithosphere and asthenosphere in these models are in excellent agreement with our three-layer model results. However, their result for asthenospheric viscosity is an order of magnitude lower than ours.

Other regional scale studies of deformation caused by surface load changes agree with asthenospheric viscosities on the order of 10^{18} Pa s (Kaufmann and Amelung, 2000; Thoma and Wolf, 2001), although the loads used in these studies are too small to allow for a determination of asthenospheric thickness. The higher viscosity required by the data presented here may be related to differences in the tectonic settings of these other studies. High heat flow associated with mantle upwelling beneath the Basin and Range province (Bills et al., 1994; Kaufmann and Amelung, 2000) and the mid-Atlantic ridge (Thoma and Wolf, 2001) may lead to lower asthenospheric viscosities found there. Our results for lithospheric thicknesses and asthenospheric viscosities are essentially median values in the "weak mechanical regime" modeled by Ivins and James (1999), who suggest that such values are characteristic of tectonically active regions.

It is difficult to compare directly the Earth model result presented here with GIA studies owing to the larger spatial- and coarser temporal- resolutions of the load models used in such studies. In general, GIA studies provide robust constraints on bulk upper and lower mantle viscosity but provide little detailed information on uppermost mantle and crustal structure (Kaufmann and Amelung, 2000). We assumed an upper mantle viscosity based on GIA results. In a study of isostatic response to the Late Wisconsinan Cordilleran ice sheet ~1000 km to the south of our study, Clague

and James (2002) find asthenospheric viscosities in the range of (0.5 - 5) x 10^{19} Pa s are required by relative sea level and tilted lake shoreline observations. Additionally, these data require a thin elastic lithosphere (35 - 60 km thickness) in excellent agreement with our results. However, they note that the effects on uplift predictions caused by reasonable Earth model variations are small compared to those brought about by plausible variations in the ice sheet history assumed.

Comparisons with Earth models based on postseismic studies can also be difficult, although here the problem is one of ambiguity. Postseismic deformation may be caused by a combination of 1) afterslip on the main fault or neighboring ones, 2) poroelastic relaxation within the crust, and/or 3) viscoelastic relaxation of the lithosphere and asthenosphere (Bürgmann et al., 1997). With that said, our results for asthenospheric viscosity are roughly consistent with that of Pollitz et al. (1999) based on deformation following the 1992 Landers, California earthquake. Moreover, the models presented here should provide a useful starting point for future studies of viscoelastic postseismic mechanisms in southern Alaska.

Conclusions.

Large sea level changes have been measured in the northern part of southeastern Alaska with tide gauges and studies of raised shorelines. The tide gauge data set depicts a regional pattern of sea level rates from 3 to 26 mm/yr, centered over upper Glacier Bay. We find that the overall magnitude and pattern has not significantly changed since previous similar measurements (Hicks and Shofnos, 1965). Raised shorelines at 14 sites show that total sea level changes in the range of 0.9 to 5.7 m have occurred since ~1790 AD, with a regional pattern of higher uplift closest to upper Glacier Bay. The onset of uplift measured at the raised shoreline sites occurred at the same time the Glacier Bay Icefield began its dramatic collapse. Comparison between the sea level rates of the tide gauge data set with the uplift rates from GPS data (Larsen et al., 2003a) provides a measurement of regional sea surface (geoid) rate of change ($\Delta\dot{S} = -0.3 \pm 0.8$ mm/yr). This value is used to estimate uplift rates and total

uplift from the tide gauge data and raised shoreline data, respectively, to facilitate viscoelastic uplift modeling and comparison with GPS uplift rates.

When the GPS uplift rates and tide gauge uplift rates are modeled independently, the two data sets require similar constraints on the Earth model parameters (lithospheric elastic thickness and mantle half-space viscosity). The uplift data from the raised shorelines require a significantly different viscosity, which we propose is due to the almost exclusive sensitivity of this data to the large ice thickness changes local to Glacier Bay. When integrated together in a combined data set, the GPS, tide gauge and raised shoreline measurements require at the 95% confidence level a three-layer Earth model consisting of a 50^{+30}_{-25} km thick elastic lithosphere, an asthenosphere with viscosity $\eta_A = (1.4 \pm 0.3) \times 10^{19}$ Pa s and thickness 110^{+20}_{-15} km, overlaying an viscous upper mantle half-space ($\eta_{um} = 4 \times 10^{20}$ Pa s). The best-fit combined model results in an overall misfit of $\chi^2_\nu = 2.5$, and is thus able to account for a total of 77 measurements of uplift from three distinctly different techniques with a low overall degree of misfit. Furthermore, we have assumed load models based solely on independent observations of glacial change, rather than iteratively modifying load models to minimize this misfit. As such, our results show that 1) uplift observations in southeast Alaska can be entirely explained by post-glacial isostatic rebound, and 2) these observations provide robust constraints on lithospheric elastic thickness, asthenosphere thickness and asthenosphere viscosity.

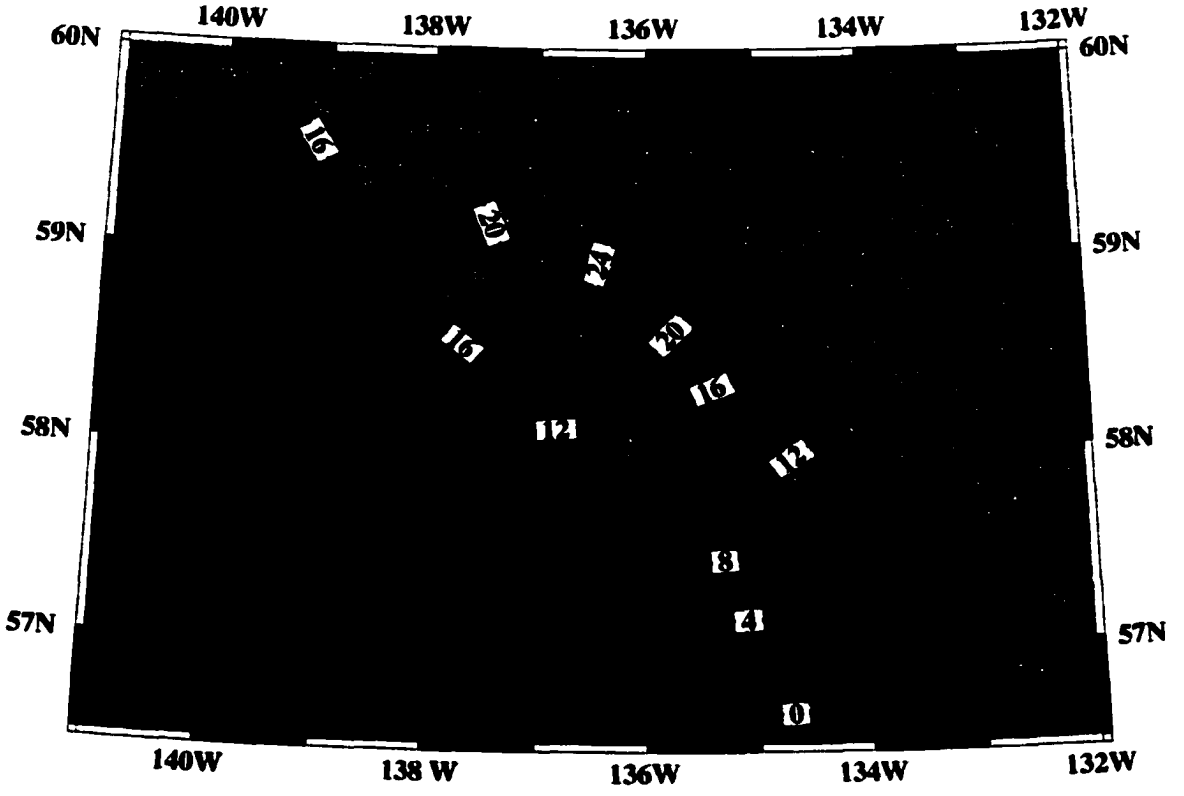

Figure 3.1. Sea level rates from tide gauge data. Contour interval is 2 mm/yr. Red diamonds indicate tide gauge sites. Glaciers and icefields are shown in light purple.

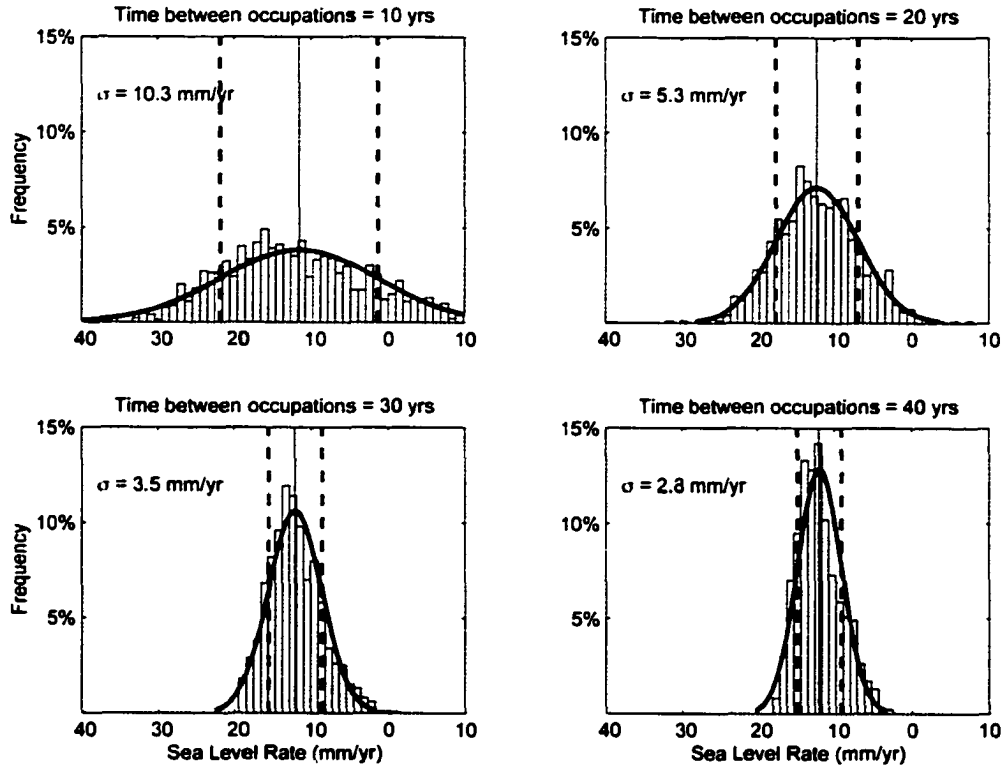

Figure 3.2. Histograms of sea level rates. Rates are found by repeatedly (1000 times each) sampling the Juneau permanent tide gauge monthly mean sea level record. Prior to sampling, the record was partially corrected for concurrent mean sea level offsets observed at the Sitka permanent gauge (see text). Rates were calculated over record subsets that simulate a typical temporary tide gauge data set. This subset is formed by randomly selecting two consecutive months from within the record, then two more consecutive months are randomly selected from within (X ± 0.5) years later, where X = 10, 20, 30, 40 years. The red curves overlaying the histograms show Gaussian distributions over the range of rates found; the solid and dashed vertical lines show the mean and standard deviation, respectively. The standard deviations (σ) found from each time span are used to assign errors to the temporary tide gauge sea level rates (see Fig. 3.3).

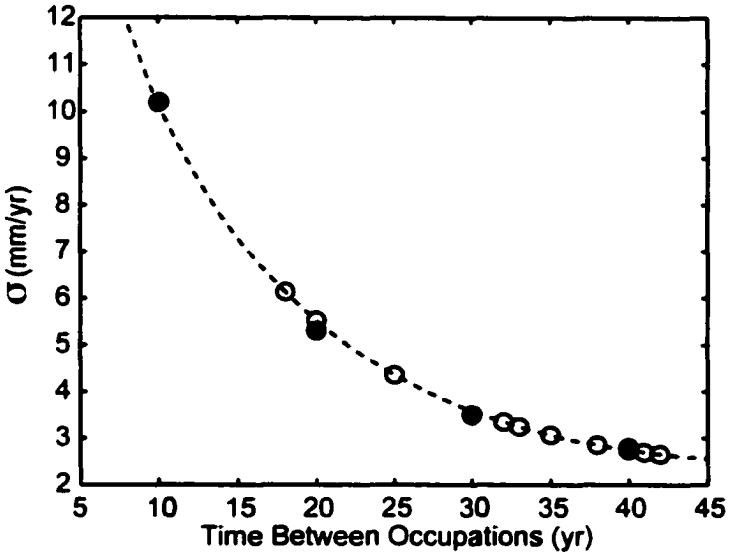

Figure 3.3. Sea level rate errors vs. time. The x-axis is time between occupations at temporary tide gauges. The points plotted as solid circles are taken from the analysis in Figure 3.2, to which a logarithmic regression was fit (dashed line). The errors assigned to the sea level rates in Table 3.1, shown by open circles, are found according to this regression and the time span between occupations.

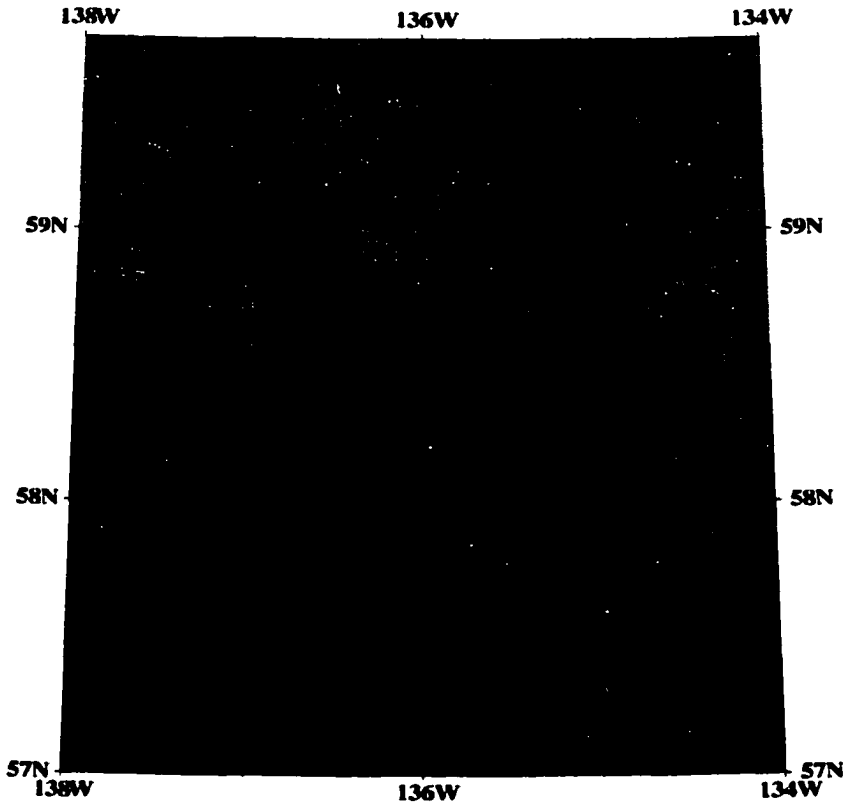

Figure 3.4. Total sea level change found at raised shoreline sites. Sea level change is indicated both in meters and by the height of the bar plotted at each site.

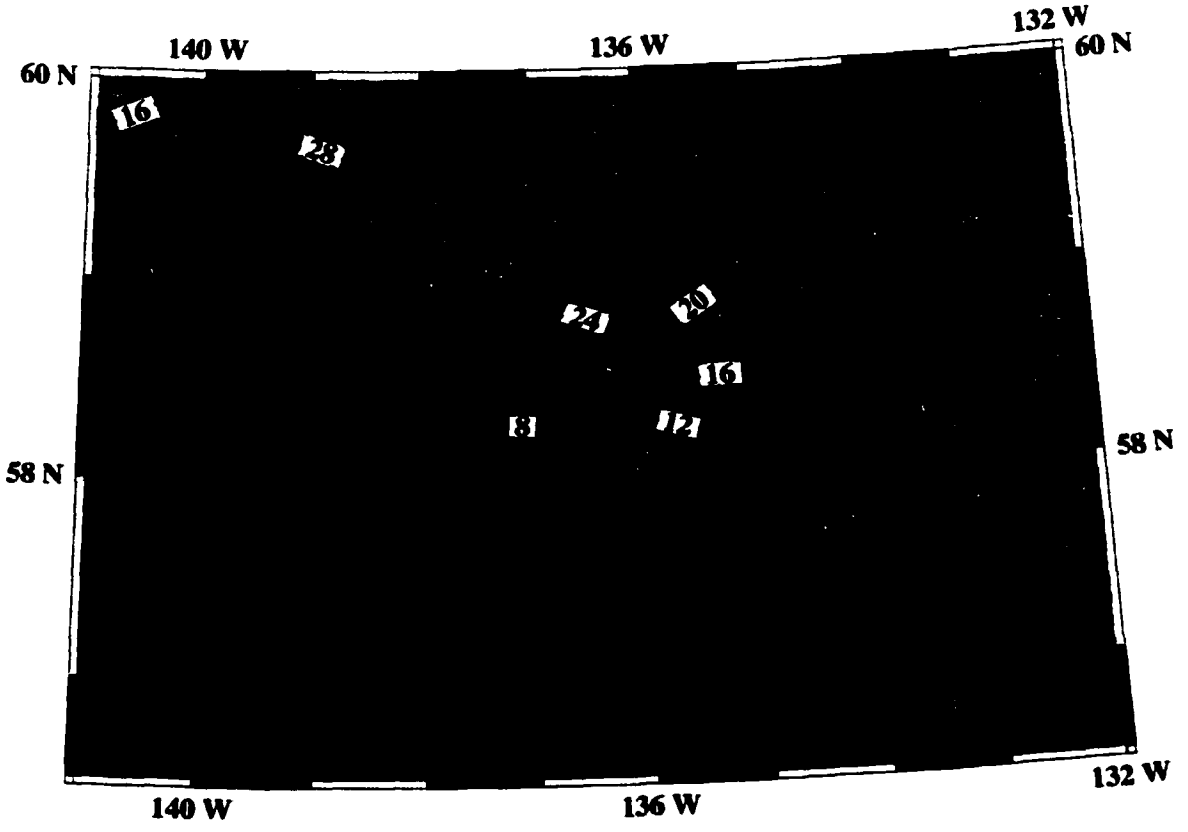

Figure 3.5. GPS uplift rates. Rates are from Larsen et al. (2003a). Contour interval is 2 mm/yr.

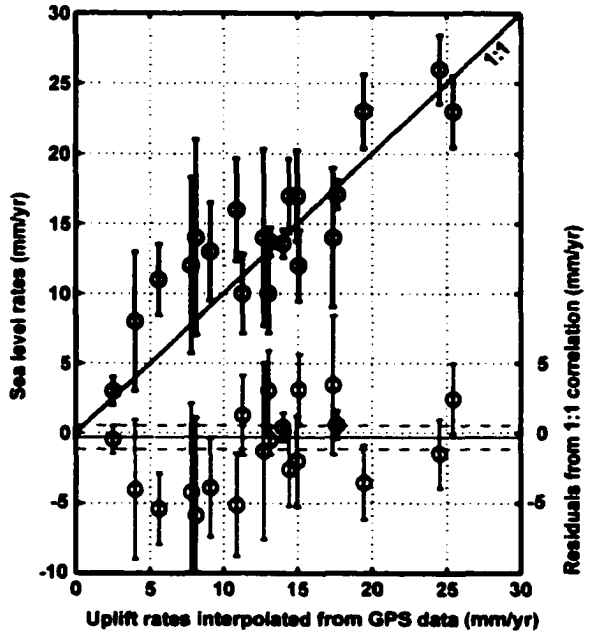

Figure 3.6. Sea level rates vs. uplift rates interpolated from GPS measurements. GPS uplift rates from Larsen et al. (2003a) were interpolated to estimate uplift at tide gauge sites (blue circles). The sea level rates are shown with the errors found in Figure 3.3; the errors for the interpolated GPS uplift rates are on the order of ± 4 – 8 mm/yr. The right hand vertical axis shows the residuals from a 1:1 correlation (red open circles). The weighted mean of these residuals is –0.3 mm/yr, shown by the solid red horizontal line with ±2σ of this mean shown by the dashed red lines.

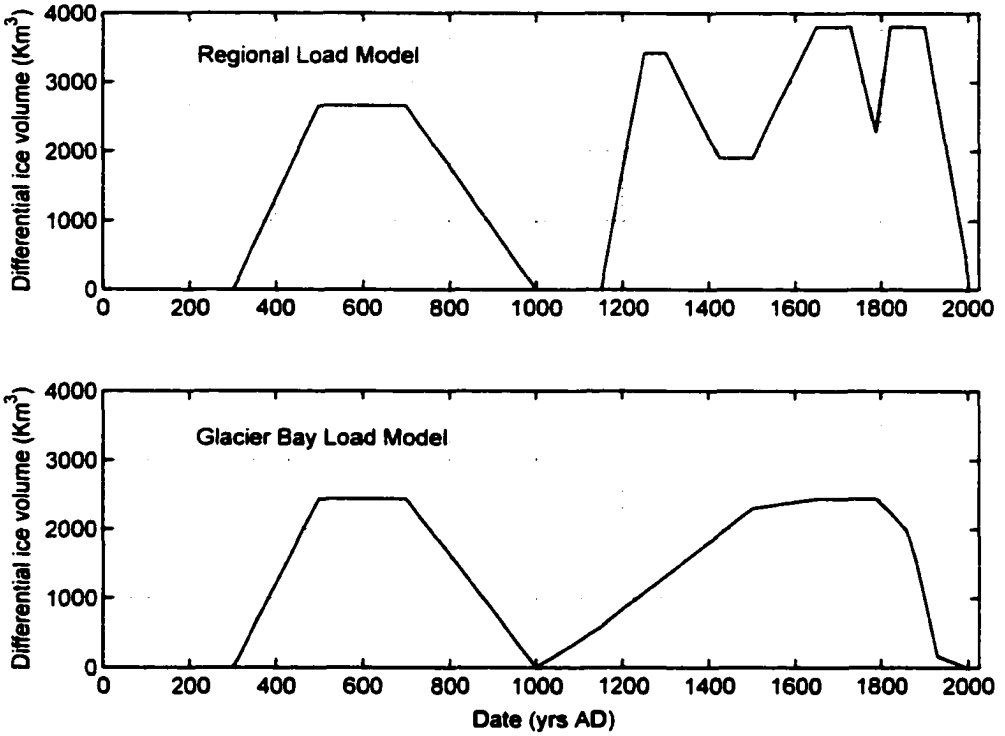

Figure 3.7. Regional and Glacier Bay ice load models used in viscoelastic modeling.

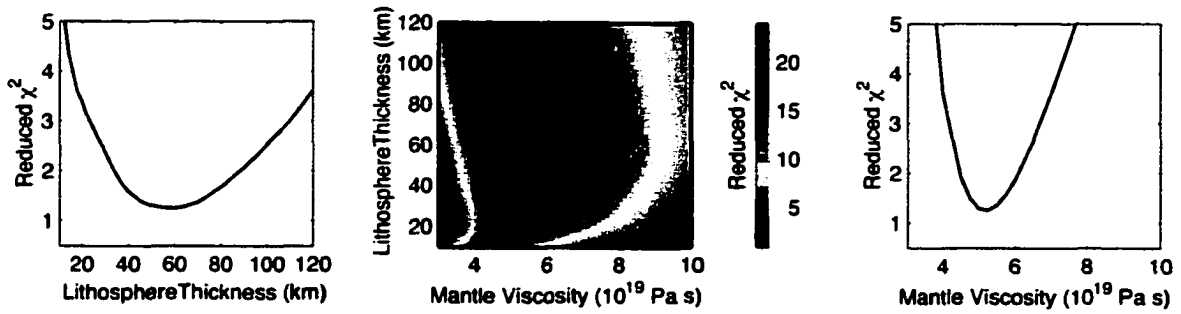

Figure 3.8. Misfit of the tide gauge uplift rates. Misfit is shown as a function of Earth model parameters, evaluated using the chi-square (χ^2) merit function; Reduced chi-square is defined $\chi^2_\nu = \chi^2/\nu$ where ν = degrees of freedom (in this case, 20). A) Misfit vs. lithospheric elastic thickness for the best-fit mantle viscosity. B) Misfit, shown by the color scale, over the range of Earth model parameters. The best-fit Earth model is shown by the red cross, and has $\chi^2_\nu = 1.3$. The 95% confidence region is shown by the red contour line. C) Misfit vs. mantle viscosity for the best-fit lithospheric thickness.

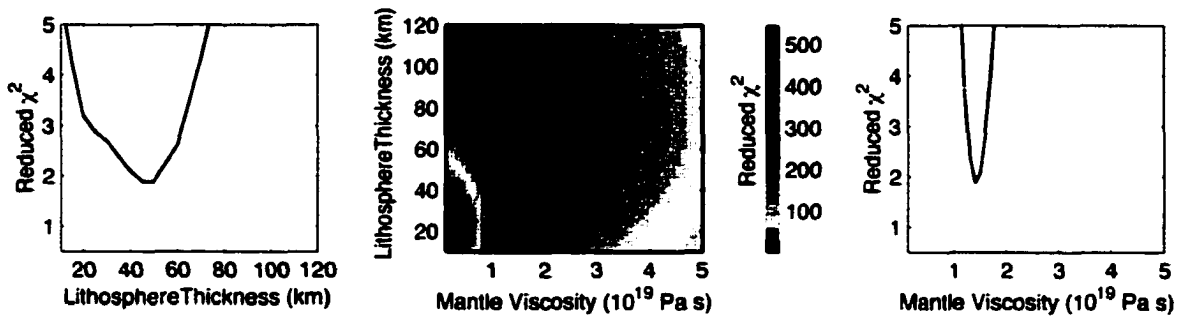

Figure 3.9. Misfit of total uplift at raised shoreline sites. Misfit is shown as a function of Earth model parameters, evaluated using χ^2_ν (in this case degrees of freedom ν = 12). A) Misfit vs. lithospheric elastic thickness for the best-fit mantle viscosity. B) Misfit, shown by the color scale, over the range of Earth model parameters. The best-fit Earth model is shown by the red cross, and has $\chi^2_\nu = 1.8$. The 95% confidence region is shown by the red contour line. C) Misfit vs. mantle viscosity for the best-fit lithospheric thickness.

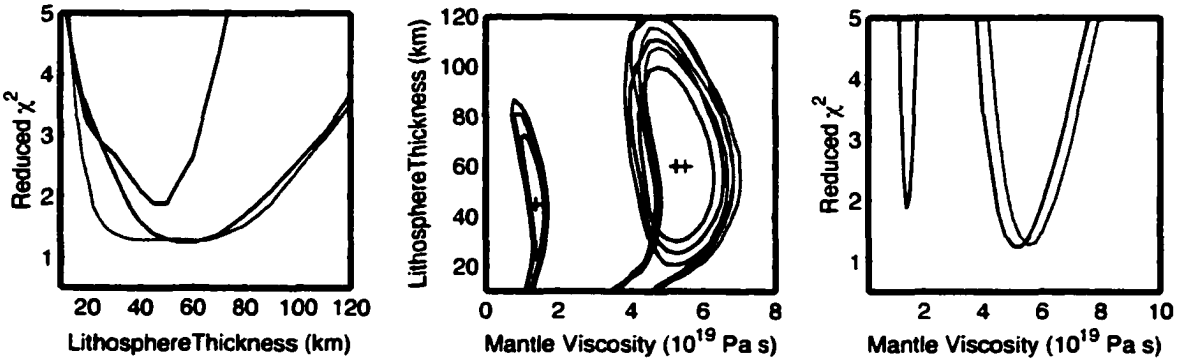

Figure 3.10. Model comparison. GPS misfit is shown in red, tide gauge misfit in blue and raised shoreline misfit in black. In left panel, the misfit of each data set is shown as a function of lithospheric thickness. The middle panel shows a contour map of $\Delta\chi^2$ confidence regions as a function of lithospheric thickness and mantle (half-space viscosity). The three contours for each data type correspond to 68.3%, 95.4% and 99.73% confidence regions of $\Delta\chi^2$. The right panel shows misfit of each data set as a function of mantle (half-space) viscosity. Note the extreme sensitivity of the raised shoreline misfit to slight variations in viscosity.

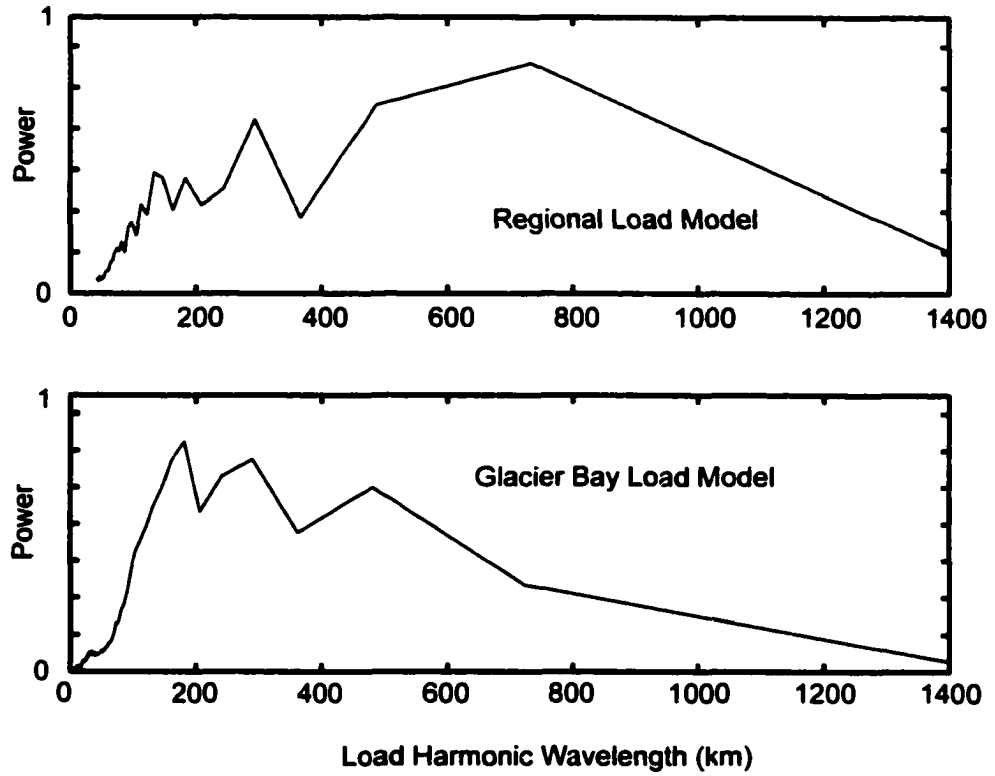

Figure 3.11. Spatial power spectrum of the two load models. Units of the y axis (power) are normalized to allow spectrum comparison. The top panel shows that the peak power of the regional load model is found at harmonic load wavelength $\lambda = 730$ km. The bottom panel shows that the peak power of the Glacier Bay load model is found at $\lambda = 180$ km.

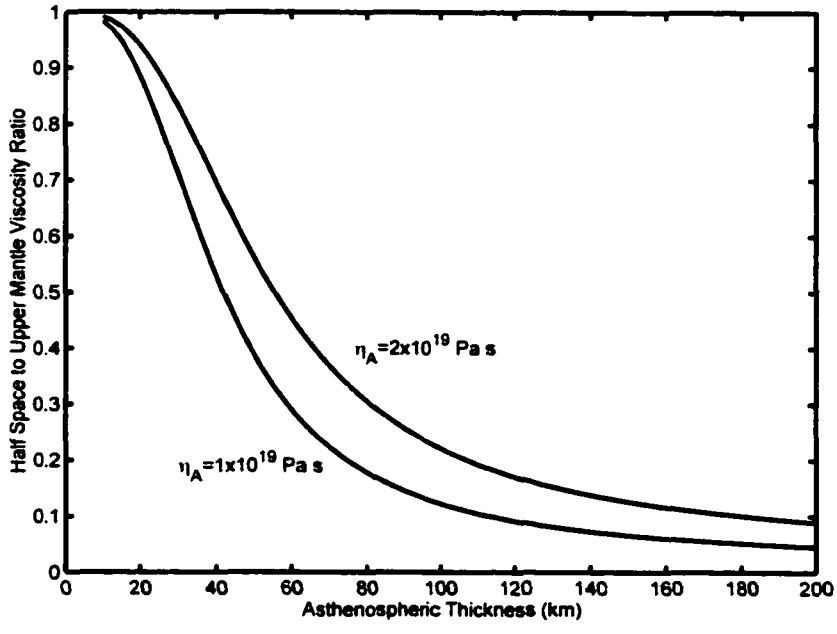

Figure 3.12. Asthenosphere thickness vs. $\Re$. $\Re$ is the ratio of upper mantle viscosity to asthenosphere viscosity as stated in equation 3. The two curves correspond to different values of asthenosphere viscosity (η_A) in equation 3, as noted on the graph. The value of κ assumed corresponds to a harmonic load wavelength of λ = 730 km, as determined from spatial filtering of the regional load model. η_{UM} is assumed to be 4 x 10^{20} Pa s.

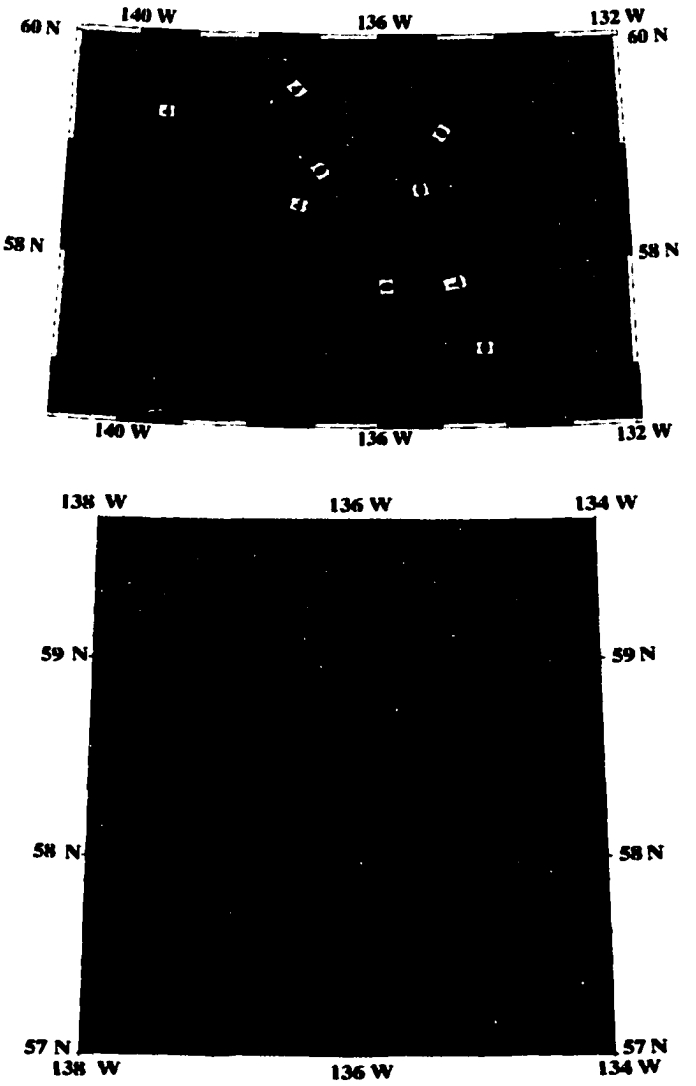

Figure 3.13. Residuals from the best fit three-layer model. This model has asthenosphere viscosity η_A = 1.4 x 10^{19} Pa s., asthenosphere thickness D = 110 km and lithospheric elastic thickness = 50 km. The upper panel shows contours of uplift rate residuals found over the combined GPS and tide gauge data sets (2 mm/yr contour interval). Tide gauge sites are shown by open blue circles and GPS sites by red diamonds. The lower panel shows the total uplift residuals found at the raised shoreline sites, indicated both in meters and by the height of the bar plotted at each site. Blue bars indicate that observations are greater than model predictions, and red bars indicate that observations are less than model predictions.

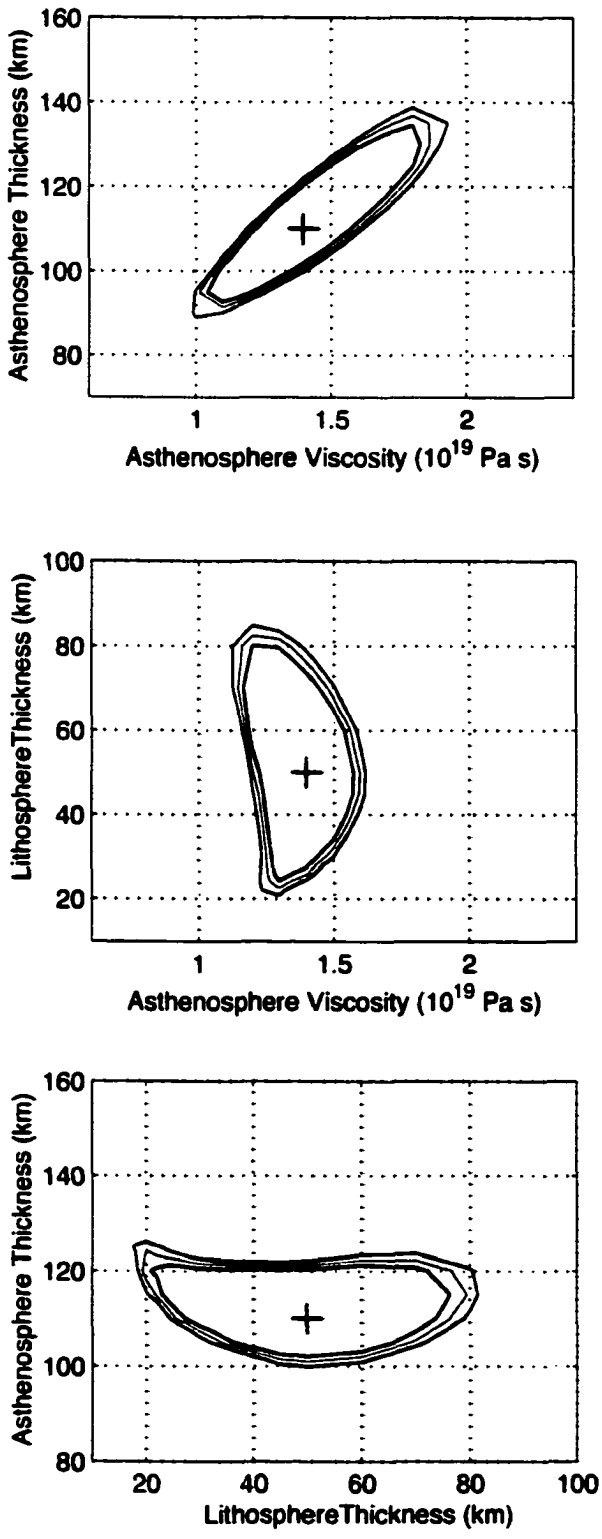

Figure 3.14. Contour maps of $\Delta\chi^2$ confidence regions for three-layer Earth models that satisfy the combined tide gauge, GPS and raised shoreline data set of 77 uplift observations. The plots are on three slices of the $\Delta\chi^2$ volume distribution through the global minimum located at asthenosphere viscosity η_A = 1.4 x 10^{19} Pa s., asthenosphere thickness D = 110 km and lithospheric elastic thickness = 50 km. Each plot has three contours that correspond to 68.3%, 95.4% and 99.73% confidence regions of $\Delta\chi^2$. The top panel shows misfit as a function of asthenosphere viscosity and thickness at a constant value of lithospheric thickness = 50 km. The middle panel shows misfit as a function of asthenosphere viscosity and lithospheric thickness at a constant value of asthenosphere thickness = 110 km. The bottom panel shows misfit as a function of lithospheric thickness and asthenosphere thickness at a constant value of asthenosphere viscosity = 1.4 x 10^{19} Pa s.

Table 3.1. Tide gauge sea level rates. Occupation dates are listed for the temporary tide gauge sites. Agency refers to who performed the second occupation of the site; all initial occupations were by NOS. Duration refers to the length of time of the second occupation. Very short occupations were a result of equipment failures.

Site	Longitude	Latitude	S.L. Rate (mm/yr)	Occupation Dates	Agency	Duration (months)
Muir Inlet	-136.11	58.91	26 ± 3	1959 & 2001	UAF	1
Willoughby Island	-136.12	58.61	23 ± 5	1961 & 2001	UAF	0.3
Composite Island	-136.57	58.89	23 ± 3	1959 & 2000	UAF	1.5
Excursion Inlet South	-135.44	58.42	17 ± 3	1964 & 1999	NOS	2
Lituya Bay	-137.62	58.61	17 ± 3	1959 & 1999	UAF	2
Inian Cove	-136.33	58.26	16 ± 4	1959 & 1991	NOS	2
William Henry Bay	-135.23	58.71	14 ± 5	1959 & 1984	NOS	3
Swanson Inlet	-135.11	58.20	14 ± 6	1960 & 1980	NOS	2
Salt Lake Bay	-135.66	57.96	14 ± 7	1982 & 2000	UAF	2
Elfin Cove	-136.34	58.19	13 ± 4	1959 & 1992	NOS	1
Auke Bay	-134.65	58.38	12 ± 3	1959 & 2000	UAF	2
Tenakee Springs	-135.21	57.78	12 ± 6	1960 & 1980	NOS	2
Miner Island	-136.34	58.01	11 ± 3	1959 & 2000	UAF	0.7
Annex Creek	-134.10	58.32	10 ± 3	1959 & 1997	NOS	1
Taku Harbor	-134.01	58.07	10 ± 3	1959 & 1997	NOS	2
Pt. Sinbad	-135.65	57.41	8 ± 5	1976 & 2001	UAF	2
Skagway	-135.33	59.45	17.1 ± 1	Permanent Gauge		
Yakutat	-139.74	59.55	13.7 ± 1	Permanent Gauge		
Juneau	-134.41	58.30	13.6 ± 1	Permanent Gauge		
Sitka	-135.34	57.05	3.0 ± 1	Permanent Gauge		

Table 3.2. Raised shoreline total sea level change. The dates listed for the start of emergence represent a minimum age of the onset of sea level change (see text).

Site	Longitude	Latitude	Total Sea Level Change (m)	Start of emergence
Sullivan Cove	-135.36	58.92	5.7 ± 0.3	1752
Pleasant Island	-135.70	58.38	4.9 ± 0.3	1815
Horse Fly Cove	-136.41	58.37	4.2 ± 0.5	1861
Excursion Inlet	-135.47	58.46	4.2 ± 0.5	1850
Graves Harbor	-136.69	58.27	4.0 ± 0.3	1825
Goose Island	-136.04	58.21	3.7 ± 0.3	1784
Boat Harbor	-135.16	58.65	3.6 ± 0.3	1822
Inian Cove	-136.33	58.26	3.5 ± 0.5	1823
Echo Cove	-134.96	58.67	3.3 ± 0.5	1815
9-mile, Juneau	-134.57	58.36	3.1 ± 0.2	1798
Bear Creek	-136.30	58.01	2.8 ± 0.5	1850
Lisianski Strait	-136.37	57.93	2.6 ± 0.5	1791
Kadashan Bay	-135.23	57.73	1.8 ± 0.3	1812
Sulioa Bay	-135.65	57.41	0.9 ± 0.3	?

References

Arendt, A.A., Echelmeyer, K.A., Harrison, W.D., Lingle, C.S. &Valentine, V.B., Rapid wastage of Alaska glaciers and their contribution to rising sea level, *Science*, **297**, 382-386, (2002).

Bills, B.G., Currey, D.R., & Marshall, G.A., Viscosity estimates for the crust and upper mantle from patterns of lacustrine shoreline deformation in the eastern Great Basin, J. *Geophys. Res.*, 99, 22,059-22,086 (1994).

Bürgmann, R., Segall, P., Lisowski, M., & Svarc, J.L., Postseismic strain following the Loma Prieta earthquake from repeated GPS measurements, in *The Loma Prieta, California, earthquake of October 17, 1989*, ed. Reasenburg, *U.S. geol. Surv. Prof. Pap.*, **1558**, 209-244 (1997).

Calkin, P.E., G.C. Wiles and D.J. Barclay, Holocene coastal glaciation of Alaska, *Quat. Sci. Rev.*, **20**, 449-461, 2001

Cathles, L.M., *The Viscosity of the Earth's Mantle*, Princeton University Press, 326-328 (1975).

Clague, J.J. & Evans, S.G., Historic retreat of Grand Pacific and Melbern Glaciers, St. Elias Mountains, Canada: an analogue for decay of the Cordilleran ice sheet at the end of the Pliestocene?, *J. Glaciology*, **39**, 619-624 (1993).

Clague, J.J. & James, T.S., History and isostatic effects of the last ice sheet in southern British Columbia, *Quat. Sci. Rev.*, **21**, 71-87 (2002).

Clark, J.A., An inverse problem in glacial geology: The reconstruction of glacier thinning in Glacier Bay, Alaska between A.D. 1910 and 1960 from relative sea-level data. *J. Glaciology*, **18**, 481-503 (1977).

Douglas, B.C., Global sea level rise: A redetermination, *Surv. Geophys.*, **18**, 279-292, 1997

Field, W.O., Glaciers of the St. Elias Mountains, in *Field, W.O., ed., Mountain Glaciers of the Northern Hemisphere*, **2**, CRREL, Hanover, NH, 143-297 (1947).

Goodwin, R.G., Holocene glaciolacustrine sedimentation in Muir Inlet and ice advance in Glacier Bay, Alaska, U.S.A., *Arctic and Alpine Res.*, **20**, 55-69, (1988).

Hicks, S.D. & Shofnos, W., The determination of land emergence from sea-level observations in southeast Alaska, *J. Geophys. Res.*, **70**, 3315-3320 (1965).

Ivins, E.R. & James, T.S., Simple models for late Holocene and present-day Patagonian glacier fluctuations and predictions of a geodetically detectable isostatic response. *Geophys. J. Int.*, **138**, 601-624 (1999).

Kaufmann, G. & Amelung, F., Reservoir-induced deformation and continental rheology in vicinity of Lake Mead, Nevada, *J. Geophys. Res.*, **105**, 16341-16358 (2000).

Klein, A., Jacoby, W., & Smilde, Mining-induced crustal deformation in northwest Germany: Modeling the rheological structure of the lithosphere, *Earth Planet. Sci. Lett.*, **147**, 107-123 (1997).

Larsen, C.F., Echelmeyer, K.A., Freymueller, J.T., Motyka, R.J. & Ivins, E.R., Rapid uplift of southern Alaska caused by recent ice loss, *Nature, submitted* (2003a)

Larsen, C.F., Echelmeyer, K.A., Freymueller, J.T. & Motyka, R.J., Tide gauge records of uplift along the northern Pacific-North American plate boundary, 1937 to 2001, *J. Geophys. Res., In Press* (2003b).

Motyka, R.J., & Beget, J.E, Taku Glacier, southeast Alaska, U.S.A.: Late Holocene history of a tidewater glacier. *Arctic and Alpine Research* **28**, 42-51 (1996).

Motyka, R.J., Little Ice Age Subsidence and Post Little Ice Age Uplift at Juneau, Alaska Inferred from Dendrochronology and Geomorphology, *Quat. Res., In Press*, (2003).

Pollitz, D.F., Wicks, C. & Thatcher, W., Mantle flow beneath a continental strike slip fault: Postseismic deformation after the 1999 Hector Mine earthquake, *Science*, **293**, 1814-1818 (2001).

Press, W.H., Teukolsky, S.A., Vetterling, W.T. & Flannery, B.P., *Numerical Recipes in C, the Art of Scientific Computing*, Cambridge University Press, Cambridge, 660-661 (1992).

Sella, G. F., Dixon, T.H. & Mao, A., REVEL: A model for recent plate velocities from space geodesy, *J. Geophys. Res.*, **107**, 2002.

Sigmundsson, F, Post-glacial rebound and asthenosphere viscosity in Iceland, *Geophys. Res. Lett*, **18**, 1131-1134 (1991).

Swanson,R.L., Variablity of tidal datums and accuracy in determining datums from short series of observations, NOAA Tech. Rep. NOS 64, Sliver Spring, MD, 41, 1974.

Tamisiea, M., Mitrovica, J.X., & Davis, J.L., A method for detecting rapid mass flux of small glaciers using local sea level variations, *Earth Planet. Sci. Lett.*, submitted (2003).

Thoma, M. & Wolf, D., Inverting land uplift near Vatnajökull, Iceland, in terms of lithosphere thickness and viscosity stratification, *Gravity, Geoid and Geodynamics 2000,* ed. by Sideris, M.G., Springer-Verlag, Berlin, 97-102 (2001).

Wessel, P. & Smith, W.H.F., New, improved version of the Generic Mapping Tools Released, *EOS Trans. AGU,* **79**, 579 (1998).

Wiles, G.C., Barclay, D.J., & Calkin, P.E., Tree-ring-dated 'Little Ice Age' histories of maritime glaciers from western Prince William Sound, Alaska, *The Holocene,* **9**, 163-173 (1999).

Woodward, R.S., On the form and position of mean sea level, *US Geol. Surv. Bull.*, **48**, 87-170, (1888).

Appendix

The survey data and reduced tide gauge records from the 8 UAF temporary tide gauge occupations are shown in Figures 3.A1-1 through 3.A-8. Listed at the top of each figure is the station name, and the year and days of our observations. The year of the most recent National Ocean Service (NOS) occupation is listed next. The serial number of the tide gauge instrument used and calibration information are shown. The name for each benchmark surveyed is shown in the schematic, as well as the height above the sensor zero point. The sensor to datum values listed are from the sensor zero point to reduced Mean Sea Level (MSL) and/or Mean Tide Level (MTL). The raw gauge output, calibrated water depth, and seasonal correction are shown in the table below the schematic. At the bottom of this table, the previous NOS determined benchmark height is listed. The difference between our height and this previous height is divided by the time elapsed between the occupations to find the rate listed beneath the table. Finally, notes about the quality of the benchmarks and the occupation are listed at the very bottom of the figure.

Station Name: Bartlett Cove
Time Span of UAF-GI Observations: Julian Days 174.5-229.7; 2001
Date of most recent NOS Survey: 1967
Logger s/n: 2901
Logger Calibraton: Slope m=1.0342; Intercept b=-0.008068

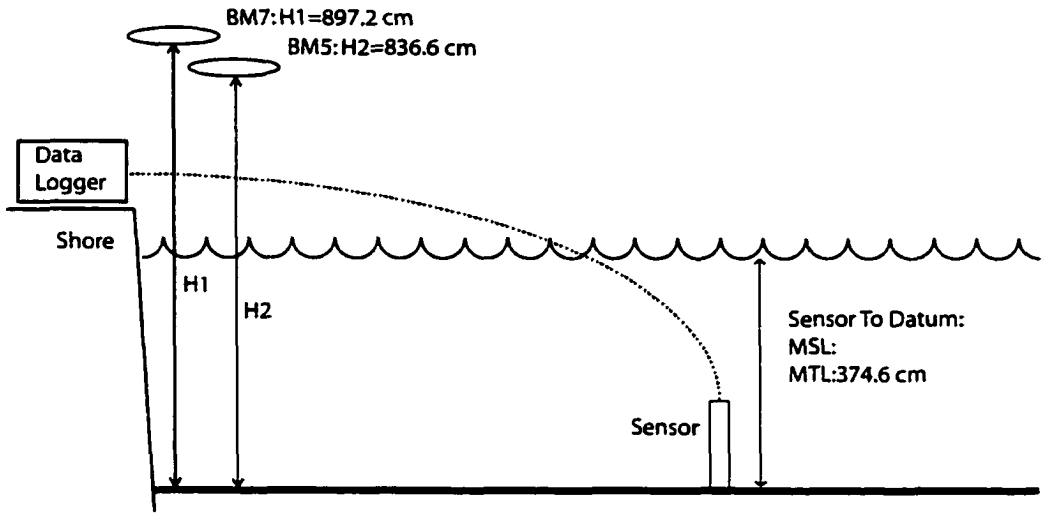

Datum	Raw Data	Calibrated	Seas. Corr. Juneau	Sensor to datum	BM 7 to Datum
MSL 2001	3.7332	3.612	-0.1135		
MTL 2001	3.7338	3.613	-0.1337	3.746	5.226
MHW 2001	5.5205				
MLW 2001	1.9468				
MTL 1967					4.523

Rate=2.1 cm/yr

Notes: BM5, and all other BM's are unstable. Poorly monumented overall.

Figure 3.A-1. Bartlett Cove tide gauge.

Station Name: Composite Island
Time Span of UAF-GI Observations: Julian Days 170-212.4; 2000
Date of most recent NOS Survey: 1959
Logger s/n:3705
Logger Calibraton: Slope m= 1.0166; Intercept b=0.000

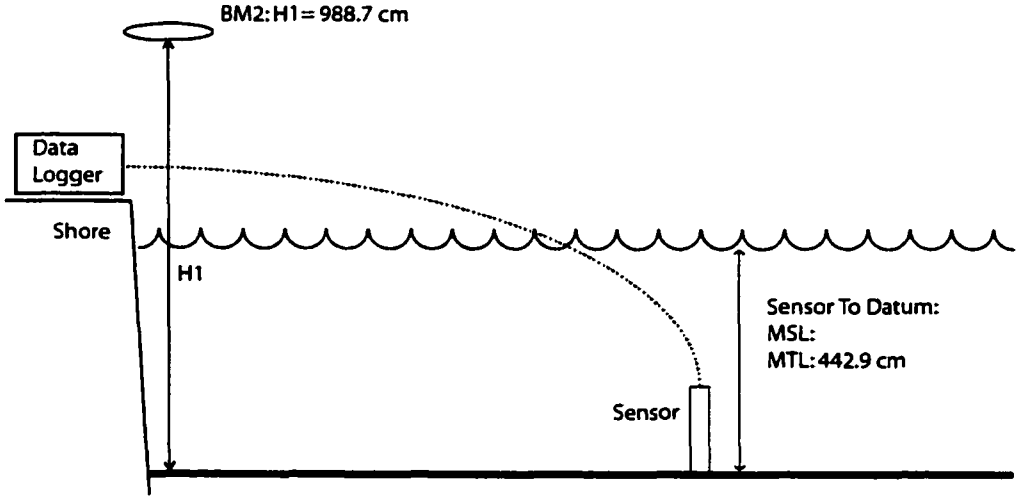

Datum	Raw Data	Calibrated	Seas. Corr. Juneau	Sensor to datum	BM 2 to Datum
MSL 2000	4.2416	4.3119	-0.1161		
MTL 2000	4.2469	4.3173	-0.1119	4.429	5.458
MHW 2000	6.3879		+1.9256		
MLW 2000	2.1058		-2.1496		
MTL 1959					4.526

Rate=2:3 cm/yr

Notes: BM2 is in bedrock.

Figure 3.A-2. Composite Island tide gauge.

Station Name: Lituya Bay
Time Span of UAF-GI Observations: Julian Days 206-268;1999
Date of most recent NOS Survey: 1959
Logger s/n: 2901
Logger Calibraton: Slope m= 1.018719; Intercept b=+0.01614

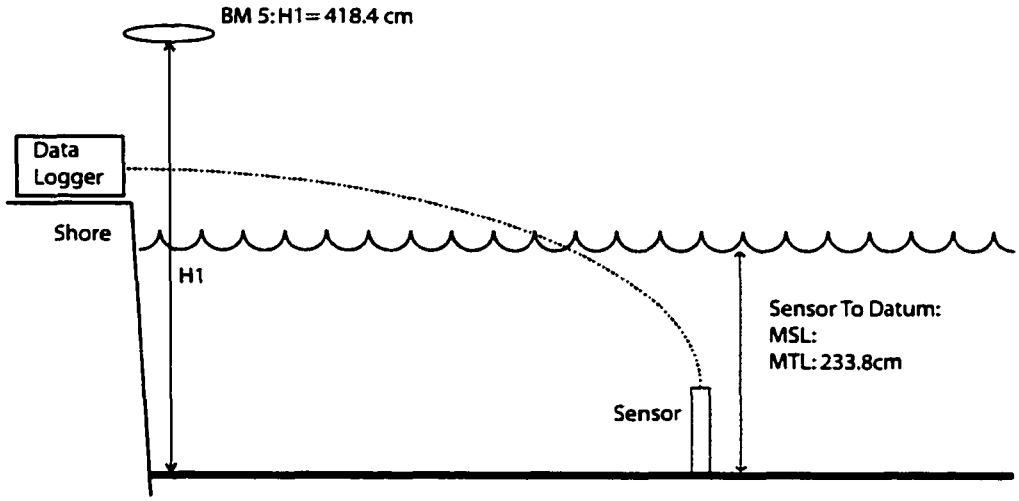

Datum	Raw Data	Calibrated	Seas. Corr. Yakutat	Sensor to datum	BM 5 to Datum
MSL 1999	2.3090	2.2618	-0.0625		
MTL 1999	2.3158	2.2684	-0.0696	2.338	1.846
MHW 1999	3.4705				
MLW 1999	1.1610				
MTL 1959					1.173

Rate=1.7 cm/yr

Notes: BM5 is in a large buried boulder or bedrock.

Figure 3.A-3. Lituya Bay tide gauge.

Station Name: Miner Island
Time Span of UAF-GI Observations: Julian Days 160.5-181.9; 2000
Date of most recent NOS Survey: 1959
Logger s/n: 2901
Logger Calibraton: Slope m= 1.0195; Intercept b=+0.00807

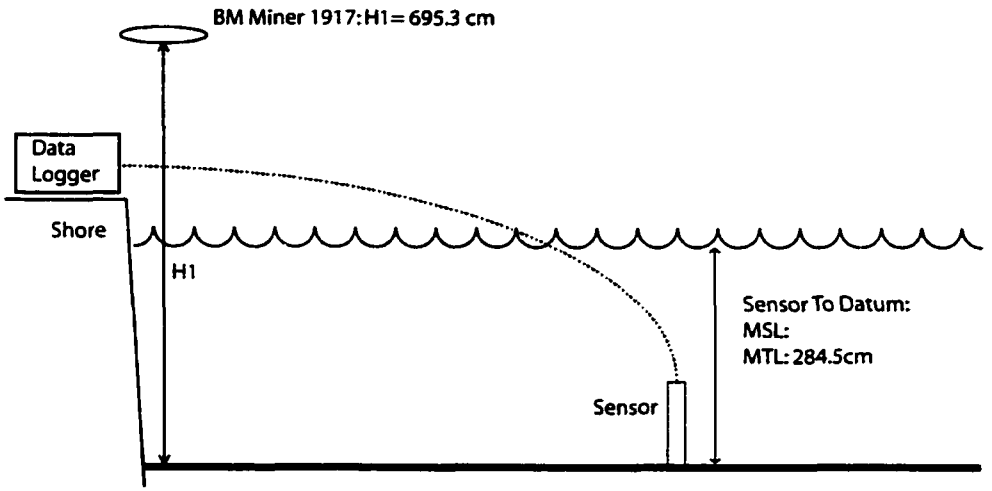

Datum	Raw Data	Calibrated	Seas. Corr. Sitka	Sensor to datum	BM 2 to Datum
MSL 2000	2.7633	2.708	-0.1772		
MTL 2000	2.7184	2.664	-0.1807	2.845	4.108
MHW 2000	4.2160				
MLW 2000	1.2206				
MTL 1959					3.679

Rate=1.1 cm/yr

Notes: Logger malfunction. Data used are from a larger data set; selected based on appearence.
BM Miner 1917 is in bedrock.

Figure 3.A-4. Miner Island tide gauge.

Station Name: Muir Inlet, Hunter Cove
Time Span of UAF-GI Observations: Julian Days 174.6-206.6; 2001
Date of most recent NOS Survey: 1959
Logger s/n:
Logger Calibraton: Slope m=1.072; Intercept b=-0.00931

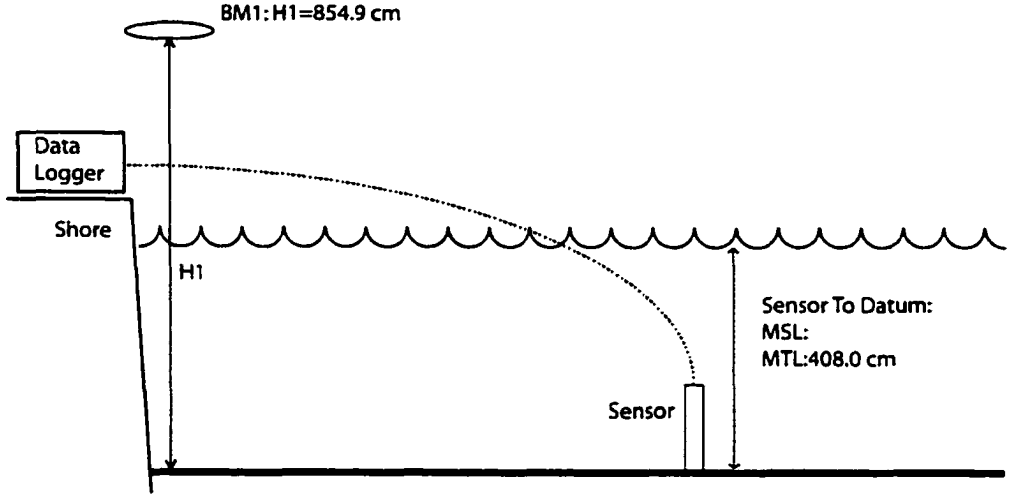

Datum	Raw Data	Calibrated	Seas. Corr. Juneau	Sensor to datum	BM 1 to Datum
MSL 2001	4.1449	3.907	-0.1362		
MTL 2001	4.1742	389.7	-0.1831	4.080	4.469
MHW 2001	6.3730		+1.8624		
MLW 2001	1.9468		-2.2286		
MHHW 2001	6.6310				
MLLW 2001	1.2370				
MTL 1959					3.368

Rate=2.6 cm/yr

Notes: BM1 is in bedrock.

Figure 3.A-5. Muir Inlet tide gauge.

Station Name: Pt Sinbad, Sergius Narrows
Time Span of UAF-GI Observations: Julian Days 235.4-299.3; 2000
Date of most recent NOS Survey: 1976
Logger s/n: 2901
Logger Calibraton: Slope m= 1.018719; Intercept b=+0.00807

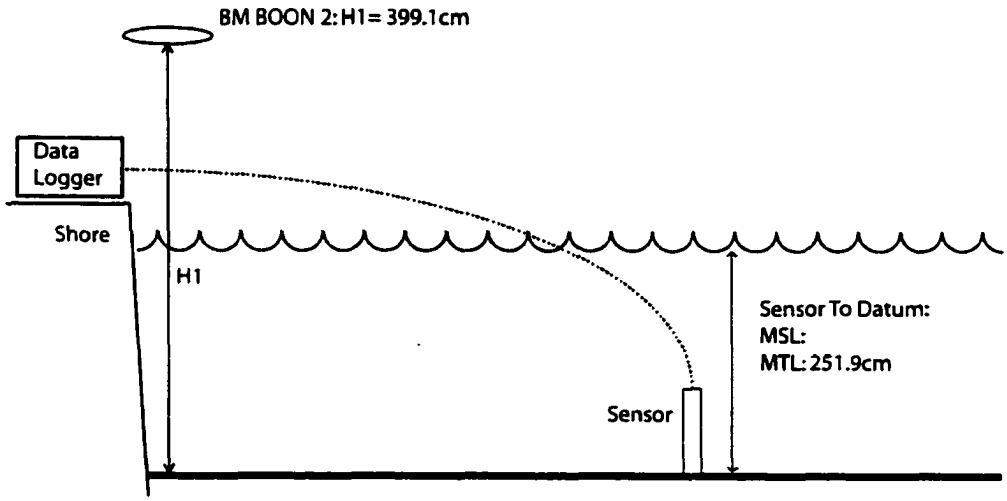

Datum	Raw Data	Calibrated	Seas. Corr. Sitka	Sensor to datum	BM 5 to Datum
MSL 2000	2.462		-0.0992		
MTL 2000	2.463	2.415	-0.1031	2.519	1.472
MHW 2000	3.765				
MLW 2000	1.160				
MTL 1976					128.6

Rate=0.8 cm/yr

Notes: BM5 is in a large buried boulder or bedrock.

Figure 3.A-6. Pt. Sinbad tide gauge.

Station Name: Salt Lake Bay
Time Span of UAF-GI Observations: Julian Days 163.1-212.2; 2000 (June 12-Aug 2)
Date of most recent NOS Survey: 1982
Logger s/n: 2902
Logger Calibraton: Slope m=1.0341; Intercept b=+0.259

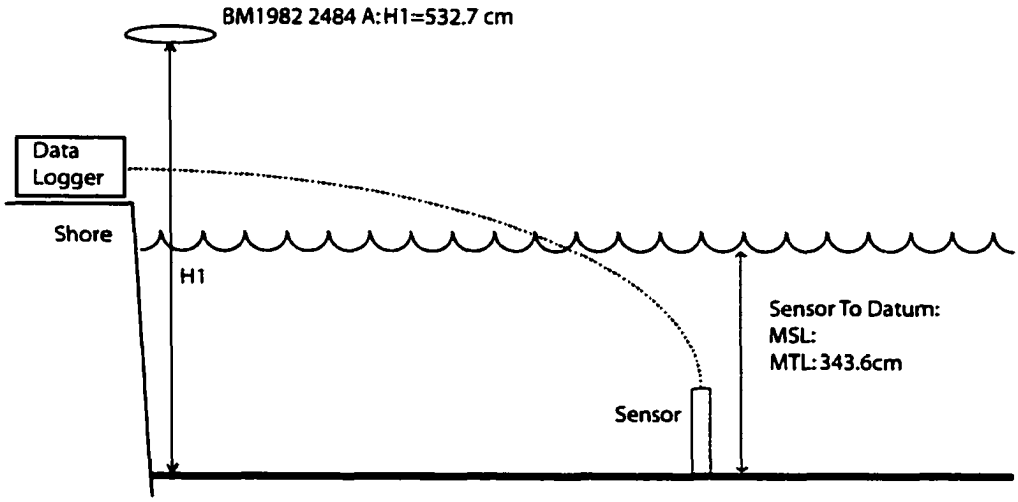

Datum	Raw Data	Calibrated	Seas. Corr. Juneau	Sensor to datum	BM 2484A to Datum
MSL 2000	3.565	3.371			
MTL 2000	3.530	3.338	-0.0981	3.436	1.891
MTL 1982					1.646

Rate= 1.4 cm/yr

Notes: BM1982 2484 A is in bedrock.

Figure 3.A-7. Salt Lake Bay tide gauge.

Station Name:Willoughby Island
Time Span of UAF-GI Observations:Julian Days 155.4-168.4;2000
Date of most recent NOS Survey: 1961.5
Logger s/n: 3704
Logger Calibraton:Slope m=0.9697;Intercept b=0.000

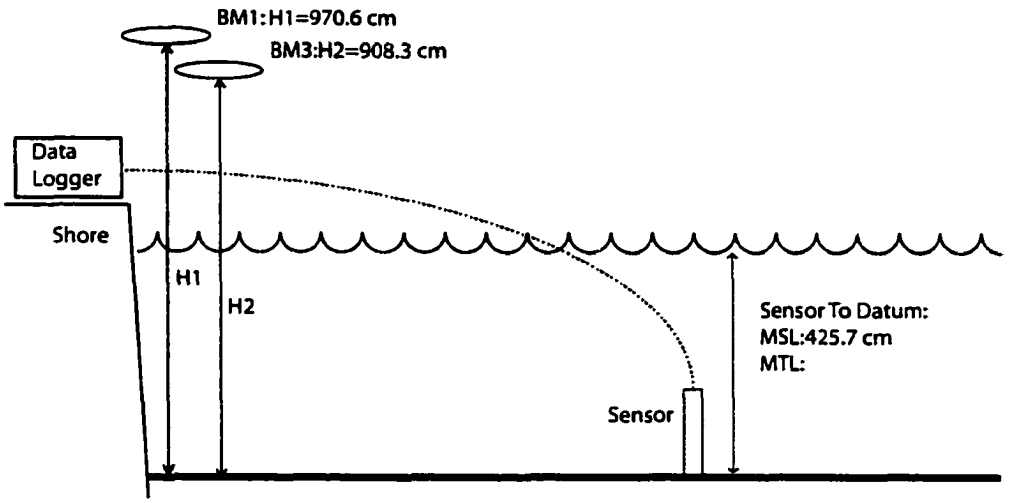

Datum	Raw Data	Calibrated	Seas. Corr. Juneau	Sensor to datum	BM 1 to Datum	BM 3 to Datum
MSL 2000	4.3113	4.1807	-0.1362	4.257	5.449	4.826
MTL 2000						
MHW 2000						
MTL 1961.5					4.584	3.953

Rate=2.3 cm/yr

Notes: Logger failed after only 13 days.

Figure 3.A-8. Willoughby Island tide gauge.

Conclusions.

A clear pattern of vertical crustal motions emerges from the analysis of sea level records at the 15 permanent tide gauge stations along the northern North America-Pacific plate boundary. The stations along the strike-slip portion of the plate boundary and away from regions of major glacial unloading exhibit small rates of uplift with linear trends. Where recent glacial unloading has been large, and still is, the records show extremely rapid uplift, also with linear trends. In the subduction zone the vertical crustal motions are predominantly non-linear, with significant shifts superimposed on the records at the times of major earthquakes. Extremely rapid uplift rates are found at Juneau, Skagway and Yakutat.

Extreme sea level changes have been observed throughout the northern part of southeastern Alaska using temporary tide gauges and studies of raised shorelines. The temporary tide gauge data set shows a regional pattern of sea level rates from 3 to 26 mm/yr, centered over upper Glacier Bay. The overall magnitude and pattern has not changed significantly over the last 50-70 yrs. Raised shorelines at 14 sites show total sea level change in the range of 0.9 to 5.7 m has occurred since ~1790 AD, with a regional pattern of higher uplift closest to upper Glacier Bay. The onset of uplift measured at the raised shoreline sites occurred at the same time the Glacier Bay Icefield began its dramatic collapse.

Global Positioning System measurements at 45 sites throughout southern Alaska describe a broad region with uplift rates 10-35 mm/yr. Peak uplift rates are found in upper Glacier Bay, and in the Yakutat Icefield. Horizontal site velocities indicate there is < 5 mm/yr of compressional strain along the Fairweather Fault, and as such the tectonic contribution to uplift rates here is likely small. Comparison between the sea level rates of the tide gauge data set with the uplift rates of GPS measurements provides an measurement of regional sea surface (geoid) rate of change ($\Delta\dot{S}$) of

-0.3±0.8 mm/yr. This value is used to estimate uplift rates and total uplift from the tide gauge data and raised shoreline data, respectively, to facilitate viscoelastic uplift modeling and comparison with GPS uplift rates.

Realistic glacial unloading models, based on direct and indirect observations of glacial mass changes, indicate that 1) viscoelastic uplift dominates over strictly elastic uplift, 2) a low viscosity upper mantle is required, and 3) isostasy related to the tidewater glacier retreat of Glacier Bay drives a large fraction of the uplift. When the GPS uplift rates and tide gauge uplift rates are modeled independently, the two data sets require similar constrains on the Earth model parameters (lithospheric elastic thickness and mantle half-space viscosity). The total uplift data from the raised shorelines requires a significantly different (lower) viscosity. We propose this is due to the almost exclusive sensitivity of this data set to the large ice thickness changes local to Glacier Bay, which contrasts with sensitivity of the uplift rates to both regional and Glacier Bay load changes.

When integrated together in a combined data set, the GPS, tide gauge and raised shoreline measurements require at the 95% confidence level a three-layer Earth model consisting of a 50^{+30}_{-25} km thick elastic lithosphere, an asthenosphere with viscosity (η_A) of (1.4±0.3) x 10^{19} Pa s and thickness 110^{+20}_{-15} km, overlaying a viscous upper mantle half-space (η_{um} = 4 x 10^{20} Pa s). The best-fit combined model results in an overall misfit of χ^2_ν=2.5, and is thus able to account for a total of 77 measurements of uplift from three distinctly different techniques with a low overall degree of misfit. Moreover, these calculations have assumed ice load models based solely on independent observations of glacial change, rather than iteratively modifying load models to minimize this misfit.

The thesis presented here, i.e. the rapid uplift of southern Alaska is due primarily to isostatic rebound, is based on the following results: 1) the long term tide gauge records show that the region's uplift has been steady and continuous, whereas tectonically driven uplift shows non-linear behavior over the same time period, 2) GPS

measurements indicate little compressional strain south and east of Yakutat, 3) raised shoreline dating indicates that the onset of uplift began at the same time significant ice unloading began, and 4) Isostatic models show that rebound caused by observed post-Little Ice Age glacial change can match the uplift observations with low misfit. In conclusion, the uplift observations in southeast Alaska can be entirely explained by post-glacial isostatic rebound. Furthermore, these observations provide robust constraints on lithospheric elastic thickness, asthenosphere thickness and asthenosphere viscosity.